
Space Systems Engineering and Operations

Professor: *Dr. Michèle Lavagna*

SOHO Mission: Solar and Heliospheric Observatory

Group n° 29



MSc in Space Engineering
Politecnico di Milano
Academic Year 2023-2024

Team members

<i>Person code</i>	<i>Matriculation Number</i>	<i>Surname</i>	<i>Name</i>
10703587	244603	Conte	Chiara
10637601	103415	Accordini	Luca
10719352	243232	Fiume	Elisa
10766758	243222	Gallo	Emanuele
10779108	244976	Loffredo	Emanuela
10727581	245128	Gardioli	Francesco

Contents

1 Mission Description	1
1.1 Abstract	1
1.2 Mission high-level goals	1
1.3 Mission Drivers	1
1.4 Functional Analysis	2
1.5 Mission Phases	2
1.5.1 Disposal Phase and Mission Extension	3
1.6 Concept of Operations	3
1.7 On-board scientific instruments	3
1.7.1 Payload	3
1.7.2 Payload functions	5
1.7.3 Phase/ConOps - P/Ls correlation	5
1.8 Mission Analysis-Functionalities/Phases correlation	6
1.9 Launch window design choices	6
1.10 Transfer trajectory design choices	6
1.11 Final orbit design choices	6
2 Mission Analysis and Propulsion Subsystem	8
2.1 Mission Analysis	8
2.1.1 Mission trajectory design understanding	8
2.1.2 Mission costs reverse sizing	8
2.1.3 ΔV budget breakdown	9
2.2 Propulsion Subsystem	10
2.2.1 Propulsion subsystem architecture and design	10
2.2.2 Propulsion subsystem reverse sizing	10
3 TMTCS Subsystem	15
3.1 TMTCS Subsystem Architecture	15
3.1.1 Space Segment	15
3.1.2 Ground Segment	16
3.2 TMTCS design and justification	16
3.2.1 Correlation with operation/phases/modes	17
3.3 Reverse Sizing	17
3.3.1 Contact Window and Data Volume	17
3.3.2 Frequency, data rate and band selection	18
3.3.3 Encoding and modulation of the signal	18
3.3.4 Link budget	18
3.3.5 Uplink reverse sizing	19
4 AOC Subsystem	20
4.1 AOCS Architecture	20
4.1.1 AOCS Hardware: Sensors	20
4.1.2 AOCS Software	21
4.1.3 Mass, power and data budgets	22
4.2 AOCS Design and Justifications	22
4.2.1 Mission modes and control	23
4.2.2 Pointing Budget	24
4.3 AOCS Reverse Sizing	25
4.3.1 Disturbances	25
4.3.2 Attitude actuators sizing	25
4.3.3 Preliminary fuel mass sizing	26
5 TC Subsystem	27
5.1 TCS Architecture	27
5.1.1 TCS Criticalities and Requirements	27
5.1.2 TCS Components and Positioning	27
5.2 TCS Design and Justification	28
5.2.1 Thermal Ranges and Phases	28
5.2.2 Units Specifically Controlled	29
5.3 TCS Reverse Sizing	30
5.3.1 Hot and Cold Case Selection	30

5.3.2	Heat Fluxes and Powers	30
5.3.3	Passive Control	31
5.3.4	Active Control	32
5.3.5	Mass, Power and Data Budget	32
6	EP Subsystem	33
6.1	EPS Architecture	33
6.1.1	Power Sources Architecture	33
6.1.2	Power Regulation and Control	33
6.1.3	Power distribution	34
6.2	EPS Design and Justifications	34
6.2.1	Operational Profiles and Power Budget	35
6.3	EPS Reverse Sizing	36
6.3.1	Solar Arrays	36
6.3.2	Secondary Batteries	37
6.3.3	Mass, Power, Data and Volume Budget	38
7	Configuration & OBDH Subsystem	39
7.1	Space segment configuration and justification	39
7.1.1	Launcher adapter and appendages	39
7.1.2	Payloads	39
7.1.3	TMTC subsystem	40
7.1.4	Propulsion Subsystem	40
7.1.5	AOCS	41
7.1.6	TCS	41
7.1.7	EPS	41
7.1.8	OBDH Subsystem	41
7.2	OBDH Subsystem	42
7.2.1	Components and Adopted Buses	42
7.2.2	Interfaces	43
7.2.3	Data	43
7.2.4	Autonomy	43
7.2.5	On Board Time (OBT)	43
7.2.6	OBDH Reverse Sizing	43
Appendix		46
Bibliography		47

List of Figures

1	Functional decomposition	2
2	ConOps	3
3	SOHO spacecraft schematic view	5
4	SOHO transfer trajectory	6
5	Sizing methodology	11
6	Sizing methodology	12
7	SOHO Propulsion Schematic [6]	13
8	SOHO thruster configuration	14
9	SOHO Spacecraft	14
10	Elementary scheme of SOHO TMTC architecture	15
11	HGA and LGAs configuration	15
12	The SOHO Ground Data System (GDS)	16
13	Generalities about SOHO and AOCS architecture	20
14	SOHO normal mode control loop (for pitch and yaw)	22
15	S/C modular design	39
16	SOHO prepared for encapsulation in the fairing	39
17	SOHO spacecraft instruments view	40
18	SOHO antennas highlighted	40
19	SOHO thruster configuration	40
20	OBDH Architecture [2]	42

List of Tables

1	Guiding questions and relative science objectives	1
2	Mission goals correlated to the measurements of the P/Ls	5
3	Phases/ConOps correlated to the P/Ls	5
4	ΔV budget breakdown. "NM" stands for "no margins"; "WM" stands for "with margins"	9
5	SOHO thrusters and manoeuvres correlation	10
6	Mass Data	10
7	Pressure Data	10
8	Masses of the propulsive subsystem components	12
9	Masses expressed as a percentage of m_{dry}	12
10	Summary of estimated vs real data."NM" stands for "no margins"; "WM" stands for "with margins" ¹	13
11	SOHO thrusters (applies to both A and B branches) [41]	14
12	Computation of the losses	18
13	Final results of the link budget preliminary sizing	19
14	Resuming table for uplink sizing results	19
15	Gyroscopes function [114]	21
16	SOHO thrusters [41]	21
17	Thrusters configuration	21
18	Pitch axis parameters	22
19	Yaw axis parameters	22
20	Mass, power and data budget of AOCS subsystem	22
21	Control modes of SOHO	24
22	Propellant mass sizing	26
23	TCS requirements	27
24	Operational temperatures of S/C components	28
25	Fluxes along the mission phases	29
26	Heat Fluxes in hot and cold cases	31
27	Heat Powers in hot and cold cases	31
28	Data Budget of TCS	32
29	Mass and Power Budget of TCS	32
30	Operational Profiles	35
31	Power Budget for phase/mode	36
32	Parameters chosen for SA sizing	36
33	Resuming table of substrates characteristics	37
34	Parameters chosen for Battery sizing	37
35	Data Budget of EPS	38
36	SOHO thrusters (applies to both A and B branches)	40
37	Data of all subsystem components	45
38	Percentage on code, data and KIPS per S/S	45
39	Final results and systems data usage per each S/S in each mode	45
40	Comparison between computed and real data	45
41	Resuming table of subsystems elements active for each mode	46
42	Systems data usage per each S/S in RMW mode	46
43	Systems data usage per each S/S in NM mode	46
44	Systems data usage per each S/S in ESR mode	46
45	Systems data usage per each S/S in CRP mode	46
46	Total results for RMW mode	46
47	Total results for NM mode	46
48	Total results for ESR mode	46
49	Total results for CRP mode	46

Nomenclature

<i>2P2T</i>	Double-Pole Double-Throw	<i>ERNE</i>	Energetic and Relativistic Nuclei and Electron experiment
<i>ACU</i>	Attitude Control Unit	<i>ESA</i>	European Space Agency
<i>AOCS</i>	Attitude and Orbit Control System	<i>ESR</i>	Emergency Sun Reacquisition
<i>AOS</i>	Acquisition Of Signal	<i>EUV</i>	Extreme UltraViolet
<i>APA</i>	Antenna Pointing Assembly	<i>FCV</i>	Flow Control Valve
<i>AU</i>	Astronomical Unit	<i>FDE</i>	Failure Detection Electronics
<i>BCR</i>	Battery Charge Regulator	<i>FDV</i>	Fill/drain valve
<i>BER</i>	Bit Error Rate	<i>FOV</i>	Field of view
<i>BOL</i>	Begin Of Life	<i>FPSS</i>	Fine Pointing Sun Sensor
<i>BRU</i>	Battery Regulator Unit	<i>FVV</i>	Fill/vent valve
<i>BSR</i>	Back Surface Reflection	<i>GOLF</i>	Global Sun velocity oscillations
<i>CCD</i>	Charge-Coupled Detector	<i>GRIST</i>	Grazing Incidence Solar Telescope
<i>CDMU</i>	Central Data Management Unit	<i>GSFC</i>	Goddard Space Flight Center
<i>CDS</i>	Coronal Diagnostic Spectrometer	<i>HED</i>	High Energy Detector
<i>CELIAS</i>	Charge, Element and Isotope Analysis System	<i>HGA</i>	High Gain Antenna
<i>CMG</i>	Control Moment Gyro	<i>HOI</i>	Halo Orbit Insertion
<i>CMOS</i>	Complementary Metal Oxide Semiconductor	<i>HOP</i>	Halo Orbit Phase
<i>CM</i>	Correction Manoeuvres	<i>HPA</i>	High Power Amplifier
<i>COSTEP</i>	Comprehensive SupraThermal and Energetic Particle Analyzer	<i>HR-STR</i>	High-Resolution Star Tracker
<i>COTS</i>	(Commercial) Off-the-Shelf component	<i>HR</i>	High Rate
<i>CRP</i>	Coarse Roll Pointing	<i>IIDE</i>	Inter Instrument Data Exchange
<i>DCU</i>	Data Compression Unit	<i>IRU</i>	Inertial Reference Unit
<i>DC</i>	Direct Current	<i>IR</i>	Infrared
<i>DET</i>	Direct Energy Transfer	<i>ISA</i>	Initial Sun Acquisition Mode
<i>DISCO</i>	Dual Spectral Irradiance and Solar Constant Orbiter	<i>JPL</i>	Jet Propulsion Laboratory
<i>DoD</i>	Depth of Discharge	<i>KIPS</i>	Kilo Instructions Per Second
<i>DSN</i>	Deep Space Network	<i>LASCO</i>	Large Angle Spectroscopic COronagraph
<i>EAF</i>	Experiment Analysis Facility	<i>LCL</i>	Latching Current Limiters
<i>EIRP</i>	Effective Isotropic Radiated Power	<i>LED</i>	Low Energy Detector
<i>EIT</i>	Extreme-Ultraviolet Imaging Telescope	<i>LEOP</i>	Launch and Early Orbit Phase
<i>EMC</i>	Electromagnetic Compatibility	<i>LEO</i>	Low Earth Orbit
<i>EOC</i>	End of Charge	<i>LGA</i>	Low Gain Antenna
<i>EOF</i>	Experiment Operations Facility	<i>LION</i>	Low Energy Ion and Electron Instrument
<i>EPHIN</i>	Electron Proton Helium Instrument	<i>LPO</i>	Libration Point Orbit
<i>EPS</i>	Electric Power Subsystem	<i>LR</i>	Low Rate
		<i>LSI</i>	Large Scale Integration
		<i>MACS</i>	Modular Attitude Control System
		<i>MA</i>	Mission Analysis

<i>MCC1</i>	Mid Course Correction 1	<i>S3R</i>	Sequential Switching Shunt Regulator
<i>MCC2</i>	Mid Course Correction 2	<i>SAS</i>	Sun acquisition sensors
<i>MDI</i>	Michelson Doppler Imager	<i>SA</i>	Solar Array
<i>MLI</i>	Multi Layers Insulation	<i>SBDL</i>	Standard Balanced Digital Link
<i>MM</i>	Momentum Management	<i>SDAC</i>	Solar Data Analysis Center
<i>NASA</i>	National Aeronautics and Space Administration	<i>SDPF</i>	Sensor Data Processing Facility
<i>NM</i>	Normal Mode	<i>SD</i>	Science Data
<i>OBDH</i>	On Board Data Handling	<i>SK</i>	Station Keeping
<i>OBT</i>	On Board Time	<i>SMOCC</i>	SOHO Mission Operations Control Center
<i>OSR</i>	Optical Solar Reflector	<i>SNR</i>	Signal to Noise Ratio
<i>OS</i>	Operating System	<i>SOHO</i>	Solar Heliospheric Observation
<i>P/L</i>	PayLoad	<i>SOI</i>	Solar Oscillations Investigation
<i>PCM</i>	Propellant Control Module	<i>SOS</i>	Silicon On Sapphire
<i>PCU</i>	Power Control Unit	<i>SRP</i>	Solar Radiation Pressure
<i>PDU</i>	Power Distribution Units	<i>SSA</i>	Solid State Amplifier
<i>PI</i>	Principal Investigator	<i>SSU</i>	Star Sensor Unit
<i>PLM</i>	Payload module	<i>SUMER</i>	Solar Ultraviolet Measurements of Emitted Radiation
<i>PM</i>	Phase Modulation	<i>SVM</i>	Service Module
<i>PPT</i>	Power Peak Tracker	<i>SWAN</i>	Solar Wind Anisotropies
<i>PS</i>	Propulsion Subsystem	<i>TAI</i>	International Atomic Time
<i>PWM</i>	Pulse With Modulator	<i>TCS</i>	Thermal Control Subsystem
<i>R-S</i>	Reed-Solomon	<i>TMT</i>	TeleMetry and TeleCommand
<i>RAM</i>	Random Access Memory	<i>TM</i>	Telemetry
<i>RCS</i>	Reaction Control Subsystem	<i>TTI</i>	Transfer Trajectory Insertion
<i>RFDU</i>	Radio Frequency Distribution Unit	<i>TTP</i>	Transfer Trajectory Phase
<i>RF</i>	Radio Frequency	<i>TT</i>	Transfer Trajectory
<i>RLP</i>	Rotating Libration Point Frame	<i>TWTA</i>	Traveling Wave Tube Amplifier
<i>RMW</i>	Roll Manoeuvre Wheels	<i>USO</i>	Ultra Stable Oscillator
<i>ROM</i>	Read Only Memory	<i>UTC</i>	Coordinated Universal Time
<i>RSL</i>	Roll Steering Law	<i>UVCS</i>	Ultraviolet Coronagraph Spectrometer
<i>RTG</i>	Radioisotope Thermoelectric Generator	<i>UV</i>	Ultra Violet
<i>RTU</i>	Remote Terminal Units	<i>VDA</i>	Vapor Deposited Aluminium
<i>RWA</i>	Reaction Wheel Assembly	<i>VIRGO</i>	Variability of Solar irradiance and Gravity Oscillations
<i>RWU</i>	Reaction Wheel Unit	<i>VUV</i>	Vacuum UltraViolet
<i>RW</i>	Reaction Wheel	<i>WDE</i>	Wheel Drive Electronics Box
<i>S/C</i>	Spacecraft		
<i>S/S</i>	Subsystems		

1 Mission Description

1.1 Abstract

The Solar and Heliospheric Observatory (SOHO) is a cooperative mission between ESA and NASA. The principal scientific objectives of the SOHO mission are to reach a better understanding of the structure and dynamics of the solar interior using helioseismology techniques and to gain better insight into the physical processes that form and heat the Sun's corona, maintain it and give rise to its acceleration into the solar wind.

The SOHO spacecraft was launched on 2 December 1995 with an initial mission duration of 29 months, 8 years after it started to be developed by European industry. Since 14 February 1996, SOHO is in a halo orbit around the Lagrangian point L_1 . From that time, SOHO images and data are used to predict 'space weather' events affecting our planet.

The aim of this report is to perform a reverse engineering analysis of this mission in order to see how the selected design of the S/C addressed the problems that arose.

1.2 Mission high-level goals

SOHO's scientific objectives group together the goals of two other earlier missions which failed to pass the ESA selection process: DISCO and GRIST.

The high-level goals are therefore diversified and comprise the investigation of the solar activity. What could have been considered a priori as a patchwork of science objectives, ultimately led to the definition of the most comprehensive solar observatory ever designed. The science objectives will then be translated into measurement objectives to be accomplished by the S/C's payloads [3].

Guiding Questions	Science Objectives
What is the structure and dynamics of the solar interior?	Study of the solar interior, using the techniques of helioseismology
Why does the solar corona exist?	Study of the heating mechanisms of the solar corona
How is the solar corona heated to the extremely high temperature of about 1 000 000°C?	Study of the interaction of the Sun with the heliosphere and the interstellar medium
Where is the solar wind produced and how is it accelerated?	Investigation of the solar wind and its acceleration processes

Table 1: Guiding questions and relative science objectives

1.3 Mission Drivers

The mission drivers lead either completely or partly the system design process being a bunch of mandatory requirements highly constrained and greatly influencing the decision making process at any level of the project.

For the SOHO mission the following drivers have been recognized [1]:

- **Pointing stability:** it is vital to ensure that the instruments are accurately aimed at the desired target. Specific attention was paid to the high frequency jitter produced by all moving mechanisms and particularly by the reaction wheels, which spin continuously for the life of the mission. During the development phase, analyses and tests of the major potential contributors to micro vibrations were performed and the integration of the spacecraft and the experiments, to show that the goals sought by certain experiments would be met.
- **Spacecraft autonomy and permanent Sun visibility:** because of the interrupted daily contact with the ground stations, the autonomy of the spacecraft in case of failures (besides the usual redundancy of critical elements), is extremely important. The unique vantage point chosen for SOHO, the Lagrangian Point L_1 , allows permanent visibility of the Sun and also an extremely stable thermal environment.
In case of failures, which may lead to depointing of the spacecraft from its nominal direction, SOHO is designed to go back into a safe Sun-pointing attitude mode, with a minimum of functions which maintain the good health of the payload and its thermal stability.
- **Cleanliness:** as several instruments are very sensitive to contamination, cleanliness was of paramount importance in the whole SOHO programme. It was achieved by careful application of various techniques (clean rooms, tents, local bagging and permanent purging), particularly during the test phase, and involved the use of facilities built specifically for SOHO.
- **Communication:** the orbit and the distance involved in the halo orbit present some operational challenges. A 5 s light time delay each way to SOHO made it difficult to perform command verification and still allow a high rate of commanding. This is why a special ground software was required to allow pipelining of commands. It used an S-band RF system, whose full coverage was allowed by a High Gain Antenna (HGA) and two Low Gain Antennas (LGA) [7].

1.4 Functional Analysis

Here below the functional analysis decomposition is shown:

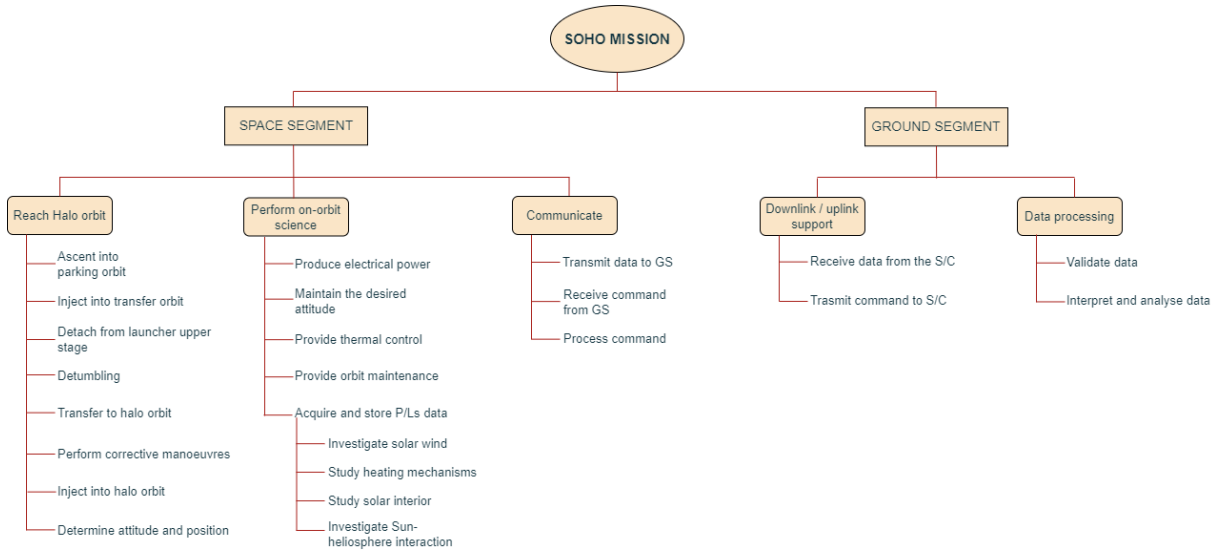


Figure 1: Functional decomposition

1.5 Mission Phases

The operational mission is divided into three main phases [7]:

- **Launch and Early Orbit Phase (LEOP):** this first phase starts at lift-off, including the coasting period in parking orbit and ends with the injection of the spacecraft into the transfer trajectory. It is divided into two subphases:
 1. *Ascent Subphase:* SOHO is launched by the Atlas II-AS using a Centaur upper stage, from Kennedy Space Center. The first burn of the Centaur injects the SOHO/Centaur composite into a near-circular parking orbit². The duration of this subphase is of 10 minutes.
 2. *Parking-Orbit Subphase:* this subphase begins at SOHO/Centaur insertion into parking orbit and finishes at the SOHO/Centaur injection into transfer trajectory.
 The Centaur/SOHO combination coasts in the parking orbit for 74 minutes. During this phase communication is not performed.
- **Transfer Trajectory Phase (TTP):** the TTP starts with the injection of the spacecraft into the transfer orbit and ends with the injection into the halo orbit. It lasts about 4 months and during this phase the priority is given to the health and status of the spacecraft bus. It is important to ensure the first Acquisition Of Signal (AOS) with a maximum duration of 35 minutes. Furthermore, housekeeping and science telemetry, telecommand, and ranging links are established during this phase. The TTP is divided in the following four subphases:
 1. *PRE-SEP Subphase:* the pre-separation lasts about 35 minutes from Transfer Trajectory Insertion (TTI) until separation from the Centaur upper stage.
 2. *PRE-OP Subphase:* the pre-operation begins at separation and ends when the anti-Sun line/spacecraft/Earth angle is less than 33 degrees. During this subphase, the S/C is detumbled and starts pointing at the Sun using the hydrazine thrusters. Subsequently, the Solar Arrays (SA) are deployed and the AOCS (Attitude and Orbit Control System) performs a reorientation using the fine pointing Sun sensor provided. From designing, PRE-OP subphase should last about 3 hours.
 3. *LR Subphase:* redundant Low Gain Antenna (LGA) are available for the low data rate only.
 4. *HR Subphase:* about 7 hours after separation, the High Gain Antenna (HGA) are deployed providing both uplink reception and medium- or high-rate telemetry downlinking for the remainder of the TTP (and mission). Two mid-course corrections are realised to maintain the correct transfer trajectory.
- **Halo Orbit Phase (HOP):** it starts at the spacecraft's injection into the halo orbit. Three daily passes of 1.6 hours and one 8 hours pass were baselined for SOHO support during 10 months per year, the remaining 2 months having 24 h/day support. The onboard data recorder provide data storage during all non-contact periods. These contacts are sufficient for complete recorder-play-back data capture and to meet all telemetry, ranging and command requirements.

²The parking orbit was at 150-200 km altitude and inclined at 28.5 degrees. The period was of 90 minutes

During the operational phase, any combination of the ranging, telemetry, and telecommanding links are nominally available. Below, HOP subphases are listed:

1. *Commissioning Subphase*: the first group of tasks in the halo orbit is the hereinafter of commissioning phase, which ends after successful check-out for all on-board instruments, thus beginning the fully operational life of SOHO. A schedule is made for commissioning operations from the first time the commanding link to SOHO is established (about 2 hours after launch) up to insertion into halo orbit, about 4 months after launch, and for sporadic activities up for two months more[4].
2. *Mission Operations Subphase*: this starts after commissioning and includes all scientific and routine operations necessary to undertake the desired experiment activities. After insertion into the halo orbit, a first station-keeping manoeuvre is performed. Every 8 weeks, an orbit maintenance manoeuvre is conducted. Momentum-wheel off-loading is coupled with orbit correction manoeuvres. During this phase, the satellite is three-axis-stabilised in a Sun-pointing attitude. In the case of safe-mode activation, it maintains this Sun-pointing attitude but to a lower accuracy.

1.5.1 Disposal Phase and Mission Extension

The mission did not foresee a disposal phase. This could depend on the fact that the awareness for the generation of space debris raised only after. Just in 2002, the Working Group 4 of the Inter-Agency Space Debris Coordination Committee worked out the "*IADC Space Debris Mitigation Guidelines*" [28] that was the first international regulatory document specialized in the field of space debris mitigation.

As a design choice, SOHO was equipped with sufficient on-board consumables for a mission duration of 6 years [2]. This redundancy aimed at mitigating potential issues during the transfer and the maintenance of the halo orbit. Additionally, at the end of the commissioning phase, the spacecraft confirmed good margins in every aspect related to orbital life. In fact, the ample reverses of fuel remained on-board due to the manoeuvre optimization and due to the excellent performances of the propulsion system, together with the low degradation rate of the solar array allowed the possibility of a following extension of the mission [1]. For these reasons, in 1997 it was possible to extend the mission until 2003. Then, in 2002 a second extension was granted for another 4 years, allowing SOHO to cover the complete 11-year solar cycle. Other multiple extensions led the SOHO mission to be still ongoing nowadays. In particular, during the years, data analysis confirmed the feasibility of extending the mission further. As a matter of fact, fuel consumption from 2008 to 2018 amounts to 5 kg with a remaining fuel of 113 kg and the degradation of the solar array after 274 months is 23.35% [31].

1.6 Concept of Operations

The mission conceptual operations are summarized in Figure 2. Orbital and corrective manoeuvres are not continuous operations; thus, the figure illustrates the periods during which they can be performed. For a clearer understanding of when the operations are carried out, the phases are outlined below.

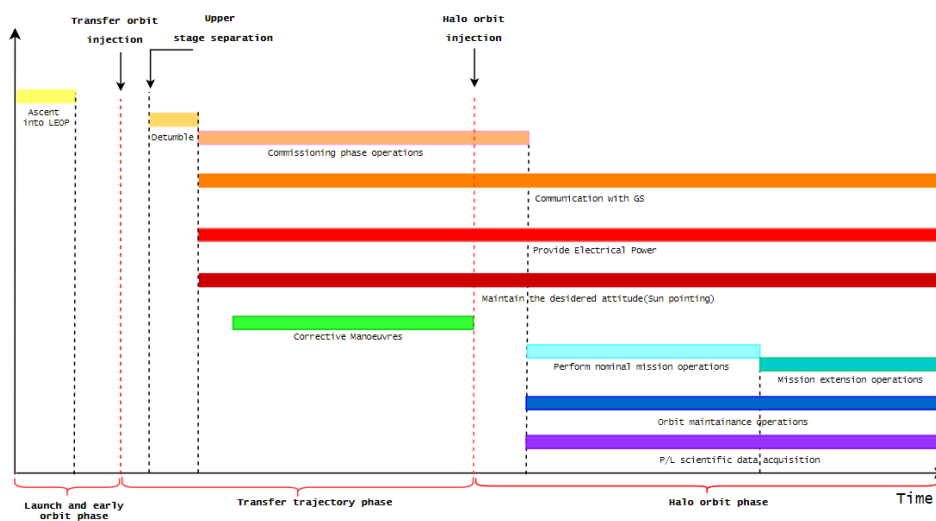


Figure 2: ConOps

1.7 On-board scientific instruments

1.7.1 Payload

The scientific payload of SOHO comprises twelve state-of-the-art instruments, as represented in Figure 3. The experiments on board SOHO can be divided into three main groups, according to their area of research: helioseismology instruments,

solar corona instruments and solar wind "in-situ" instruments.

- **Global Sun velocity oscillations (GOLF):** it studies the internal structure of the Sun by measuring velocity oscillations in the frequency range 10^{-7} to 10^{-2} Hz over the entire solar disc. A sodium vapour resonance filter is used in a longitudinal magnetic field to sample the two wings of the solar absorption line. This provides not only an internal calibration of the instrument sensitivity, but also opens the possibility to recognise, and correct for, the solar background signal produced by the effects of solar magnetically active regions. The use of an additional rotating polariser enables also measurement of the mean solar line-of-sight magnetic field [14].
- **Variability of Solar irradiance and Gravity Oscillations (VIRGO):** this instrument provides the following observational and derived data: continuous high-precision measurements of the solar total and spectral irradiance and spectral radiance variation, continuous measurements of the solar polar and equatorial diameters and frequencies, amplitudes and phases of oscillation modes in the frequency range of 1 uHz to 8 mHz. In this way it can characterise solar intensity oscillations and measures the total solar irradiance to quantify its variability over periods of days to the duration of the mission [16].
- **Michelson Doppler Imager/Solar Oscillations Investigation (MDI/SOI):** it measures the longitudinal component of the Sun's magnetic field and records the vertical motion ("tides") of the Sun's surface. By measuring the acoustic waves inside the Sun as they perturb the photosphere, the structure and dynamics of the Sun's interior can be studied [17].
- **Solar Ultraviolet Measurements of Emitted Radiation (SUMER):** this vacuum ultraviolet (VUV) telescope and spectrometer perform a detailed spectroscopic plasma diagnostics of the solar atmosphere, from the chromosphere through the transition region to the inner corona, measuring its flows, temperature, density and dynamics [19].
- **Coronal Diagnostic Spectrometer (CDS):** this spectrometer detects emission lines from ions and atoms in the solar corona and transition region, providing diagnostic information on the solar atmosphere. The spectra recorded provide information on temperature, density, elemental composition and flows of very hot plasma trapped in the Sun's magnetic field [20].
- **Extreme-Ultraviolet Imaging Telescope (EIT):** is a telescope able to image the solar transition region and inner corona in four selected bandpasses in the extreme ultraviolet (EUV). Using either full-disk or subfield images, the EIT can image active regions, filaments and prominences, coronal holes, coronal "bright points", polar plumes, and a variety of other solar features. The detector in the EIT is a backside-thinned charge-coupled detector (CCD) [21].
- **Ultraviolet Coronagraph Spectrometer (UVCS):** it is composed of three reflecting telescopes with external and internal occultation, creating an artificial solar eclipse, and a spectrometer assembly consisting of two toric grating spectrometers and a visible light polarimeter, providing valuable information about the microscopic and macroscopic behaviour of the highly ionised coronal plasma [22].
- **Large Angle Spectroscopic CORonagraph (LASCO):** it is a set of three coronagraphs (telescope designed to block direct light coming from the solar, in order to see the extremely faint emission from the region around the sun) that image the solar corona, each one looks at an increasingly large area, from 1.1 to 32 solar radii [23].
- **Solar Wind Anisotropies (SWAN):** this instrument is the only remote sensing one on SOHO that does not look at the Sun. It watches the rest of the sky, measuring hydrogen that is 'blowing' into the Solar System from interstellar space. By studying the interaction between the solar wind and this hydrogen gas, SWAN determines how the solar wind is distributed [24].
- **Charge, Element and Isotope Analysis System (CELIAS):** it is designed to study the composition of the solar wind and of solar and interplanetary energetic particles, as they sweep past SOHO. It consists of three different sensors with associated electronics, which are optimized each for a particular aspect of ion composition. These aspects are the elemental, isotopic, and ionic charge composition of solar wind or energetic ions emanating from the Sun. It warns of incoming solar storms that could damage satellites in Earth orbit [25].
- **Comprehensive SupraThermal and Energetic Particle Analyzer (COSTEP):** it consists of two instruments, which are called EPHIN (Electron Proton Helium Instrument) and LION (Low Energy Ion and Electron Instrument). The first one is a telescope for the measurement of energy spectra of electrons and of hydrogen and helium isotopes; the second is a stack of semiconductor detectors to measure energetic particles. Both instruments are measuring energetic particles emitted by the Sun, in order to understand stationary processes in the solar atmosphere, energy deposition and particle acceleration in the solar atmosphere, composition of the solar atmosphere and to learn more about processes in the interplanetary medium [26].
- **Energetic and Relativistic Nuclei and Electron experiment (ERNE):** it is a complementary instrument to COSTEP and will investigate the solar atmosphere by detecting charged particles produced in various solar energy release processes, using two energetic particle sensors: the Low Energy Detector (LED) and the High Energy Detector (HED) [27].

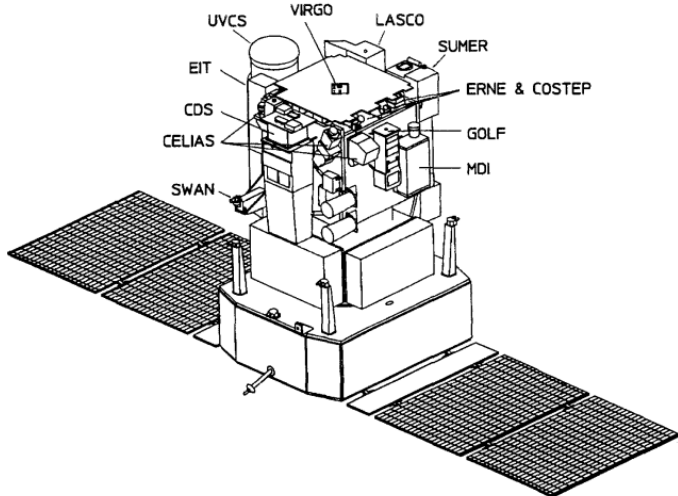


Figure 3: SOHO spacecraft schematic view

1.7.2 Payload functions

Scientific Objectives	Measurement Objectives
Study of the solar interior, using the techniques of helioseismology	Global and low resolution imaging of oscillating and solar constant (VIRGO); high resolution imaging of velocity oscillations (MDI); global sun velocity and magnetic field oscillations (GOLF)
Study of the heating mechanisms of the solar corona	Evolution of low coronal structure and activity (EIT); density and temperature in the corona (UVCS); structure and evolution of the corona (LASCO)
Investigation of the solar wind and its acceleration processes	Solar wind mass flux anisotropies (SWAN); ion and electron composition in the solar wind (CELIAS and COSTEP)
Study of the interaction of the Sun with the heliosphere and the interstellar medium	Plasma flows, temperature and density in the solar atmosphere (SUMER); density, temperature and flows in the solar atmosphere (CDS); detection of charged particles in the solar atmosphere produced in various solar energy release processes (ERNE)

Table 2: Mission goals correlated to the measurements of the P/Ls

1.7.3 Phase/ConOps - P/Ls correlation

SOHO's P/Ls operate simultaneously during the Mission Operations, indeed, unlike many space-based and ground telescopes, there is no time formally allocated by the SOHO program for observing proposals on individual instruments.

Phase/ConOps	Payloads
Transfer Trajectory Phase (TPP)	Service module switch-on; check whether GOLF door is closed and if not, close to prevent contamination of entrance window; verify and tune GOLF channel; MDI start and functional tests; CCD bakeout; SUMER switch-on and start outgassing; early VIRGO switch-on to protect SPM and enhance outgassing; UVCS functional tests and calibrations; early experiments of GOLF, MDI, SUMER, CDS, LASCO, EIT, UVCS, SWAN, CELIAS, CEPAC; determination of off-pointing sensitivity of VIRGO and monitoring of performance of detectors over time; joint calibrations; joint activities with service module.
HOP: Commissioning Subphase	Experiment of GOLF, VIRGO, MDI, SUMER, EIT, UVCS, SWAN, CELIAS, CDS, LASCO; remaining commissioning activities.
HOP: Mission Operations Subphase	All P/Ls operate simultaneously, as commissioning demonstrated that timelining for experiment operations was unnecessary [1]. Regarding communication CELIAS, VIRGO, GOLF, and SWAN operate automatically and don't need near real-time operational control except for surveillance of housekeeping data. Other instruments, those of the coronal imaging investigators, operate interactively every day in real (or near real-) time [12].

Table 3: Phases/ConOps correlated to the P/Ls

1.8 Mission Analysis-Functionalities/Phases correlation

In this section an in-depth analysis of the SOHO transfer trajectory, already presented in Section 1.5, is carried out. In Fig. 4 the entire trajectory is shown in detail.

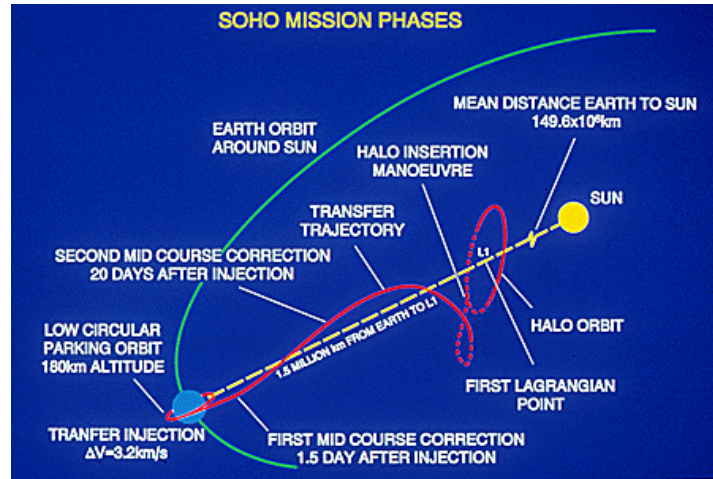


Figure 4: SOHO transfer trajectory

The selection of some specific aspects of mission analysis (i.e. launch windows, transfer trajectory and final orbit) is driven by the high scientific goals and specific functionalities of the mission. The following design choices are taken to benefit the SOHO mission.

1.9 Launch window design choices

The launch window for the SOHO mission, spanning from November 23 to December 15, was determined primarily by the aim to avoid lunar perturbations, with daily launch times optimized based on transfer orbit geometry. Moreover, the launch time span choice is influenced by the benefits coming from launching during a minimum of the solar cycle.

This can be seen in Fig. 5a, where ① is the transfer to halo orbit, ② is the nominal operation time, ③ is the initially expected operation extension. These peculiar timing choices minimize perturbations during the initial phases of the transfer, making the S/C avoid passage through electrically active zones, thus reducing the damage to electronics and external structure. This enhances the transfer stability, the mission efficiency and the goals achievements [34].

1.10 Transfer trajectory design choices

The transfer trajectory design has its basis in manifold dynamics. Manifolds are geometric structures that describe the dynamical behaviour of trajectories near equilibrium points. The transfer orbit design starts by choosing some requirements to be respected. The initial requirements considered are an uninterrupted view of the Sun and minimization of the background noise due to particle flux. Those requirements generate Lissajous amplitude constraints: $A_X = 206448 \text{ km}$, $A_Y = 666672 \text{ km}$ and $A_Z = 120000 \text{ km}$.

Given this Lissajous orbit, a transfer trajectory is sought. Initially, a limited set of points is selected along some specified parts of the Lissajous trajectory. It is already known that the manifolds associated with these points will pass close to the Earth. This particular region along the nominal path is designated as the "Earth Access region". Each point in the Earth Access region can be defined as a fixed point and the corresponding one-dimensional stable manifold globalized. Together, these one-dimensional manifolds form a two-dimensional surface associated with this region of the nominal orbit. From the analysis of this surface, it's possible to select the one trajectory that passes closest to the Earth as the initial guess for the transfer path. Given the initial guess, the transfer is differentially corrected with the aid of numerical algorithms to meet the requirements of the other constraints. By proceeding in this way, a deep understanding of the final orbit and the transfer trajectory can be obtained, thus, selecting them in order to minimize the cost and respect the requirements of the mission [15].

1.11 Final orbit design choices

SOHO's final operational orbit is referred to as halo orbit belonging to Class II, which means that it's characterised by an anticlockwise rotation (when looking at the Sun from Earth), at a distance of about 1.5 million kilometres from Earth. The SOHO orbit is a quasi-periodic halo orbit, where the frequencies of the in-plane and out-of-plane motions are practically equal. Such an orbit is seen to repeat itself with a period of approximately 178 days around the L_1 point. As motion about the L_1 point is inherently unstable, station-keeping manoeuvres are necessary to prevent orbital decay and eventual escape

from the L_1 region. Strictly speaking, the station-keeping technique does not maintain a periodic halo orbit, but instead, a Lissajous path that is so close to the nominal halo orbit's dimensions and behaviour that in a practical sense it is equivalent to the nominal halo orbit [18].

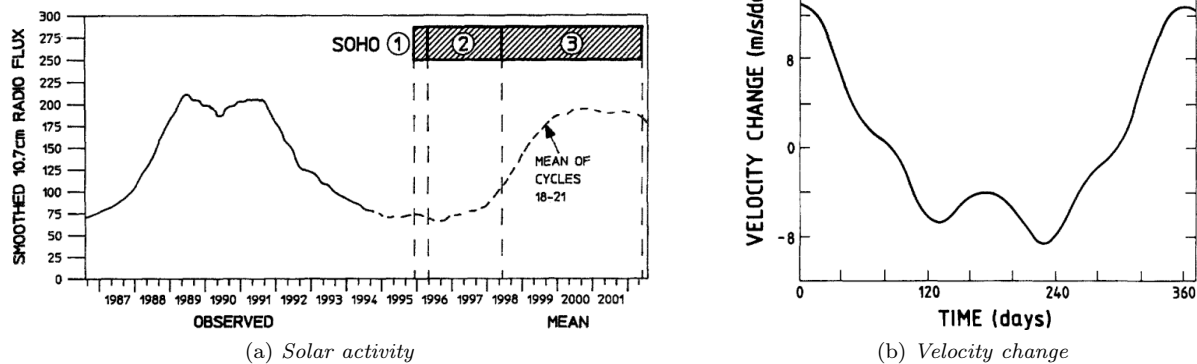
The RLP-frame³ oscillation amplitudes determined in the design phase corresponding to the halo orbit followed by SOHO are: $A_X = 206448\text{ km}$, $A_Y = 666672\text{ km}$ and $A_Z = 120000\text{ km}$. The actual values closely match those previously reported, with this particular selection aimed at minimizing both insertion cost and time spent within the vicinity of the exclusion zone by delineating a large-amplitude orbit, instead of a smaller one.

The halo orbit offers several advantages over the low Earth orbit (LEO) adopted by previous solar observatories [34]:

1. Uninterrupted view of the Sun, which is beneficial for power generation and all the instruments and scientific observation to be carried out.
2. It is permanently outside the magnetosphere: this allows to neglect its influence, and so to obtain an appropriate and more accurate "in-situ" sampling of solar wind and particles.
3. The smooth S/C velocity change in its orbit with respect to the Sun enables to attain accurate helioseismology measurements. In fact, for the halo orbit, the velocity change with respect to time can be highlighted in Fig.5b.
4. It guarantees view of the Earth, enabling almost continuous communication with the ground stations. This is due to the fact that L_1 orbits around the Sun every 12 months as it is coupled with the motion of the Earth.

For SOHO, halo orbit is preferred over orbiting around L_1 point for two reasons: the unstable orbit at the L_1 point and facility of communication in a halo orbit. If SOHO was sitting directly at the L_1 point, it would always be right in front of the Sun. The trouble is that the Sun is very noisy at radio wavelengths, which would make it very difficult to tune into the radio telemetry from the spacecraft. By placing it into a halo orbit, we can place it so that it is always a few degrees away from the Sun, making radio reception, thus, communication much easier [33]. The privileged position of the L_1 point, at 0.01 AU from Earth, allows also a fast exchange of information in reception and transmission. Moreover, the SOHO orbit offers an extremely stable thermal environment [1].

The amount of fuel needed for halo orbit station-keeping for SOHO satellite is just over 2 m/s per year with manoeuvres performed four times a year [18]. This small amount of necessary fuel makes it possible to extend the mission, thus increasing the amount of data coming from the attainment of mission goals for a more precise analysis.



³The RLP (Rocket, Linearized, Perturbed) frame is a coordinate system used in orbital mechanics to simplify the equations of motion for spacecraft undergoing orbital manoeuvres. It's a rotating reference frame where the x-axis points along the direction of the velocity vector, the z-axis is perpendicular to the orbital plane, and the y-axis completes the right-handed coordinate system.

2 Mission Analysis and Propulsion Subsystem

2.1 Mission Analysis

2.1.1 Mission trajectory design understanding

The correlation between trajectory design and functionalities/phases has already been developed in Section 1.8, so this paragraph aims to analyse the trajectory design of the mission according to the ΔV budget per manoeuvre.

Starting from the launch trajectory design, both possible trajectory solutions for the parking orbit, the short and the long coast, were acceptable since there were no mission constraints that favoured one choice over the other. For this reason, the selection of the mission trajectory design can be made solely considering the transfer and the target orbit. For the transfer trajectory, the SOHO mission designers considered various options: the three-impulse, the lunar swingby-assisted and the direct transfer. From cost analysis the direct transfer was by far the most convenient one, so it was selected for this mission, while the others were taken into account only as recovery plans [52]. Moreover, to achieve even smaller ΔV costs, the transfer was designed in order to target an orbit around L_1 point instead of the point itself. This is one of the reasons why the Class-2 halo orbit was chosen as the target: not only it is a quasi-periodic orbit around L_1 point but it is also a large-amplitude orbit, whose injection ΔV is smaller with respect to the one of standard periodic halo orbits.

2.1.2 Mission costs reverse sizing

The reverse sizing of the mission will be carried out by performing preliminary analytical simulation according to the design of a heliocentric Hohmann transfer between Earth and L_1 . The first impulse of the Hohmann transfer is related to the launcher, thus it is neglected in the present analysis, while the second one models the HOI. For the SOHO transfer, the Hohmann model is reasonable to be exploited since the following observations hold:

- both the planet and the lagrangian point orbit around the main attracting body, the Sun, describing trajectories characterized by low eccentricity. Therefore, they can be approximated as circular at first instance;
- since the libration point L_1 is in between the Sun-Earth line, it is on the same ecliptic plane of the Earth. Thus, the orbits related to Earth and L_1 can be well approximated as co-planar;
- as an elementary approximation it can be said that the SOHO motion is mainly led by the Sun's gravitational field, the Earth-Moon gravitational field, and other disturbances, such as SRP can be neglected.

In the following paragraphs, the real mission and its model are simultaneously deepened.

2.1.2.1 Launch and injection into transfer orbit

To reach an L_1 halo orbit, the transfer trajectory from Earth must have a characteristic velocity of $C_3 \sim -0.7 \text{ km}^2/\text{s}^2$, and be directed approximately sunward [52]. This value is similar to the escape energy from Earth's gravitational field, which is a reasonable choice since the required orbiting point L_1 has small Earth gravitational field influences. The launcher Atlas IIAS with a Centaur upper stage was used to achieve the required characteristic energy. In the real transfer, the launcher was firstly injected into a near-circular parking orbit, and then, after a brief coasting period, the Centaur upper stage supplied the 3193.9 m/s burn for the TTI injection, placing SOHO on a direct transfer trajectory to L_1 [34].

2.1.2.2 Correction manoeuvres

Correction manoeuvres must be taken into account for execution errors and tracking uncertainties. It is quite obvious that the simplistic Hohmann transfer is not capable of including correction manoeuvres, therefore they cannot be modelled but their uncertainties are included in the margins of the other impulses.

In the real transfer, the first mid-course correction (MCC1) was designed to be divided into two impulses, namely X-1 and X-2 segments, to provide an initial assessment of the thruster performance due to their first use. The impulses had a magnitude of 3.04 m/s and 1.878 m/s , respectively. The second midcourse correction (MCC2) would be performed, if needed, to correct errors from MCC1. Because of additional anomalies, the MCC2 logic changed to reduce the total cost. Actually, from a simple error correction, the manoeuvre became an orbit-shaping one given in the x-z plane. This was chosen to reduce the sum of the total impulse to be provided to arrive at the final orbit, thus considering HOI also. The resulting impulses values were 15.7 m/s (Z-1 segment), 10.0 m/s (Z-2 segment) and 6 m/s (X-1 segment). The manoeuvre along the z-direction was split up as previously mentioned for MCC1. The total impulse for the MCC2 is 31.7 m/s .

2.1.2.3 Halo Orbit Insertion

In the Hohmann model developed for this reverse sizing, the halo orbit insertion corresponds to the second impulse. This has a magnitude of 75.12 m/s and it is performed 181 days after the first impulse.

The real HOI manoeuvre was performed on the first useful date, which was 14^{th} February 1996, 106 days after the launch. This choice was made since it corresponded to the lowest cost possible of 14 m/s .

2.1.2.4 Stationkeeping

Libration point orbits (LPOs), whether halo or Lissajous, are inherently unstable and must be maintained via occasional propulsive manoeuvres, as it has been done for the SOHO mission since its arrival to the nominal operational orbit. These manoeuvres are widely referred to as “stationkeeping” manoeuvres. In absence of the indicated stationkeeping, LPO perturbations lead to exponential decay away from the libration point region. However, being in an invariant manifold, the associated costs of stationkeeping are small and recurring with low frequency. In particular, the amount of time allowed to elapse between SK burns depends on the particular mission and its requirements, constraints, fuel budget and attitude control. In the considered case, both in model and reality, the constraints were to make the manoeuvres less frequent as possible to allow uninterrupted periods of scientific observation and at the same time to keep ΔV values as low as possible to avoid damaging the scientific instruments.

In order to model the required stationkeeping manoeuvres some assumptions are done:

- only the most relevant perturbation effect, which is the SRP, is taken into account. The estimated magnitude of the acceleration acting on the S/C due to this disturbance evaluated in L_1 is: $a_{SRP} \sim 8.84 \times 10^{-8} \text{ m/s}^2$;
- in order to simplify the model, the satellite is assumed to be exactly at L_1 point at the beginning of the simulation, where nominal displacement and velocity are null (before introducing perturbations). Then, due to the presence of the acceleration, the S/C will move with a linear accelerated motion along the Earth-Sun line;
- the manoeuvres are performed along the Sun-Earth line: this assumption is not so far from reality since the SK manoeuvres are performed along X_b direction (X in body axes), with the goal of bringing the x-component of the velocity (V_X) in RLP-frame coordinates, to zero;
- the possibility of having manoeuvres with different magnitude occurring at different time intervals is not taken into account.

The result is obtained by imposing a constraint on the maximum admissible ΔV which is set to 0.75 m/s per manoeuvre [42], in order to determine the time interval between two impulses. This leads to a manoeuvre every 98 days, which also respects the requirement of having the manoeuvre less frequent as possible. This result is not so far from reality, in which they were performed with different time intervals, following a roughly fixed 90-day cadence. The model leads to an annual cost of $\Delta V_{SK} \sim 2.80 \text{ m/(s · year)}$, slightly higher with respect to the real annual cost of $\Delta V_{SK} \sim 2.31 \text{ m/(s · year)}$ in the Early Mission years. The real SK design is based on an orbital energy balancing technique which allows to keep SOHO’s orientation unchanged and to optimize velocity components at specific points along the Sun-Earth line, reducing sensitivity to Earth’s orbit eccentricity [37]. The real annual SK manoeuvre cost has gradually decreased in the recent years, making the adopted model less reliable.

2.1.3 ΔV budget breakdown

The following table summarizes the costs analysed in the previous paragraph:

Manoeuvres	Model NM [m/s]	Margins [m/s]	Model WM [m/s]	Real [m/s]
MCC1	-	-	-	4.92
MCC2	-	-	-	31.70
HOI	75.12	10	85.12	14
Total (transfer)	75.12	10	85.12	50.62
SK (per year)	2.80	10	12.80	2.31

Table 4: ΔV budget breakdown. "NM" stands for "no margins"; "WM" stands for "with margins"

The margin applied to the deterministically calculated manoeuvres is 10 m/s , instead of 5% which would be lower than the chosen one. In the simulation, the correction manoeuvres are considered in the margins adopted for the HOI. This is due to their unpredictability at the design phase and to their typical low magnitude. As can be noted, there are discrepancies between the model and the real costs, due to all the hypotheses made when referring to a Hohmann transfer. The most relevant one is considering only the gravity of the Sun. In a deep analysis, this cannot be deemed correct, since SRP and Earth-Moon gravitational disturbances certainly and greatly affect SOHO celestial path. It can be observed that the model tends to oversize the real transfer because it is not capable of considering the beneficial effect for mission costs deriving from the exploitation of manifold dynamics. Other discrepancies are related to the different times spent to complete the transfer: according to the model it can be achieved in almost 181 days, while the real transfer duration is 106 days. So, the model overestimates both the costs and the time of flight but it can be used as a first guess. On the overall, the SK model is suitable for the problem. From literature [41] the final output of the MA is a total budget allocation of $\Delta V = 275 \text{ m/s}$ for further analyses at the subsystem level. This assumption is strongly conservative because SOHO was the second S/C to orbit around L_1 , after ISEE-3 mission, that shared almost the same final orbit. Similarly to the latter mission, SOHO had the luxury of a large supply of fuel, to allow for uncertainties in the insertion and maintenance of the new orbit [40].

2.2 Propulsion Subsystem

2.2.1 Propulsion subsystem architecture and design

The selection of SOHO's propulsion subsystem architecture is a direct response to fulfill the mission's requirements and to address its drivers.

Entering the analysis, generally, there are two types of onboard propulsion systems: primary and secondary.

Primary propulsion systems are dedicated to the execution of major manoeuvres such as orbit transfers and trajectory corrections, that often involve significant ΔV s and require a relatively high level of thrust. On the other hand, secondary propulsion systems, also known as attitude control or stationkeeping propulsion, are used mainly for the spacecraft's attitude control, to perform TCMs⁴ and for maintaining its orbit.

In the case of the SOHO mission, the adopted architecture is a low-thrust monopropellant blowdown system, whose choice is driven by several factors and considerations. Firstly, the manoeuvres involved in the mission are of relatively low magnitude (in the order of m/s as described in Section 2.1.3), and therefore do not necessitate the capabilities of a primary propulsion system, but rather a low thrust secondary system is chosen. This is, in fact, able to fulfill the required ΔV budget throughout the whole mission, starting from launcher detachment. Additionally, the choice of a bi-propellant architecture instead of a monopropellant one, despite the potential for higher thrust, would introduce increased complexity and cost to the spacecraft design. Moreover, it could pose a higher risk of contamination to the sensitive scientific instruments onboard, whose cleanliness is of primary concern.

The final design incorporates sixteen thrusters, divided into primary (A) and redundant branches (B), strategically positioned around the spacecraft to provide both the necessary ΔV and roll, yaw, and pitch control [42]. The details about the chosen configuration are further analysed in the Subsection 2.2.2.4.

In particular, the correlation of the thrusters with the manoeuvres is shown in Table 5:

Manoeuvre	Segment	Thruster Pair
MCC1	X-1	1A,2A
	X-2	1A,2A
MCC2	Z-1	7A,8A
	Z-2	7A,8A
	X-1	1A,2A
HOI	X-1	1A,2A

Table 5: SOHO thrusters and manoeuvres correlation

2.2.2 Propulsion subsystem reverse sizing

The aim of the following paragraph is to explain the procedure utilized for the sizing of the propulsion subsystem. The propellant used by SOHO monopropellant engines is hydrazine. The choice of this propellant is correlated to several advantages that make it one of most used in space application:

- for spacecraft that contain optical instrument (i.g. telescopes, star tracker or IR radiation seekers) such as SOHO, the exhaust plume must be free of possible contaminants that may deposit or condense on optical surfaces, and monopropellant hydrazine reaction gases satisfy this requirement;
- proven reliability: hydrazine-based propulsion systems can be throttled, allowing precise control of thrust levels useful for orbit adjustment and attitude control;
- storability: it has a relative stability under normal storage conditions.

The propulsive subsystem is composed of a single blowdown tank of hydrazine and helium, which is used as pressuring gas. Indeed, the gases typically used for this purpose are helium and nitrogen, but since He is lighter than N_2 , it has been chosen in order to save weight despite its higher tendency towards leakage.

2.2.2.1 Sizing

For computing the sizing of the subsystem, the following data regarding the mission are kept from literature [1] [39] [42]:

Data	Value [kg]
Total mass at launch	1863.7
Dry mass	1612.7
MRE-1.0 monopropellant mass	0.5

Table 6: Mass Data

Pressure	Value [MPa]
Initial pressure of pressurizer	22
Final pressure of pressurizer	10

Table 7: Pressure Data

⁴Trajectory Control Manoeuvres (mm/s or cm/s): they are performed just to tune a long way trajectory to get to the final target

Starting the sizing with the tank, it is known from the literature that it has a prolate spheroidal shape [44]. It is housed in the Service Module (SVM) upper panel, aligned with the principal axis of the spacecraft and with the centre of mass on it. This positioning avoids the large change in the principal inertia matrix during the consumption of the fuel and it also avoids the generation of external disturbance torques due to the sloshing of the propellant. Furthermore, the tank position is exploited to defend the electronics from radiation and to keep warm the hydrazine at the same time.

The tank is made out of titanium alloy *TI-6Al-4V* (the most common Ti alloy used for in-space applications) with the following characteristics: $\rho = 4430 \text{ kg/m}^3$ and $\sigma_{ultimate} = 950 \text{ MPa}$. The choice of this material is due to its properties: firstly its compatibility with the hydrazine which is an extremely corrosive liquid especially with other metal such as aluminum and steel; then for its resistance to high temperatures without significant deformation or loss of mechanical properties and also for its high strength-to-weight ratio that allows for the design of lightweight tanks.

The specific impulse of the MRE-1.0 monopropellant thrusters used during the mission can be taken from the datasheet [39] and it amounts to $I_{sp} = 220\text{ s}$.

From literature [41], the total velocity budget amounts to $\Delta V = 275 \text{ m/s}$, which was allocated during the design phase. Comparing it with the real costs of the mission (Subsection 2.1.3), it could be pointed out that the budget under consideration is conservative. This reflects the results of a risk analysis, which identifies the direct transfer as the optimal choice, but that could quickly escalate in cost due to potentially misleading occurrences. Those occurrences might be injection errors, and capabilities and limitations of both the spacecraft and ground support, particularly regarding the promptness of initiating emergency manoeuvres [52].

The sizing starts from the computation of the mass of propellant using the Tsiolkovsky equation:

$$\Delta V = I_{sp} g_0 \ln \left(\frac{m_0}{m_f} \right)$$

Using the constant value of $g_0 = 9.81 \text{ m/s}^2$, the final mass (m_f) can be determined from the dry mass of the spacecraft (in Table.6), adding a 20% margin in order to express the difference between the nominal and real values (R-M1-1 [49]). Then, the propellant mass is computed as the difference between the initial (m_0) and the final mass. The operating pressure of the engine is provided by a pressurization blowdown system, as it will be analysed in Subsection 2.2.2.3. As mentioned in Table 7, the range of pressure is between 22 MPa and 10 MPa. In order to size the system some margins shall be added to the propellant mass:

- 3% taking account of the ullage;
 - 2% for propellant residuals that could remain in the tank (MAR-MAS-080);
 - 0.5% for the loading uncertainties.

In this way, the total hydrazine mass amounts to 277.5 kg. Following with the sizing, in order to take into account the unusable volume, a 10% margin must be added to the volume of fuel, giving a result of 295.7 L. Then, the initial volume of pressurizing gas can be computed knowing the blowdown ratio⁵ $B = 2.2$ using the expression below:

$$V_{gas,i} = \frac{V_{prop}}{\beta - 1}$$

Exploiting the perfect gas law, the mass of helium is determined, adding a 20% margin:

$$m_{press} = \frac{P_{tank} V_{gas,i}}{R T_{tank}}$$

The tank volume is then calculated as:

$$V_{tank} = V_{gas,i} + V_{prop}$$

A margin of 1% shall be added to the result in order to account for the bladder volume.

The scheme below graphically represents the steps taken so far:

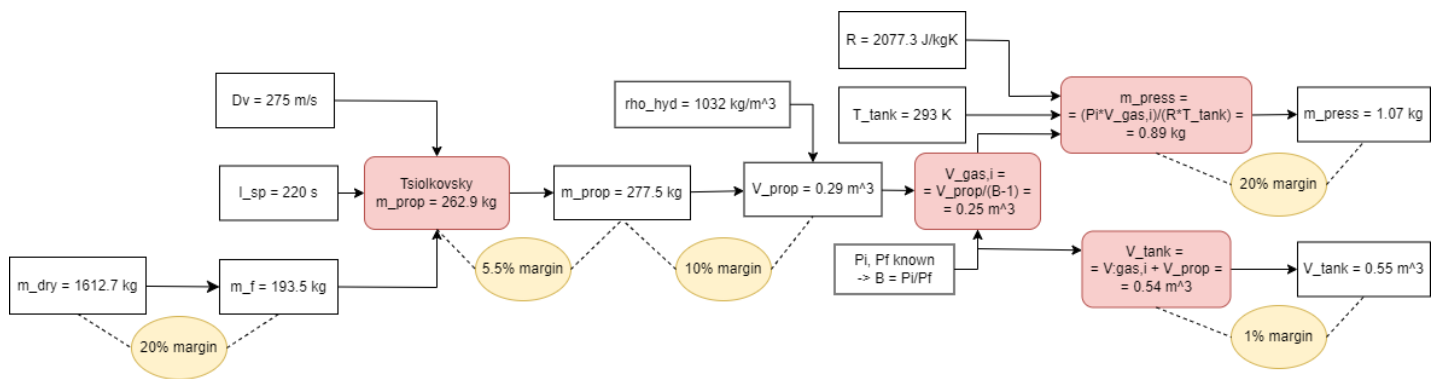


Figure 5: Sizing methodology

⁵Having a low value of B can give a more homogeneous thrust and pressure decay but, at the same time, it causes a reduction in the volume of fuel

The COTS tank used has a prolate spheroid, as mentioned before, but it can be approximated to a sphere. With such approximation, the radius and the thickness can be evaluated as:

$$r_{tank} = \left(\frac{3}{4} \frac{V_{tank}}{\pi} \right)^{\frac{1}{3}} = 0.51 \text{ m} \quad t_{tank} = \frac{P_{tank} r_{tank}}{2\sigma} = 0.6 \text{ mm}$$

From here, the mass of the tank can be computed as:

$$m_{tank} = \frac{4}{3} \rho \pi [(r_{tank} + t_{tank})^3 - r_{tank}^3]$$

Finally, the total mass of the propulsive subsystem is calculated as:

$$m_{PS} = m_{tank} + m_{press} + m_{thrusters}$$

Where $m_{thrusters} = 16 \cdot m_{thruster}$.

A further 10% margin is added to take into account cables, so the mass of the feeding system results to be 1.75 kg.

	Mass [kg]
m_{tank}	8.44
m_{press}	1.07
$m_{thrusters}$	8.00
m_{cables}	1.75
m_{PS}	19.26

Table 8: Masses of the propulsive subsystem components

The final mass of the subsystem is 19.26 kg, as it can be seen from the Table 8.

It is then necessary to verify, through the following inequality, the actual feasibility of the mission by making sure that the launcher is indeed capable of delivering the spacecraft to the desired position.

$$m_{dry} + m_{prop} + LVA + margins < LM$$

The LVA is deduced through the linear regression in Figure 6, obtaining a value of 190.9 kg, having a supported mass of 1863.7 kg. It is now possible to compute the sum of dry mass, propellant mass and LVA (with margins) which amounts to 2081.1 kg, margins included.

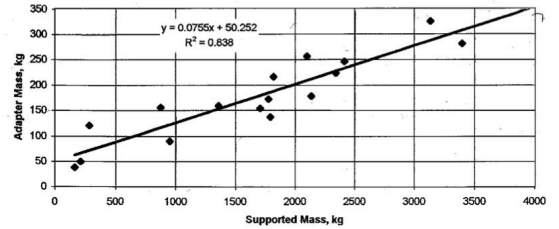


Figure 6: Sizing methodology

It is then known from the literature that the Atlas IIAS launcher is capable of delivering up to 8610 kg to low Earth orbit [48], which indeed satisfies the inequality and confirms the correct choice of the launcher.

The Table 38 summarizes the percentage of the propulsion unit and the payload with respect to the dry mass.

	% of m_{dry}
m_{PS}	1.19
$m_{P/L}$	40.62

Table 9: Masses expressed as a percentage of m_{dry}

2.2.2.2 Comparison with real data

In this section a comparison between computed and real data is reported.

	Computed NM	Margins		Computed WM	Real
Tank mass [kg]	8.44	-	-	8.44	34.50
Mass of pressurant [kg]	0.89	20%	0.18 kg	1.07	-
Mass of propellant [kg]	262.99	5.5%	14.46 kg	277.50	250
Tank volume [L]	542.20	1%	5.40 L	547.60	461.60
Tank radius [m]	0.51	-	-	0.51	1.02 x 0.81
Tank wall thickness [mm]	0.60	-	-	0.60	-

Table 10: Summary of estimated vs real data."NM" stands for "no margins"; "WM" stands for "with margins" ⁶

As it can be seen from the results in Table 10, the mass of the tank results being quite smaller than the real one. This difference originates first of all from the fact that the tank actually selected for the mission is an off-the-shelf component with a fixed shape and mass. Furthermore, the differences in the design process might also add to this gap, since the mass of the tank depends on both the radius and the thickness which have been calculated using a simplified spherical tank model.

2.2.2.3 Feeding strategy selection

The feeding strategy selected for moving the hydrazine from the tank to the thrust chambers consists in a blowdown feed system. The ullage gas, that is helium in the present case, is stored in the same tank of the liquid propellant and it is separated from it by an elastomeric diaphragm. The expansion of the ullage pushes the hydrazine out towards the thrusters. A blowdown system was preferred to a regulated pressure one for this mission for several reasons: firstly, it can be pressurized at different levels if necessary [43], allowing to have different thrust values during the operational life; secondly, it avoids the need of additional gas pressurant vessels thereby reducing mass, volume and propulsion systems complexity; thirdly, it is less expensive since it only needs few components.

The architecture of the blowdown system has been illustrated in the Fig. 7 and consists of:

- Fill/vent valve (FVV) and fill/drain valve (FDV) which are used for filling, venting or draining the propellant, when needed;
- Tank containing the liquid propellant and the pressurized inert gas;
- Propellant Control Module (PCM) which includes latch valves for activating and de-activating the thrusters and a pressure transducers to measure the pressure and convert it into an electric signal.

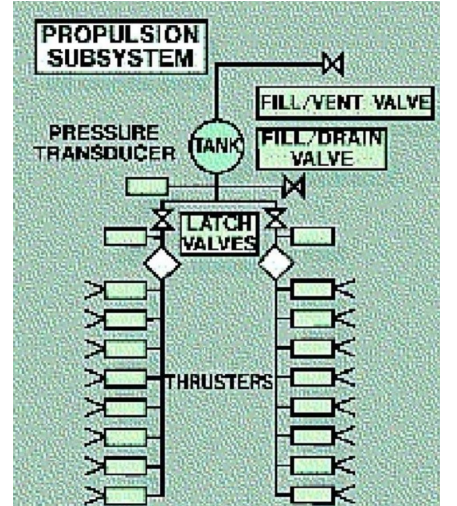


Figure 7: SOHO Propulsion Schematic [6]

⁶Recalling that the tank has a prolate spheroidal shape, here the semi-major axes are reported

2.2.2.4 Thrusters configuration design

SOHO is equipped with sixteen 4.4 N MRE-1.0 monopropellant hydrazine thrusters [39] organized into two branches, with eight thrusters in each. The primary branch, known as the A-branch, is employed for regular operations, while the redundant B-branch is activated during the autonomous fail-safe mode. This dual-branch configuration ensured redundancy and reliability in propulsion and control systems, enhancing the overall robustness of the mission architecture. The configuration adopted is described in Table 16, in which the roles of each thruster pair regarding ΔV and attitude control are also highlighted:

Thruster Pair	Thruster Locations	ΔV Direction (body frame)	Primary Attitude Control
1 and 2 (1 is canted 30° down and 2 is 30° up)	Fore (Sunward $+X_b$)	$-X_b$	Pitch
3 and 4	Aft (Earthward $-X_b$)	$+X_b$	Yaw
5 and 6	Top ($+Z_b$)	$-Z_b$	Roll
7 and 8	Bottom ($-Z_b$)	$+Z_b$	Roll

Table 11: SOHO thrusters (applies to both A and B branches) [41]

Figure 8 illustrates the adopted thrusters layout, detailing their arrangement and orientation, while Figure 9 clarifies the spacecraft's body axes direction relative to Earth and Sun.

The *rationale* behind the chosen configuration for SOHO thrusters is driven by multiple factors, including the cleanliness mission driver, manoeuvres needed for operational tasks and effective attitude control along the three axes to fulfill the pointing performance mission driver.

Considering firstly the mission cleanliness driver, this needs careful thruster positioning to minimize the impact of thruster plumes on sensitive equipment. In particular, thrusters 1 and 2, which are dedicated to negative x-axis thrust, are canted 30° out to minimize plume impingement on the payload module, since $+X_b$ direction is that along which the instrument bore-sights are intended to point at the Sun [34]. This is particularly relevant for maintaining the integrity of scientific observations and data collection onboard [2].

Additionally, the performed manoeuvres are designed so that they consist of two main components: those along the Earth-Sun line and those perpendicular to it, corresponding to the x-axis and z-axis manoeuvres, respectively. For this reason, thrusters are aligned along X_b and Z_b directions, so that all nominal thrust components are in the XZ plane.

Furthermore, effective attitude control on all three axes is essential for spacecraft operational stability. This configuration ensures that thrusters are capable of performing three-axis attitude control so that SOHO can maintain its desired orientation in space, enabling scientific observations and fulfilling mission scientific objectives.

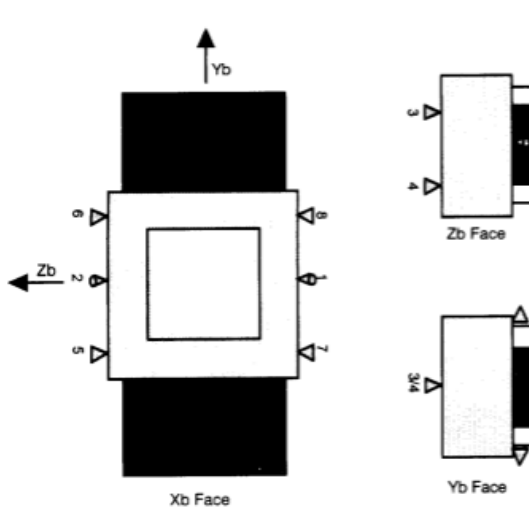


Figure 8: SOHO thruster configuration

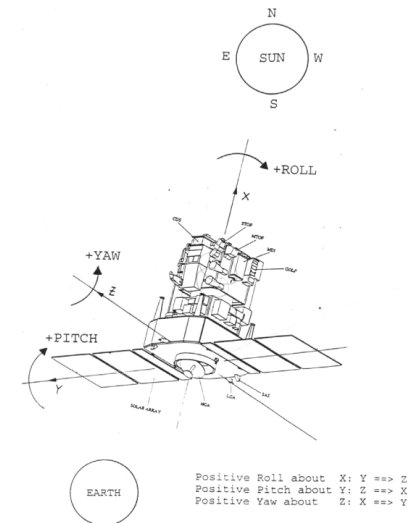


Figure 9: SOHO Spacecraft

3 TMTTC Subsystem

3.1 TMTTC Subsystem Architecture

3.1.1 Space Segment

In this section, the architecture of SOHO and its components will be analysed. The links between the spacecraft and the ground are direct, which means without conveying the transmitted data through other satellites. The ground-to-satellite and satellite-to-ground connection will be provided by an S-band RF system, whose frequencies are 2245 and 2067 MHz for downlink and uplink, respectively.

The TMTTC on-board architecture of SOHO mission includes the following components: antennas, RFDU, amplifier and transponder. The overall architecture, without considering the doubling of hardware and lines for redundancy, can be depicted as follows:

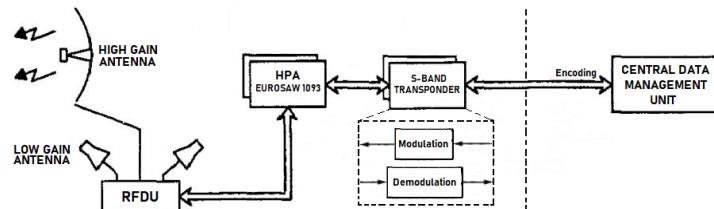


Figure 10: Elementary scheme of SOHO TMTTC architecture

Based on this architecture, two transmission paths are possible [48]:

- **transmission (downlink):** the TMTTC subsystem processes two digital bit streams. One originates from either stored data or real-time from the payload, while the other is sourced from command and data handling, containing telemetry data regarding health and status. These two data streams undergo modulation onto subcarriers, which are subsequently modulated onto the carrier output. The resulting composite signal is then amplified and routed through the RFDU, so through the 2P2T switch and the diplexer, activating the appropriate antenna for transmission;
- **reception (uplink):** the modulated signal is received by the subsystem via the antennas. Subsequently, the signal passes through the RFDU, which determines the appropriate antenna for signal reception, and then is amplified. After being demodulated, the digital command bit stream is forwarded to the command and data handling subsystem.

The encoding/decoding is performed in the Central Data Management Unit (CDMU), which belongs to the On-Board Data Handling (OBDH) subsystem. The algorithm chosen is the Reed-Solomon (R-S) code for the uplink. The downlink data are both R-S (interleaved to a depth of five) and convolutional encoded. The **antennas** present in the SOHO TMTTC architecture are one high-gain antenna (HGA) and two low-gain antennas (LGAs). The following image clarifies the configuration of the antennas in the spacecraft geometry [2].

The HGA is integrated into the spacecraft's central tube and it points directly at the Earth, being placed along $-X_b$ direction in body frame⁷, as it can be seen in Fig.11. The LGAs are mounted on fixed booms at the bottom section of the service module and protrude from the main body along $\pm Z_b$ sides of the S/C to provide full geometrical coverage. For high-rate scientific data, RF coverage is provided by a pointable HGA. Practically, the HGA operates in S-band, right or left-handed circular polarization for both uplink and downlink. Two LGAs ensure omni coverage, usable only with low-rate telemetry. Each LGA operates in S-band right-handed circular polarization at both uplink and downlink. The antenna pattern is quasi-rotationally symmetric and quasi-isotropic in the region of elevation between 0° and 108.5° (LGA reference axis). In the end, full RF coverage is provided by the total three antennas selected for this mission.

From a structural point of view, the HGA is a S-band shallow reflector antenna of 804 mm diameter, with an associated mechanism. It comprises a carbon fibre reflector, an aluminium feed cone with a crossed dipole feed and a reflective disk on top. Instead, the two LGAs are quadrifilar short resonant helix mounted on a short skirt [2].

An S-band **RFDU** is necessary to connect the three spacecraft antennae with receivers and with the S-band transmitters, guaranteeing a high degree of flexibility and redundancy. Inside the RFDU there are diplexers and double-pole double-throw (2P2T) RF switch. The first separates the incoming signal into different frequency bands, allowing the transponders to simultaneously handle signals in multiple frequencies, such as those used for uplink and downlink communication. Diplexers also help isolate the transmitter (or receiver) from the receiver (transmitter) port at its centre frequency, so the transmitter (receiver) does not lock, jam, or damage the receiver (transmitter). Instead, the 2P2T switch selects the antenna, HGA

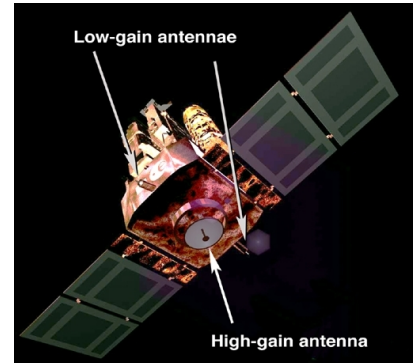


Figure 11: HGA and LGAs configuration

⁷The body frame, as already pointed out in other assignments, is $\{X_b, Y_b, Z_b\}$, where X_b is the Sunward direction, Z_b is the S/C top direction and Y_b is orthogonal to them.

or LGAs, and the mode of the system, reception or transmission. The **High Power Amplifier** (HPA) chosen for this mission is EUROSAY 1093 [2], a Solid-State Amplifier (SSA). This choice is compliant with the power output required by the system, which is about 10 W in high power mode and 3.2 W in low power mode. SSAs tend to be more reliable, lighter and smaller. For redundancy reasons, two amplifiers are inserted into the system.

The TTMTTC includes two redundant **transponders**, each consisting of a receiver, which receives commands and ranging signals, a modulator, and a S-band transmitter, which produce the radio frequencies needed for transmission or telemetry and ranging signals to the Earth.

3.1.2 Ground Segment

Tracking/ranging functions, telemetry data transmission to ground and routine telecommanding for SOHO are provided by NASA's Deep Space Network (DSN). This consists of three facilities located around the world, at approximately 120° apart in longitude, where each of these sites has at least one antenna capable of communicating in S-band. These sites are at Goldstone, California; near Madrid, Spain; and near Canberra, Australia. DSN antennas range in size from 26 to 70 metres and the strategic placement of its sites permits constant communication with spacecraft as our planet rotates: before a distant spacecraft sinks below the horizon at one DSN site, another site can pick up the signal and carry on communicating [50]. JPL (located in Pasadena, CA) provides DSN interface coordination, central communications, scheduling, and facilities management. As it can be seen in Fig.12, the experiment PI representatives at SOHO Experiment Operations Facility (EOF), located at NASA's Goddard Space Flight Center (GSFC), receive real-time and playback flight telemetry data, process these data to determine instrument commands and send commands to their instruments, both in near real-time and on a delayed execution basis.

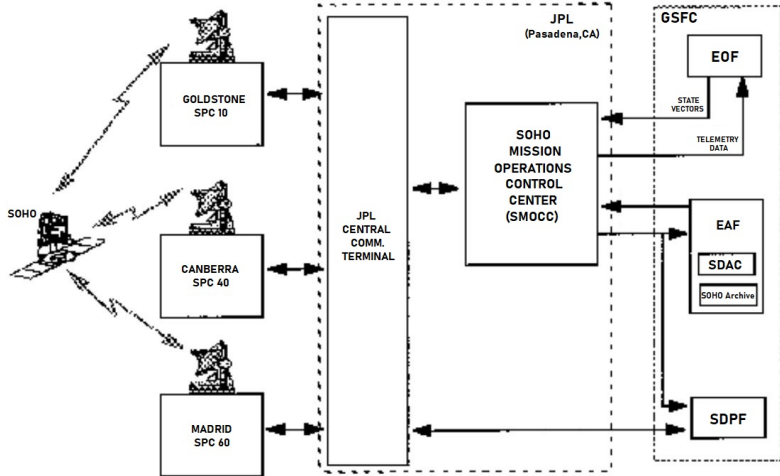


Figure 12: The SOHO Ground Data System (GDS)

There are connections from the EOF to external facilities to allow transfer of incoming data from GSFC support elements, remote investigator institutes, other solar observatories, and ESA facilities. EOF interacts also with the SOHO Mission Operations Control Center (SMOCC) and other required elements at GSFC for scheduling and commanding the SOHO flight experiments. The Experiment Analysis Facility (EAF) is the focal point for science and data analysis and it includes the Solar Data Analysis Center (SDAC) and the SOHO Archive. The Sensor Data Processing Facility (SDPF) provides the functions necessary for data capture, intermediate data processing, and the creation, compilation, and mailing of distributed data [7] [2].

3.2 TMTTC design and justification

The TMTTC subsystem is critical for carrying out spacecraft operations effectively, therefore, it shall be thoroughly designed in order to ensure continuous operation even in case of system failure. In this paragraph, the main TMTTC design choices are highlighted and justified. As an RF system, the S-band circular polarization was selected, as mentioned in Section 3.1.1. This choice is due to the S-band efficiency as a conduit for supplying vital real-time data and for high resilience to environmental interference. Also, all the antennas on board operate in circular polarization since they are expected to be used during spinning spacecraft attitude modes. In particular, the chosen architecture includes two LGAs and one HGA as highlighted in Section 3.1.1. The presence of almost omnidirectional antennas (LGAs) is of vital importance for the mission, in particular regarding the first phases, where a low telemetry rate is required, and for the safe mode. Under such circumstances, precise pointing capabilities may be unavailable, making the HGA unusable, necessitating the ability to maintain traceability regardless of the spacecraft's attitude conditions. These aspects will be deepened in Subsection 3.2.1. Moreover, the two LGAs are positioned in opposite directions to obtain total coverage around the spacecraft. This is also the reason why they protrude from the main body. Instead, a single HGA was utilized for high data rate communication. The choice of a single HGA was driven by the substantial dimensions and complexity inherent in this component. A parabolic reflector was selected for this antenna type due to its lightweight structure and its ability to provide high gain and directivity. In fact, unlike isotropic antennas that disperse power uniformly in all directions, a parabolic reflector concentrates power in a specific direction, enhancing the efficiency of communication. The HGA is mated into the aft part of the central cylinder [9] of the spacecraft, oriented in the $-X_b$ direction. This placement serves two main purposes: firstly, it satisfies the Earth-pointing requirement, and secondly, it ensures the antenna is positioned in a shadowed area, minimizing potential interference. Additionally, the HGA is gimbaled to allow a maximum deviation of 32° from the anti-Sun direction. This adjustment is essential for avoiding S-band radio interference from the Sun during downlink transmissions. Furthermore, the HGA's two degrees of freedom, guaranteed by the presence of a mechanism, enable precise pointing towards both Earth and DSN, irrespective of the highly elliptical orbit traced by the spacecraft around the L_1 point [51].

3.2.1 Correlation with operation/phases/modes

The *rationale* behind the choice of the TMTC subsystem architecture is driven by the need of allowing communication throughout all the phases (starting from launcher detachment) and modes included in the mission. It is also important to consider the three different telemetry rates achievable by SOHO which are: *Low rate*, 1.3 kbps only due to HK; *Medium rate*, 55 kbps splitted into 5% HK and 95% Science; *High rate*, 246 kbs with 1% needed for HK, 20% for Science and 79% for MDI [1]. Starting with the phases, already analysed in Section 1.5, it is possible to highlight the antennas main functions and operations [7]:

- **Launch and Early Orbit Phase (LEOP)**: during this phase, where SOHO is still attached to the launch vehicle, no communication with the ground is foreseen. During launch the HGA is rigidly attached to the spacecraft.
- **Transfer Trajectory Phase (TTP)** : following the separation from the Centaur upper stage, the spacecraft enters the *LR subphase*. During this phase, both low-gain antennas are utilized exclusively for low data rate transmission. This ensures the initial Acquisition of Signal (AOS) and enables the first low telemetry downlink. Approximately 7 hours post-separation, the *HR Subphase* begins. In this phase, the high gain antenna is deployed, facilitating both uplink reception and medium to high telemetry downlinking for the duration of the Transfer Trajectory Phase (TTP) and the entirety of the mission. After the first three days of continuous contact normal operations contact sequence begins, as will be described in the Halo Orbit Phase.
- **Halo Orbit Phase (HOP)**: the normal operation contact sequence entails three daily passes of 1.6 hours each and one 8-hour pass over 10 months per year, with continuous contact with the DSN for helioseismology data return during the remaining 2 months. Specifically, the 8-hour period is dedicated to real-time communication with the DSN, three periods of 3.73 hours each to on-board recording without ground communication, and three periods of 1.6 hours each to real-time communication to dump previously recorded data to the DSN. This communication time window is dictated mainly by the observing programs of the MDI which is the most demanding instrument with a high data rate stream, which is transmitted only during long passes ("campaign program"). The "dynamic program" operates for 2 months with high-rate telemetry, conducting campaigns that cannot be completed within an 8-hour timeframe. These contacts are sufficient for complete recorder-play-back data capture and to meet all telemetry, ranging and command requirements. During the operational phase, any combination of the ranging, telemetry, and telecommanding links will nominally be available. In this phase, during normal operations, continuous tracking of the Earth is not necessary to transmit the HGA RF signal with the requested RF gain but a certain depointing is acceptable. Therefore, it is only necessary to realign the HGA three times every 24 hours [2].

Regarding, instead, the correlation with the modes of the mission [63]:

- **Normal Mode (NM)** : in the context of normal operations full knowledge of SOHO orientation can be acquired. Thanks to that, the HGA can be steered to point at the Earth providing a high rate downlink of telemetry using 26-meter ground stations.
- **Emergency Sun Reacquisition Mode (ESR)** : as with most space crafts, SOHO occasionally experiences interruptions to normal operations, with the S/C going into a safe mode in order to preserve it from being harmed or lost. This mode can be defined as the "*ultimate safety net*" for SOHO. In this situation, the HGA cannot be used since the S/C is not capable of pointing at the Earth properly. Instead, almost omnidirectional LGAs are used to transmit vital information to ground controllers. With 26-meter ground stations only LR telemetry can be transmitted through LGAs furnishing only the bare minimum information about health and condition of the S/C and instruments. On 34- meter ground stations the MR telemetry can be downlinked through the LGA allowing science data transmission, which cannot happen in LR. With 70-meter stations even High Rate telemetry can be achieved.
- **Coarse Roll Pointing Mode (CRP)**: this is the first step "up" from ESR and in this mode SOHO can be commanded to point correctly at the Sun and it is stable enough to guarantee absolute roll determination. In this case, the HGA can be oriented towards Earth, guaranteeing a high rate downlink.
- **Roll Manoeuvre Wheels Mode (RMW)**: it is the intermediate mode between CRP and NM, where SOHO has full knowledge of its attitude and control of its orientations but with more relaxed steering laws. This is used for thruster manoeuvres such as stationkeeping (SK) and momentum management (MM). Also in this case communication is guaranteed in high rate downlink through the HGA which can be correctly pointed at the Earth.

3.3 Reverse Sizing

When discussing the TMTC reverse sizing, both the downlink and uplink phases are taken into account. The workflow is fully deepened for the downlink, while for the uplink only the results are shown in Section 3.3.5.

3.3.1 Contact Window and Data Volume

The choice of using three facilities equidistant from each other around the world, at approximately 120° apart in longitude, guarantees that the signal will be received, being the Earth always in the transmitter's field of view. Regarding the uplink, the contact window is simply related to the amount of time it takes to transmit the necessary command data. In terms

of downlink, the critical situation corresponds to the transmission of the full data volume of 467 GB over 12 months. The computation was performed considering that for 10 months a year at high rate during long passes and medium rate during short ones. For the remaining two months the data transmission is continuous at high rate.

3.3.2 Frequency, data rate and band selection

For the sizing, the worst case scenario in terms of data rate shall be considered: for the HGA this condition corresponds to the NM operation during the "dynamic program" paired with the 26 m GS antenna, while for the LGAs the worst case scenario is obtained during the ESR considering the 70 m GS antenna, since in this case antennas with a lower diameter for high rate telemetry would not be sufficient. For both HGA and LGAs, the worst case assumes high-rate telemetry. With this in mind, the nominal data rate can be computed as the sum of the telemetry (TM) and the science data (SD) ones. Due to that, the total rate can be expressed as $R = TM + SD = 246$ kbps for both the HGA and the LGAs. SOHO uses only one frequency for telecommunications: 2.245 GHz (S-band). This choice is mainly related to the fact that the band is not excessively affected by atmospheric losses. The disadvantages with this type of frequency band are: firstly, the size of the antenna that is larger compared to the one that can be obtained using the X-band (common band frequency used in space applications) and secondly for the longer time needed to download the data. Also, the uplink communication is designed in S-band since it requires less transmission power.

3.3.3 Encoding and modulation of the signal

The encoding process stands for protecting data from transmission errors by increasing the size of the signal. As it has already been said in Subsection 3.1.1, SOHO uses for the downlink both R-S (255.233) encoding and convolution one. Since the two encoding strategies are not simultaneous, the sizing is chosen to be done considering the worst condition in terms of energy per bit to noise ratio (E_b/N_0), having so a R-S encoding. Due to this choice, the encoding coefficient is selected to be $\alpha_{enc} = 1.14$. From a graphical estimation, a minimum value of $(E_b/N_0)_{min}$ can be defined in order to guarantee the capability of the subsystem of successfully transmitting and translating the signal: considering a value BER equal to 10^{-5} (typical for downlink) the relative $(E_b/N_0)_{min}$ is 5.2 dB.

PCM/PM and, in particular QPSK, is selected to be used by SOHO, as the spacecraft can be catalogued as Medium Data Rate (200 ks/s - 2 Ms/s), as it can be seen in literature [53], with a modulation coefficient of $\alpha_{mod} = 2$.

3.3.4 Link budget

The link budget preliminary sizing starts from the knowledge of the available power given by the amplifier and the signal frequency. The output power of the amplifier is $P_{out} = 10$ W [1]. In the SOHO architecture two Solid State Amplifiers (SSA) [57] are used. These are preferred for power outputs up to 10 W (except at frequencies below 2 GHz, but it is not SOHO case) because their lower mass with respect to the Traveling Wave Tube Amplifier's (TWTA) one is advantageous, despite their reduced efficiency. Moreover, SSAs are more reliable and require lower voltages. Using the plot contained in [48], the empirically estimated input power and amplifier efficiency are $P_{input} = 52$ W and $\eta = 0.22$. Then, considering the modulation and encoding process, the real data rate can be estimated as $R_{real} = 140.22$ Kbps.

Regarding the information on the shape of the antenna, the gains can be computed in the following way, defining $\lambda = \frac{c}{f}$ with $f = 2245$ MHz:

- HGA: Analytic formula $G_{tx,HGA} = 10 \log \left(\frac{\pi^2 D_H^2 \mu_H}{\lambda^2} \right)$, with $\mu_H = 0.55$ for the parabolic antenna.
- LGA: Experimental formula: $G_{tx,LGA} = 10 \log \left(\frac{D_L^2 L}{\lambda^3} \right) + 20.2$, with $D_L = 2\lambda$ and $L = 0.156\lambda$, these two values can be taken from literature [54] [56] for helix antennas.

The cable losses are considered to be -3 dB, to be conservative in the sizing. Considering the other losses (free-space, pointing and atmospheric), the results can be summarized in the following Table 12

<i>Free space losses [dB]</i>	<i>Pointing error losses [dB]</i>	<i>Atmospheric losses [dB]</i>
-222.96	-0.011	-0.038
-222.96	-0.077	-0.038

Table 12: Computation of the losses

The free-space losses are evaluated for both the antennas by considering a maximum distance between SOHO and Earth of 0.01 AU⁸. For the atmospheric losses, the value can be defined graphically as the sum of the losses due to the rain and the ones related to the GS position: the first ones are neglected since the S-band, as seen before; while the second are the one computed and shown in the table.

Moreover, the pointing losses depend on the DSN that receives the signal, in particular on its accuracy and its beamwidth. The pointing accuracy for the DSN is considered to be $\eta = 0.01$, much lower than the one of other GSs.

The beamwidth of the receiver can be computed by considering the DSN antennas to have a parabolic shape and utilizing the following formula:

⁸This value is an approximation of the actual one between the S/C and Earth during the mission.

$$\theta_{rx} = \frac{65.3\lambda}{D_{rx}}$$

where λ is defined as before, given that the DSN also operates in the S-band. Regarding the diameter of the receiver antenna, different values are considered for the HGA receiver and the LGA receiver. The worst condition for transmitting, from the perspective of the HGA, occurs when using a 26-meter receiver. Generally, larger antennas result in stronger signals and enable the antenna to send and receive more information. For the LGA, instead, the worst case is considering the DSN antenna with a diameter of 70 m (with this type of stations, even High Rate telemetry can be achieved [63]). Subsequently, the gain of the GS antenna can be computed using the analytical expression for the parabolic antenna already seen. The Table 13 condenses the results obtained until now in terms of gains.

Type of antenna	Output Power [W]	G_{tx} [dB]	θ_{tx} [°]	θ_{rx} [°]	D_{rx} [m]	G_{rx} [dB]
HGA	10	22.93	10.85	0.34	26	53.13
LGAs	10	7.07	75.24	0.12	70	61.73

Table 13: Final results of the link budget preliminary sizing

Analyzing the obtained value for the antenna gains, it is noticeable that they are almost consistent with those found in literature [9]: the HGA exhibits a gain of 22.7 dB, which is very close to the one computed. However, for the LGAs, the gain from the reference is -31 dB, indicating a discrepancy from the computed value. Nevertheless, the value of $G_{tx} = 7.07$ dB aligns perfectly with the typical range for a helix antenna, usually falling between 5 and 20 dB. The difference observed can be attributed to the assumptions made regarding the dimensions of the helix antenna mentioned earlier.

Concerning the GS antenna, still from literature it is possible to verify the gains obtained for the 26 m antenna and the one for the 70 m [55] [58]: for both the gains the results are aligned with the data from literature ($G_{rx} = 51.4$ dB for the 26 m-receiver and $G_{rx} = 62.95 - 63.59$ dB for the 70 m one). This reaffirms the utilization of the DSN within the S-band frequency range. At this point it is possible to evaluate the receiver power as: $P_{rx} = EIRP + G_{rx} + L_{space} + L_{atm} + L_{point}$ where $EIRP$ is the effective isotropic radiated power, computed as the sum of the transmitted power, the gain of the transmitter and the cable losses.

Another important parameter that needs to be computed is the system noise density $N_0 = 10 \log(kT_s)$, which is obtained from the Boltzmann constant k and the sensor temperature, equal to 21K for the DSN [48].

Finally, the error per bit to noise density is: $E_b/N_0 = P_{rx} - N_0 - 10 \log(R)$

This is a crucial parameter since it proves the correctness of the sizing. In particular, if $E_b/N_0 - (E_b/N_0)_{min} > 3$ dB then the receiver is capable of translating the signal and distinguishing it from the noise. The margins, which is the left-hand side of the previous inequality, for HGA and LGAs are 18.76 dB and 11.43 dB, respectively. It is also important to check whether or not the receiver is capable of tracking the signal and distinguishing it from the noise. Firstly, the carrier modulation index reduction (which is the power removed from the carrier due to the modulation), is computed thanks to the modulation index β , assumed to be 78°: $P_{mod,loss} = 20 \log(\cos(\beta))$

Therefore, the Carrier Power is computed as the sum of the transmitter power and the carrier modulation index reduction and from this value it is possible to obtain the Signal to Noise Ratio (SNR) of the carrier: $SNR_{carrier} = P_{carrier} - N_0 - 10 \log(B)$, where $B = (1 + \alpha) \cdot R_{real} = 210.33$ Hz with $\alpha = 0.5$ is the receiver noise bandwidth dependent on the modulation [48]. The SNR margin can then be computed as the difference between the SNR of the carrier and the minimum SNR depending on the ground station, which is 10 dB for the DSN.

In this case, the margins for HGA and LGAs are 28.56 dB and 21.23 dB, respectively, both higher than 3dB, which means that the receiver is indeed capable of tracking the signal and distinguishing it from the noise.

3.3.5 Uplink reverse sizing

The sizing for the uplink is conducted with the same procedure for the downlink. With respect to the downlink the receiver and transmitter are switched, the frequency used is $f_{uplink} = 2067$ MHz and the data rate is $R_{uplink} = 2$ kbps. The output power is $P_{out,uplink} = 20$ kW, $BER = 10^{-7}$, $\alpha_{mod} = 1$ [58], the pointing accuracy $\eta = 0.1$ °. The temperature assumed for the HGA, being always in shadow, is assumed to be $T_{HGA} = 250$ K, while for the LGAs, being partially exposed to the Sun, is supposed $T_{LGA} = 290$ K. The following table highlights all the meaningful results:

	G_{tx} [dB]	G_{rx} [dB]	θ_{tx} [°]	θ_{rx} [°]	L_{tot} [dB]	Margin [dB]
GS 26 m to HGA	52.41	22.17	0.36	11.85	-222.29	57.15
GS 70 m to LGA	61.01	5.99	0.14	85.17	-222.29	48.93

Table 14: Resuming table for uplink sizing results

As it can be seen in the table, both the HGA and the LGA are capable of receiving the telecommands from the GS. This confirms the capability of SOHO to establish both uplink and downlink correctly with the DSN.

4 AOC Subsystem

4.1 AOCS Architecture

The Attitude and Orbit Control System (AOCS) in SOHO mission provides the satellite with the means to: point the spacecraft optical reference axis X_0 ⁹ accurately to the Sun, control the roll angle around the Sun pointing axis, and perform orbit manoeuvres. The general architecture for SOHO AOCS is reported in Figure 13a.

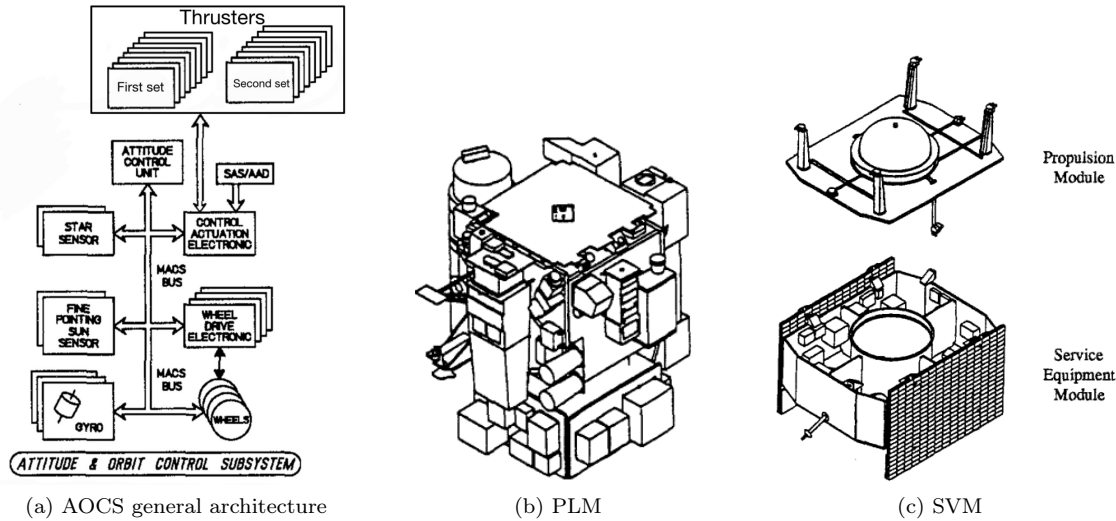


Figure 13: Generalities about SOHO and AOCS architecture

The other two images, 15c and 15, highlight the fact that SOHO design is based on a modular concept with two main elements: the Service Module (SVM) and the Payload Module (PLM). The SVM can itself be split into two sub-assemblies: the service equipment module and the propulsion module. This setup facilitates straightforward installation and access to the payload instruments, meeting all functional requirements of the instruments, especially regarding viewing direction, field-of-view clearance, straylight prevention, and pointing stability. Attitude sensors are installed on the PLM to allow the achievement of the highest possible alignment stability, while the SVM carries the actuators [2].

The SOHO spacecraft utilizes a 3-axis stabilized configuration, designed to maintain attitude stabilization and precise pointing control (further information in Subsections 4.2.1 and 4.2.2) through a closed-loop system (Subsection 4.1.2) throughout its mission. To do so, the system must be provided with sophisticated sensors to determine the attitude precisely and fine actuators to maintain the desired pointing.

4.1.1 AOCS Hardware: Sensors

The sensors used for the SOHO mission are:

- **Two Fine-Pointing Sun Sensors (FPSS):** provide unambiguous Sun angle data immediately upon application of power. The electronics unit contains no software and performs without any internal forbidden states, latch-up, or lost in space conditions. Their FOV is $\pm 4.5^\circ$ and their accuracy is 15 to 20 arcsec [72]. FPSSs are installed in the PLM, so the measurements and accuracy benefit from its high-pointing stability and they point toward the $+X_b$ direction [2]. The second FPSS is present for redundancy reasons.
- **Two star trackers, also referred to as SSU (Star Sensor Unit):** the chosen hardware is the High-Resolution Star Tracker (HR-STR). This is a narrow field star tracker based on an optical system with catadioptric objective built with radiation-hardened glasses [68]. A SSU can track up to five stars. One of the stars is designated as guide star and is used as input for the control of the roll axis. When a single event upset occurs on the cameras for detectors (CCD) inside or close to the guide star image, the star data becomes unusable for control. The accuracy is better than 1 arcsec and the FOV is $3^\circ \times 4^\circ$ [67]. The star trackers are oriented perpendicularly to the Sun-Earth line along the Y_b direction, so as not to be hindered by their radiations and disturbs in their FOV. The second star tracker is present for redundancy reasons.
- **Three gyroscopes:** they compose the Inertial Reference Unit (IRU) [73], located into the PLM for the advantages already discussed. They are not required during normal mission operation but only for thrusters based activities, such as momentum management, Emergency Sun Reacquisition (ESR) and Initial Sun Acquisition (ISA) [61]. They are aligned to measure incremental changes in the roll attitude. Each one is designed to be used only for its specific independent function [70]. The functions of the gyroscopes are summarized in the following Table 15:

⁹The spacecraft optical axes are defined with respect to the optical alignment cube of the Fine Pointing Sun Sensor (FPSS), with the optical X axis (X_0) nominally perpendicular to the spacecraft launcher separation plane and pointing from the separation ring through the spacecraft.

Gyroscope	Function
Gyro A	connected to the Failure Detection Electronics (FDE) for roll rate sensing for ESR to allow spacecraft roll-rate control using thrusters
Gyro B	connected to the FDE for excessive roll-rate (anomaly) detection
Gyro C	connected to the Attitude Control Unit (ACU) for roll attitude sensing during computer-based control modes using thrusters

Table 15: Gyroscopes function [114]

- **Three Sun Acquisition Sensors (SAS):** pyramid Sun sensor which provides 2-axis coarse Sun position information in the form of analog voltage signals in a near hemispherical FOV. The accuracy in the central portion of the FOV is better than $\pm 2^\circ$ and on sensor boresight is better than $\pm 1^\circ$ [69]. These are placed in a configuration giving omni-directional coverage.

As a final remark, additional temperature and pressure transducers can be thought to be inserted to monitor the exhibited sensors and actuators conditions, ensuring they are maintained in the operative and safe range.

AOCS Hardware: Actuators The actuators used for the SOHO mission are:

- **Two sets of eight thrusters:** SOHO is equipped with sixteen 4.4 N MRE-1.0 monopropellant hydrazine thrusters [39] divided into primary (A) and redundant branches (B). Each branch can be divided into pairs which actuate on the same direction. Thrusters are strategically positioned around the spacecraft as highlighted in the following Table 16 and Figure 17:

Thruster Pair	Thruster Locations	ΔV direction	Primary Attitude Control
1 and 2	Sunward $+X_b$	$-X_b$	Pitch
3 and 4	Earthward $-X_b$	$+X_b$	Yaw
5 and 6	Top $+Z_b$	$-Z_b$	Roll
7 and 8	Bottom $-Z_b$	$+Z_b$	Roll

Table 16: SOHO thrusters [41]

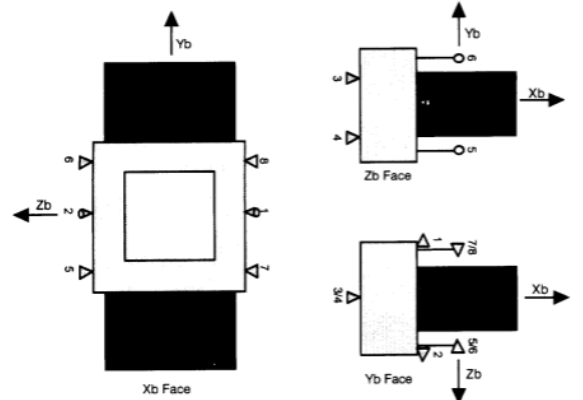


Table 17: Thrusters configuration

As an additional note, thruster 1 is canted 30° down and 2 is 30° up. Thrusters are needed for orbital manoeuvres, attitude control and desaturation of reaction wheels [6]. The propulsion equipment is mounted onto the SVM upper platform except for two thruster blocks located on the lower floor.

- **Four reaction wheels (RW):** a rotating inertial mass, driven by a brushless DC electric motor. When power is applied to the motor, the wheel accelerates, causing the satellite body to which the motor housing is attached to rotate in the opposite direction due to the induced counter torque. These are used to provide control torques to control spacecraft attitude. The control torques are needed to counteract internal and external disturbance torques experienced by the S/C and to slew the S/C for special off-pointing and roll-offset manoeuvres. The Reaction Wheel Unit (RWU) channel, located in the SVM, consists of a Reaction Wheel Assembly (RWA) and one Wheel Drive Electronics Box (WDE) [74]. Three reaction wheels are used for control, while the fourth is present for redundancy. The configuration can be thought to be pyramidal, which guarantees different control capacities along the three axes (useful if the disturbances are not uniform) and ensures the closing of the control problem also when one of them stops working.

This configuration enables to provide means of controlling the roll angle around the Sun pointing axis to any position commanded from ground. Moreover, it guarantees the possibility of controlling all axes during ΔV for mid-course corrections, operational orbit insertion and orbit maintenance [64].

4.1.2 AOCS Software

In this subsection, the focus is on delving deeper into the controller algorithm. The Normal Mode controller (Subsection 4.2.1) is employed to ensure precise spacecraft $+X_b$ axis Sun pointing during standard on-station operations. Pitch and yaw attitudes of the spacecraft are monitored using FPSS, while the roll attitude is tracked using the SSU. Actuation is carried out using reaction wheels. Due to stricter requirements on lateral axes, the discussion is narrowed down to these two axes, which utilize identical control logic, so just one of the two is analysed.

The control loop block diagram is provided below [64]:

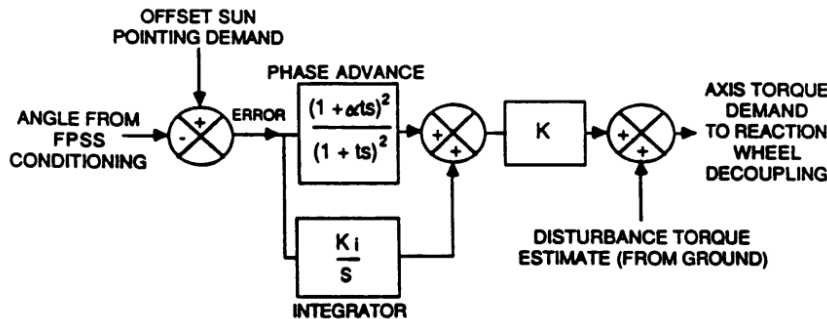


Figure 14: SOHO normal mode control loop (for pitch and yaw)

Parameter	Value
α^t	0.66
t	0.2
K	5623
K_i	TBD

Table 18: Pitch axis parameters

Parameter	Value
α^t	0.6
t	0.125
K	3467
K_i	TBD

Table 19: Yaw axis parameters

The pitch attitude, derived from FPSS conditioning, undergoes a comparison process with the off-set pitch attitude demand, resulting in an attitude error. This error then passes through a second-order phase advance filter and is combined with the output of an integrator. The resultant sum is then multiplied by the gain K to generate a torque demand concerning the pitch axis. The integral component serves to compensate for factors such as wheel friction torques. Estimates of anticipated disturbance torques are supplied by ground sources.

4.1.3 Mass, power and data budgets

The subsystem mass, power and data budgets (per single component) are:

Component	Number	Redundancy level	Mass	Power	Size [Kwords]		Typical throughput [KPIS]	Execution frequency [Hz]
			budget [kg]	budget [W]	code	data		
FPSS	2	1	0.95 (1.08)	0.5	0.5	0.1	1	1
HR-STR	2	1	7.2	10	2	15	2	0.01
IRU	1	-	7.1	43	0.8	0.5	9	10
SAS	3	-	0.210	null	0.5	0.1	1	1
Thrusters	16	1	0.5	8.5	0.6	0.4	1.2	2
RWs	4	1	7.45	29	1	0.3	5	1

Table 20: Mass, power and data budget of AOCS subsystem

Data taken from the datasheets are highlighted in the yellow cells, while the others are taken from their reference values [48]. The data volume is referred to the typical execution frequency reported. The values are based on 1750A-class Instruction Set Architecture and assumed that software is developed in a higher-order language. This is reasonable since the 1750A is a general-purpose processor and it is the one used in SOHO mission [76], thus, the numbers reported represent a good first estimate. It can be noted that the data size produced by the star trackers is the most significant one.

As a final remark, it must be considered that the data budget must be increased including the kinematic integration and the error determination, both present in the SOHO software architecture, as exposed in Subsection 4.1.2. Their data budgets are 2.2 Kwords (0.2 for data and 2.0 for code) and 1.1 Kwords (0.1 for data and 1.0 for code), respectively.

4.2 AOCS Design and Justifications

Pointing stability, particularly along the boresight axis of the scientific payload, is a key design driver for the mission. To meet this requirement, the AOCS subsystem must ensure stability and high accuracy throughout the operational lifespan. Structurally, this implies addressing potential sources of micro vibrations and high-frequency jitter, notably from continuously operating mechanisms like RWs [1]. In efforts to minimize these effects on the payload and sensors, they are housed within the dedicated and vibration-resistant Payload Module (PLM).

The *rationale* behind the chosen AOCS architecture derives from the stringent pointing demands set by the payloads, requiring precision levels well below 0.1°, as well as inertial pointing requirements. This dictates the need of a 3-axis stabilization approach and a precise combination of actuators and sensors. In particular:

- **Sensors:** achieving accurate attitude determination throughout the most demanding modes requires sophisticated sensors, including star trackers, Sun sensors, and highly precise gyroscopes. The combination of gyroscopes and star trackers is used when the mission requires the highest accuracy and justifies a high cost, such as in the SOHO case.

²Numbers outside the parentheses refer to the components only, while the ones inside parentheses also comprise the integrated electronics.
³It means it is passive.

These two sensors complement each other nicely: gyroscope can be used for initial stabilization and in periods of Sun or other interferences in the trackers FOV, such as in safe mode. Instead, the star trackers can be used to provide a high accuracy, low frequency and external reference unavailable to the gyros [48]. Furthermore, the combination of FPSS and star tracker is utilized in the normal mode (fine-pointing mode), where very high precision needs to be guaranteed, as already described in Subsection 4.1.2. Additionally, Sun Acquisition Sensors (SAS) facilitate initial attitude acquisition, crucial for orienting the solar panels towards the Sun to initiate power generation. The sensors possible combinations enable attitude determination across various operational modes, ranging from high-precision demanding modes to lower ones, as detailed in Subsection 4.2.1.

Alternatives Trade-off: considering alternatives to this configuration, horizon sensors are discarded due to the fact that they are more suitable for low Earth orbits where the accuracy would be the highest, whereas in SOHO mission the distance from the Earth is too high. Moreover, since the primary scientific goals are based on the observation of the Sun, the knowledge of S/C position with respect to it may be more relevant than the one with respect to the Earth. Then, magnetometers are not taken into account both for their low accuracy and the absence of a strong magnetic field. In addition, these would require the knowledge of a model of the magnetic field in the halo orbit region to determine attitude and this is not well known in the environment of interest.

- **Actuators:** the chosen architecture corresponds to the most common combination for achieving very high accuracy and 3-axis control. This is composed of RWs supplemented by thrusters for momentum unloading and coarse control. The latter is performed during initial mission phases and safe mode. Notably, the chosen 3-axis architecture operates as a zero momentum system, where RWs respond to disturbances on the vehicle. Thrusters, instead, are used for desaturation, orbital manoeuvres and redundant attitude control, being placed in a configuration guaranteeing 3-axis control. The rationale behind the chosen thruster configuration has already been discussed in the propulsive subsystem analysis.

Alternatives Trade-off: a commonly adopted alternative for desaturation is made by the magnetorquers, whose choice can be easily discarded due to the fact that SOHO stays out of the Earth's magnetosphere. Instead, Control Moment Gyros (CMGs) are usually employed when missions require a greater momentum exchange and faster slews. However, for missions like SOHO, where rapid manoeuvres are not necessary and could potentially harm the instruments, CMGs would be excessive. Additionally, they would add unnecessary mass and power demands to the spacecraft.

4.2.1 Mission modes and control

As already said in the previous reports, the mission is divided into three different phases: LEOP, TTP and operational phase. During the operational phase, different modes can occur within the mission. Below, the main requirements for attitude control are expressed, as it can be seen in literature [63]:

- **Normal mode (NM):** attitude and roll are controlled by spinning up or braking down three reaction wheels, oriented in a triangular fashion to each other. If one wheel is spun up, the spacecraft will rotate in the opposite direction around the axis of that wheel, due to the conservation of angular momentum. The inputs to the control mechanism come from the FPSS and the star tracker. The Roll Steering Law (RSL) dictates the movement of the stars in the star tracker to keep SOHO oriented exactly in line with the Sun's North-South axis.
- **Emergency Sun Reacquisition Mode (ESR):** this can be considered as the "*ultimate safety net*" for SOHO, a configuration entered autonomously by the spacecraft in the event of anomalies. In ESR, the spacecraft attitude is controlled entirely by hardware that senses the approximate position of the Sun and fires thrusters autonomously to ensure that the spacecraft is pointed towards the Sun ($\pm 2^\circ$ on each axis). The spacecraft roll is not controlled by the hardware, but it can be controlled by ground intervention. In ESR mode, the RWs are not used autonomously by the spacecraft and they eventually spin down after a while (in the process they impart their angular momentum on the rest of the spacecraft, which is counteracted by the thruster firings when the pointing reaches the 2-degrees limits of the "error box"). After the wheels are spun down, the spacecraft pointing "bounces around" within the error box. Through ground intervention, however, the RWs can be spun up (this is part of a normal recovery). They then provide gyroscopic stability to the spacecraft. When tuned correctly, the spacecraft can be left in ESR mode with wheels spun up with practically no thruster firings. In this mode, the pointing is not strictly controlled: it will drift slowly (and occasionally bounce) within the error box, or it will be adjusted by ground control (spinning up/down RWs).
- **Coarse Roll Pointing Mode (CRP):** in this mode the RWs are used for attitude and roll control (i.e. no thruster firings) and this is the first step "up" from ESR. Pitch and yaw rates are determined through the FPSS, while the roll rate is measured by gyroscopes. A conservative usage of SOHO's gyroscopes has always been implemented because gyroscopes are recognised as being life-limited items: activating or disabling them when necessary. This mode can be operational even in the event of gyroscope malfunction, thanks to the possibility of using of RWs also for measuring the roll rate [114].
- **Roll Manoeuvre Wheels Mode (RMW):** in RMW, the intermediate mode between CRP and Normal Mode, SOHO is controlled by the FPSS and the star tracker, ensuring that SOHO has full knowledge and control of its orientation. However, the steering laws are a bit more "relaxed" and a strict alignment with Solar North-South is not

maintained. This mode is used for thruster manoeuvres: Station Keeping (SK) manoeuvres are used to trim SOHO's orbit, and Momentum Management (MM) manoeuvres are used to spin up/down the RWs when necessary. The wheel speeds must be kept within certain ranges (not too slow, not too fast) to maintain stable control.

- **Initial Sun Acquisition Mode (ISA):** this mode makes use of the SAS-1 sensor only, leading to less than hemispheric coverage (ESR uses three SAs, and thus has omni-directional coverage). Also during this mode gyros are employed as attitude sensors. Immediately after SOHO's separation from the Centaur upper stage, the AOCS cancels the angular rates imparted by the separation and coarsely aligns the spacecraft towards the Sun. Since that time, ISA is only commanded after any ESR events, in order to recover control of the spacecraft's attitude [61] [62].

In Table 21 the pointing requirement for the main modes is highlighted:

Control mode	Requirement	Type of control	Sensors	Accuracy
Normal mode (NM)	Establish and maintain accurate the S/C +X-axis Sun pointing	Three-axis control using actuators (RWs)	FPSS, SSU	APE [2]: roll: <15 arcmin lateral: <5 arcmin RPE : medium term lateral: <10 arcsec (6 months) short term roll: <1.5 arcmin (15 min)
Emergency Sun Reacquisition Mode (ESR)	Control and reorient the S/C towards the Sun in the event of a loss of communication or orientation	Three-axis control through autonomous thruster firings using B-branch in a hard-wired mode	Three SAs, Gyroscopes	Pointing not strictly controlled, ± 2 -degree limit on each axis
Roll Manoeuvre Wheels Mode (RMW)	Pointing while doing thrusters manoeuvres (SK, MM)	Three-axis control using actuators (A-branch thrusters)	FPSS, SSU, Gyroscopes	APE : <15 arcsec [64]
Slew Manoeuvre	Soft slew rate to avoid payload damages during S/C special roll-off pointing manoeuvres [41]	Three-axis control using actuators	Three SAs, Gyroscopes	<0.5 °/s [48]
Initial Sun Acquisition (ISA)	Detumbling and coarsely align the S/C towards the Sun in the first phase of the mission	Three-axis control using actuators (A-branch thrusters)	SAS-1, Gyroscopes	Low (value not retrieved)

Table 21: Control modes of SOHO

Regarding the slew manoeuvre, no information about the required sensors could be retrieved. It was supposed to employ a configuration similar to the one used in ESR and ISA modes, where the Sun might be within the FOV of the SSU, potentially causing damage to it. For a general slew (along an arbitrary axis of an arbitrary angle variation) the FPSS sensors are neglected because the performed manoeuvre might cause the Sun to exit their FOV, thus making it impossible to determine the attitude.

4.2.2 Pointing Budget

The SOHO satellite uses five different reference frames (as seen in literature [2]), in particular in this section the *absolute attitude frame* $\{X_a, Y_a, Z_a\}$ is presented. It is time-varying and can be defined as:

- the origin coincides with the spacecraft centre of mass;
- X-axis is along the spacecraft-Sun line and oriented towards the photometric centre of the Sun;
- Z-axis is such that the (X, Z) plane contains the normal to the ecliptic plane as defined in the J 2000 inertial reference frame, being it oriented towards the north ecliptic hemisphere;
- Y-axis completes the right handed orthogonal reference frame, i.e. it will be parallel to the solar equatorial plane pointing towards the east (opposite to the solar rotation direction).

The subsystems having the stricter requirements in terms of pointing are the payload and the telecommunication ones. In particular, some of the requirements are listed below:

- **Payload:** the scientific instruments shall always point the Sun with an accuracy as good as 1 arcsec for around-the-clock data gathering [41]. For instance, the MDI instrument provides high precision solar images with an absolute pointing performance in orbit of $2' 34''$ for the Y-axis and $1' 25''$ for the Z-axis [11].

- **Telecom:** the halo orbit requires the HGA to be capable of pointing in all directions within a $\pm 32^\circ$ cone [76]. During normal operations, a certain depointing is acceptable ($< 0.7''$) and the realignment of the HGA occurs three times every 24 hours. In order to have smooth movements, a very low driver speed is used ($0.001^\circ/\text{s}$). The worst case depointing associated with this action is lower than $0.27''$ [2], which is the maximum drift of the subsystem. Regarding the LGA, since it is quasi omni-directional antenna, it does not require any demanding pointing.

4.3 AOCS Reverse Sizing

4.3.1 Disturbances

The primary external disturbance acting on SOHO is the Solar Radiation Pressure (SRP). This is because SOHO operates in a halo orbit positioned at Sun-Earth Lagrangian Point 1 (L_1), where other disturbances are minimal. As a matter of fact, SOHO is unaffected by the Earth's magnetic field as it resides outside the magnetosphere. Additionally, its distance from the Sun (approximately 0.99 AU) ensures that the influence of the Sun's magnetic field can also be disregarded. Moreover, being in an equilibrium point with respect to gravitational forces, the gravity gradient can be safely ignored.

In the subsequent preliminary sizing for SRP, only the torque affecting SOHO in the nominal operational orbit is considered. Hence, for an initial estimate, the mean disturbance over a year post-insertion is calculated using ephemerides to determine the correct distance magnitude. The torque from SRP is computed at each time step, considering that the spacecraft continuously points toward the Sun along its $+X_b$ axis, with contributions from the upper face and the two solar panels. This torque arises due to a small offset (set to 0.05 m along Y_b) between the geometric and mass centers of the spacecraft, for which no literature data could be found. For each face, the generated torque is expressed by the following equation:

$$T_{srp} = \frac{F_s}{c} A(1+q)\cos(I)(c_{sp} - c_g) \quad (1)$$

where c is the speed of light, A the surface area, q is the reflectivity coefficient of the surface (0.3 for solar arrays (SA) and 0.5 for S/C surface), I is the incidence angle, considered in the worst case scenario as 0° , and $(c_{sp} - c_g)$ is the distance between surface centroid (assumed as centre of pressure) and satellite centre of mass.

Moreover, F_s is the solar constant, determined starting from

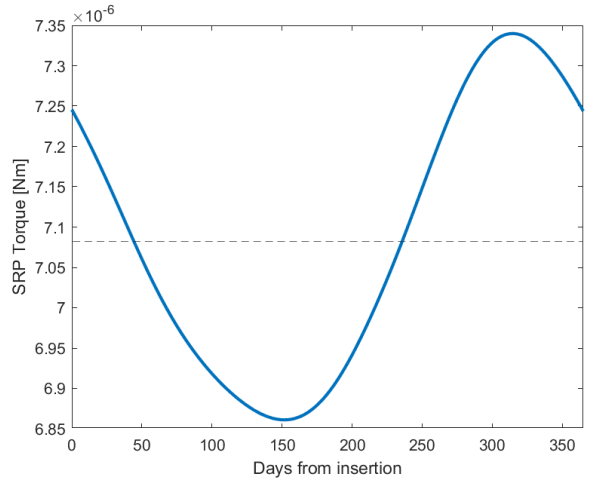
the solar constant at 1 AU using the relation:

$$F_s = F_{s@1AU} \left(\frac{AU}{r} \right)^2 \quad (2)$$

Where $F_{s@1AU} = 1367 \text{ W/m}^2$. The total torque applied to the S/C is then retrieved by appropriately summing and subtracting the contributes:

$$T_{\text{tot}} = T_{\text{SA1}} - T_{\text{SA2}} + T_{\text{upper}} \quad (3)$$

Then the mean value is computed, obtaining a torque due to the SRP disturbance of $7.08 \times 10^{-6} \text{ Nm}$, which is similar to the value of the estimated torque retrieved from literature ($\sim 10^{-7}$) [60].



4.3.2 Attitude actuators sizing

4.3.2.1 Reaction Wheels

For the reverse sizing of the spacecraft's reaction wheels [71], the following data were considered as inputs:

- Maximum and minimum moments of inertia: $I_{\max} = 3600 \text{ kgm}^2$, $I_{\min} = 2000 \text{ kgm}^2$ [59];
- Maximum angular rate, in order to not damage the payload: $0.5^\circ/\text{s}$ [48];
- Maximum angular momentum storage of the reaction wheels: 45 Nms ;
- Maximum gross torque provided by a reaction wheel: 0.248 Nm .

All the reasoning is carried out considering the halo orbit phase. RWs can be used by SOHO to dump the SRP disturbance, therefore it is clear that after some time they will need to be desaturated. Firstly, the torque needed by the RW to counteract the external disturbances torque is computed as:

$$T_D = T_{srp} + 100\% \text{ margin} \quad (4)$$

In order to obtain an approximated value of the desaturation time interval, it is possible to estimate the approximated average of the angular momentum accumulated by a reaction wheel around one orbit as follows:

$$h_{RW} = T_D \cdot t_{orbit} \quad (5)$$

The maximum storable angular momentum (45 Nms) divided by the latter value found (220 Nms) indicates that SOHO needs to be desaturated approximately once every $\Delta t_{desat} = 4 \text{ weeks}$, corresponding to approximately 1/6 of the orbit

period. However, comparing the desaturation intervals resulting from the reverse sizing with the ones found in literature [34], a discrepancy was revealed. In fact, as a mission requirement, the wheels need to be unloaded through the use of thrusters at eight weeks intervals, to be performed in conjunction with the station keeping manoeuvres required to maintain the halo orbit. Yet, from the analysis, the interval resulted to be almost halved: this may be due to the overestimate of the external disturbance torque and to the applied margin. As mentioned in Section 4.1.1, the RWs are also employed to slew the S/C for special off-pointing and roll-offset manoeuvres. The worst-case scenario considered for their sizing corresponds to the slew manoeuvre with $\theta_{max} = 180^\circ$, a real-case scenario that occurred during the commissioning phase and once every three months after the anomaly of 1998 [65] [66]. To model it, constant acceleration and braking are considered around the roll axis. Since the torque corresponding to $t_{min} = \theta/\dot{\theta}_{max} = 360\text{ s}$ is higher than the available one, the minimum time t_{min} to perform the slew is computed starting from the available data of the maximum torque provided by the RW, retrieved from data, and considering the maximum possible acceleration (half of the distance in half of the time):

$$t_{min} = \sqrt{\frac{4\theta_{max}I_{max}}{T_{max,RW}}} \quad (6)$$

From this computation, a value of 427 s is found. The maximum angular rate achieved during the slew manoeuvre is $\dot{\theta}_{max} = 0.42^\circ/\text{s}$, which is still quite close to the limit.

4.3.2.2 Thrusters

As previously mentioned, thrusters are both used for redundant attitude control during particular operational modes and to desaturate the RWs. For this preliminary analysis, the manoeuvre was considered to be performed with two of the 4.4 N thrusters, in such a way that the rotation happens around the roll axis. As done for the RWs, also the thrusters slew manoeuvre is sized considering the worst scenario in which $\theta_{max} = 180^\circ$ with constant acceleration and braking. The maximum angular rate employed for the computations is still $0.5^\circ/\text{s}$, to avoid damages to the payload. The required force to perform the slew manoeuvre depends on the required slew rate and can be calculated as:

$$F_{th} = \frac{I_{max}\theta_{max}}{nLt_{min}^2} \quad (7)$$

where $n = 2$ is the number of thrusters, $L = 1.85\text{ m}$ is the lever arm and $t_{min} = 360\text{ s}$ is the minimum time required for the manoeuvre, retrieved through the ratio between θ and $\dot{\theta}_{max}$. The requested thrust value results to be 0.0236 N, well within the thrusters capabilities, so the slew manoeuvre can actually be computed in the minimum time. This value should be compared to the minimum impulse bit of the selected thrusters model but, since it could not be retrieved from literature, it was considered acceptable in first approximation. Thrusters are also employed to desaturate the RWs (Section 4.1.1). The desaturation time is estimated through the following expression:

$$t_{des} = \frac{h_{max,RW}}{nLF} \quad (8)$$

The final value resulted to be 2.76 s.

4.3.3 Preliminary fuel mass sizing

The propellant mass estimation can be carried out considering two different thrusting phases: slew manoeuvre and RWs desaturation. Therefore, the computation considers the following expressions to quantify the amount of propellant consumed during every slew and desaturation manoeuvre:

$$m_{prop,slew} = \frac{nF_{th}t_{min}}{I_{sp}g_0} \quad m_{prop,des} = \frac{t_{des}F_{th}}{I_{sp}g_0} \quad (9)$$

Afterwards, the total propellant mass requested for the desaturation of the RWs during the entire nominal mission, which lasted 29 months, was obtained by multiplying the value of $m_{prop,des}$ by the number of RWs and by the ratio between the nominal duration and the time interval between successive desaturations Δt_{desat} , to which a 20% margin is applied. The latter ratio corresponds to the number of desaturations that occur. Results are summarized in Table 22:

	Slew manoeuvre	Desaturation of 1 RW	Desaturation for nominal mission duration of all RWs
$m_p [\text{kg}]$	0.0079	0.0056	0.6667

Table 22: Propellant mass sizing

The total propellant mass used for desaturation is quite small due to the sporadic nature of this event, taking place only almost 30 times during the nominal mission duration. Notably, since SOHO has a large amount of fuel (251 kg at launch [41]), it is clear that an extension of the mission can occur without any problems related to fuel shortage for control.

5 TC Subsystem

5.1 TCS Architecture

5.1.1 TCS Criticalities and Requirements

SOHO, as already pointed out, is a Sun-oriented spacecraft placed in a halo orbit around L_1 point, therefore it is characterized by the absence of eclipses and its thermal environment appears very stable. Consequently, designing thermal control for SOHO seems comparatively straightforward at first glance. Nevertheless, it shall be paid great attention in the Thermal Control Subsystem (TCS) design for the following reasons. Firstly, it shall be considered that the S/C experiences different thermal configurations depending on the mission phases. Secondly, to comply with the failure cases, the thermal design must be compatible with very different environmental conditions. It is also crucial to avoid mass overload of the structure and contamination of PLM¹⁰ experiments . Overall, the TCS shall guarantee the requirements shown in Table 23 [80]:

TCS requirements for PLM	TCS requirements for SVM
Maintain all equipment mounted on the PLM structure within acceptable temperature range limits (see Table 24)	Minimum heat interchange with the PLM, including reflection of external sheets of MLIs
Provide a stable thermal environment to meet all the pointing requirements of the AOCS and experiment sensors	External surfaces shall be electrically conductive
Provide an acceptable radiative environment for the experiment sensors	Thermal stability of PLM-SVM interface, for both short and long terms [75]

Table 23: TCS requirements

5.1.2 TCS Components and Positioning

The TCS components selected for the architecture and their positioning inside the S/C are listed below and will be motivated in Section 5.2 [80] [75]:

- **Sunshield:** it is permanently pointing to the Sun during the S/C operations, therefore, it is placed on the $+X_b$ panel. It is made of optical solar reflectors consisting of mirror glass tiles glued on a supporting panel. In particular, Pilkington Optical Solar Reflectors (OSR) have been selected for this architecture [96].
- **Sunshield Heaters:** they are foil heaters with different impedance values, placed underneath the $+X_b$ panel. They provide a quite flexible power adjustment that compensates for the temperature differences on the Sunshield, as will be described in Section 5.2.
- **Substitution Heaters:** they are used for the overall equipment to minimize any modification of the thermal gradients caused by the switching on/off of the single unit.
- **Structure Heaters:** these independently commendable foil heaters are placed on the four areas of the $+X_b$ panel and on both vertical areas of the lateral panels.
- **Radiators:** they are mounted on lateral walls, on corner panel $+Y_b/-Z_b$ and on lower platform. They are painted with PSG 120 FD, a matt-white thermal-control paint made of silicone and zinc oxide [93].
- **MLI Blankets:** they are a type of high performance insulators that use multiple radiation-heat transfer barriers to retard the flow of energy. The S/C uses a series of MLI blankets made by an electrically conductive polymer film (Kapton). They can be divided in Type A, B, C and D [94], depending on the performance requests:
 - *Type A* is a high efficiency MLI for general purpose and it is composed of 16 layers. The external sheet is a black conductive Kapton, perforated and internally covered with Vapor Deposited Aluminum (VDA). The 14 intermediate sheets are made of embossed Kapton (0.00762 mm) with VDA on both sides (2VDA) and perforated. The internal sheet is Kapton (0.0254 mm) 2VDA both sides and perforated.
 - *Type B* has the same composition as Type A, except for the first sheet that is black painted externally with Electrodag 501C, because with this final coating the specularity to the PLM is minimized. It is used on the upper platform area and thruster blocks.
 - *Type C* is composed of 12 layers: the external and the internal sheet are Kapton (0.0254 mm) 2VDA and perforated. The intermediate sheets are the same as Type A but the number is 10. This MLI type C is used on the hydrazine tank (top and bottom parts).
 - *Type D* is a low efficiency MLI and it is composed of 4 layers. It is equal to Type C but with only 2 intermediate layers. It is installed on Reaction Wheels (RWs), Attitude Control Unit (ACU), Antenna Pointing Assembly (APA) motors, and Reaction Control Subsystem (RCS) elements.
- **Coatings:** they are the paints used to cover the different spacecraft's surfaces, depending on the requirements of the area. One example of coating is the already mentioned Electrodag 501, used on the Type B MLI blankets, which is an electrically conductive black paint made of fluorinated binder [95]. Another coating used for this architecture is Chemglaze Z306, a black paint [97] present on all the surfaces but the central cylinder. Finally, as already mentioned, the radiators are covered by PSG 120 FD white paint, a coating characterized by high ratio emissivity over solar absorptivity, needed during the parking phase.

¹⁰the differences between PLM and SVM have already been treated in Section 4.1

Furthermore, the heating lines are regulated by dedicated thermistors, while a series of mechanical thermostats has been integrated into the design to ensure resilience against exceedingly high temperatures and software failures accompanied by heater malfunctions [80].

5.2 TCS Design and Justification

The *rationale* adopted for the TCS architecture originates from the strict pointing requirements imposed by the payloads and by the autonomy requirement, which are both crucial drivers for the mission design.

Firstly, the TCS shall be mostly passive, enhancing reliability by strategically minimizing power usage, reserving active technologies solely for specific components or instruments requiring rigorous environmental control. To mitigate structural distortions, caused by variable loads, all the payload units locations must be optimised to regroup all units belonging to the same experiment on the same panel or on adjacent ones, with an autonomous internal control system. The remaining TCS components rely on heaters, finely tunable active components strategically placed throughout critical zones [48] [82]. Radiators, as explained in Subsection 5.1.2, are placed on deep space facing sides to ensure that they can efficiently emit heat into the vastness of space without being obstructed by other components or structures on the spacecraft. This helps preventing overheating and maintaining optimal operating conditions for the spacecraft's systems.

All the various types of MLI blankets and coatings shall be chosen guaranteeing: no contamination of the PLM experiments, thermal stability between PLM and SVM, electrical conductivity and minimal heat interchange with the PLM, including reflection of external sheets of MLIs. For these reasons, the MLI shall be realized with embossed kapton, offering benefits in terms of both contamination risk and mass budget when compared to classical MLI with flat kapton plus spacer.

Because of the Sun-facing configuration, the Sunshield shall be placed on the $+X_b$ panel (as said in Subsection 5.1.2), covering the S/C Sun-facing side and simultaneously accomplishing the task of protecting the most Sun exposed parts thanks to highly reflective materials and removing excessive solar inputs. It also acts as a radiator for the instruments and electronics mounted on the $+X_b$ panel [80]. It can be assumed that the only significant source of thermo-optical degradation comes from the Sunshield, because of the increasing value of the absorptivity over time. This phenomenon is due to several factors like UV and cosmic particles, the importance of which is magnified by the presence of contaminants, like glue residues, deposited on the glass. The end result is a modification of the Sunshield temperature, which creates both a change in the thermal maps of the upper (Sun-facing) part of the PLM structure and thus thermo-elastic distortions, but also direct thermo-elastic effects coming from the distortion of the Sunshield panel itself, although some kind of mechanical decoupling has been inserted between this panel and the rest of the structure.

To compensate for the temperature differences on this component and prevent optical and structural distortions, Sunshield heaters, with a flexible power adjustment, shall be placed underneath it. In order to satisfy a thermo-elastic stability, to maintain a stable S/C pointing and to counteract experimental additional uncertainties, substitution heaters are attached to the instrument units and to other subsystem electronics, minimizing any modification of the thermal gradients caused by their switching on/off and keeping them in the right operating temperature range. For the same reason, structural heaters must also be placed on each lateral panel section, guaranteeing a homogeneous temperature across the various panels [75].

5.2.1 Thermal Ranges and Phases

In order to achieve the mission goals, it is important to maintain each component of the S/C within its operational thermal range, reported in Table 24, and to protect them from the internal and external thermal fluxes throughout the entire mission listed in Table 25.

Component	Operational temperature ranges [°C]	
	Minimum	Maximum
Batteries (Ni-Cd)	-30	55
PLM/SVM interface	15	25
Power Unit	-20	50
Power Box Baseplates	-10	50
Reaction Wheels	-10	40
Gyros	0	40
Star Tracker	0	30
OBDH Box Baseplates	-20	60
Hydrazine Tanks and Lines	15	40
Antenna Gimbals	-40	80
Antennas	-100	100
Solar Panels	-150	110
Data Processing Units	-20	50
Sun Sensors	-30	50

Table 24: Operational temperatures of S/C components

In the table above, the data highlighted in yellow are taken from datasheet [88] and from literature [2], while the others are typical thermal requirements found in literature [48].

Phases	Description	Heat source	Heat sink
LEOP	Launch and Early Orbit Phase	Sun, Earth albedo, Earth IR, internal power	Deep Space
TTP	Transfer Trajectory Phase	Sun, internal power	Deep Space
HOP	Halo Orbit Phase	Sun, internal power	Deep Space

Table 25: Fluxes along the mission phases

During the LEOP and the insertion in the transfer orbit, the Earth presence in the near surroundings of the spacecraft implies non negligible contributions of albedo and IR radiations, that add up to the solar input and to the internal power of the units. Moreover, during LEOP, the S/C configuration is totally different from the thermal point of view with respect to principal nominal operational phases [80]. Instead, during the HOP and the majority of TTP, the S/C is $+X_b$ Sun oriented with solar arrays open. The distance from the Earth suggests to consider no external heat input other than direct solar. Concerning the internal power contribution coming from the S/C units, its value is higher compared to previous phases since the SOHO spacecraft only activates its instruments entering the halo orbit, as will be detailed in Subsection 5.3.2

5.2.2 Units Specifically Controlled

Here below the temperature ranges of the main subsystems are analyzed more in detail, along with the corresponding TCS solution designed to ensure their maintenance:

- **Payload:** since the ground assembly temperature is 20°C, the mean instrument temperature shall be 20°C in orbit, in order to prevent expansion or contraction of the structure relative to the assembly and calibration conditions. To guarantee an adequate thermal environment the instruments are mounted on isostatic mounts on the four lateral panels $\pm Z_b / \pm Y_b$ and under the $+X_b$ panel of the PLM, covered in MLI. For achieving a satisfactory thermal stability even for the most demanding instruments, it is required a specific heating concept which avoids the classical switch on/off regulation but which is powered over a cycle of 10 seconds, with a duty cycle varying between 0 and 100% [82]. A major thermal design requirement is provided by the Charge Coupled Device (CCD) detector which requires an operational temperature of less than -80°C to limit dark current to acceptable levels [79]. This results in the need of thermally decoupling this component and the immediate environment, which runs at vastly different temperatures. For this purpose, the thermal control embeds a passive radiator and a fixed power heater [83], and specific materials are selected for their isolation properties, such as titanium and copper [99]. Moreover, the PLM/SVM interface is set to be at a temperature of 20 °C \pm 5 °C [2], to achieve a decoupling.
- **Propulsion subsystem:** for this subsystem the temperature requirements are derived from two constraints, the temperature range of the fuel and the design temperature of the Flow Control Valve (FCV), defined by the manufacturer. As already known, SOHO's thrusters use hydrazine as monopropellant; therefore, a lower temperature limit of 5°C needs to be imposed due to hydrazine's freezing point. Furthermore, an operating temperature range of the FCV before firing from 9 °C to 90 °C can be found in literature [77]. In order to ensure these temperatures, an MLI enclosure with a dedicated radiative window is envisaged for the thermal control of the FCV, and a TCS heater is mounted on the FCV to cope with cold environmental conditions avoiding to reach the freezing condition of hydrazine.
- **TMTC subsystem:** the thermal control requirements for antennas usually involve ensuring that temperatures remain within the acceptable range for the materials utilized in their construction. In particular, solid-dish antenna reflectors like the HGA installed on SOHO spacecraft, are generally painted white on the exposed reflecting side and covered with MLI on the back. This thermal control strategy limits the thermal distortions due to uneven illumination of the dish, that degrade RF-beam quality. On the other hand, helix antennas, such as the LGA on SOHO, have usually less severe distortion problems compared to dish reflectors ones; therefore, they do not present challenging thermal design problems. Indeed, helix antennas temperatures can generally be maintained with paints and bare metal finishes [91].
- **AOC subsystem:** each sensor is individually controlled i.e. isolated from the S/C structure through isostatic mounts. The Sun sensors usually have the inside face painted black to give good thermal coupling to the relatively stable temperature of the internal spacecraft hardware. Concerning the star sensors, they not only require an operating temperature range (Table 24) but they also include limitations on temperature gradients which could misalign the optical elements.
- **EP subsystem:** in order to limit the structural thermal gradients, some S/S electronics are accommodated on the 3 lower lateral panels $\pm Z_b$ and $-Y_b$, well decoupled conductively from the upper panels. Their temperature has to be as close as possible to the panels temperature of 20°C, achieved through MLI blankets application. These units are thermally controlled through a single black Kapton sheet radiator. When non-operational, the temperature of the electronic subsystem is maintained by a S/C powered substitution heater (described in Section 5.1.2) through duty cycle adjustment. Instead, for the electronics mounted on the $+X_b$ panel, the Sunshield facing the Sun acts as a radiator [75]. Regarding the Ni-Cd batteries, most of the times they are simply painted black to radiate the waste heat from charge and discharge inefficiencies to the spacecraft interior [91].
- **OBDH subsystem:** in order to avoid degradations coming from the radiation environment of the space [100], these units are protected by a shielding made of dense metals that absorb and deflect the radiation.

5.3 TCS Reverse Sizing

SOHO satellite has almost the shape of a rectangular parallelepiped, whose dimensions are $4.3 \times 2.7 \times 3.7 \text{ m}^3$ [80] with a total surface area of $A = 75.02 \text{ m}^2$. To develop a baseline understanding of modelling the thermal dynamics of the SOHO satellite and simplify its calculation, the following assumptions are made:

- an analysis employing a **single-node** and **lumped mass** approach is conducted. In this method, the satellite is simplified as an equivalent sphere having the same total surface area of the S/C. The resulting radius, computed starting from the knowledge of the total area, is $r = 2.44 \text{ m}$, with a corresponding cross-sectional area of $A_{cross} = 18.76 \text{ m}^2$. Simplifying the spacecraft architecture to a sphere overlooks the variety of possible configurations of passive and active elements. Its focus is on determining the necessity, rather than the specifics, of these elements in maintaining the spacecraft within acceptable temperature thresholds. Additionally, this simplification neglects the potential for different emitting or absorbing areas. Finally, the model assumes uniform material and temperature distribution across the spacecraft, disregarding differences arising from distinct surface orientations toward the Earth, the Sun or the deep space;
- both the hot and cold cases are examined under **steady state conditions**. This implies that temporal changes in the thermal equilibrium equation are disregarded, and any transient behaviour is deemed insignificant. This will be further discussed in Subsection 5.3.1;
- prior to its transfer trajectory injection, SOHO remains connected to the Centaur, resulting in a thermal configuration and control strategy that significantly deviates from the standard setup, with the majority of subsystems and all instruments still inactive. For example, the Centaur/SOHO composite rotates at a nominal rate of 0.2 rpm to regulate temperature [80]. Due to these complexities, analyzing this segment requires a more in-depth approach than simple node and steady state approximations. For this reason, the sizing of the TCS takes into account only the TTP, considered only after the detachment from launcher upper stage occurring approximately 35 minutes after the injection in the TT [7], and HOP as candidates for the hot and cold cases selections. This consideration also acknowledges that SOHO's duration in the parking orbit is merely 80 minutes, a brief period compared to the TTP and HOP, which highlights the importance of focusing on these phases.

Thus, the mono-node analysis serves primarily as an initial tool for grasping the thermal dynamics of the spacecraft, since it cannot be considered a realistic model for the heavy simplifying hypotheses considered. To ensure that the SOHO subsystems and components are fully operational from TCS point of view, the related operating temperature ranges must be of primary concern. Their values are reported in Table 24. For the analysis, the temperature must remain between $T_{min} = 15^\circ\text{C}$ and $T_{max} = 25^\circ\text{C}$, which are the maximum of minimum and minimum of maximum temperatures in the analysed ranges. Since this range is already quite strict, no margins have been added. In case this range results in unrealistic outcomes, the possibility of excluding the most restrictive units from the mononodal analysis may be considered to broaden the thermal range. However, these units would still be relevant for subsequent development, such as a multi-nodal analysis.

5.3.1 Hot and Cold Case Selection

The initial stage of the preliminary sizing involves the selection of the hot and cold cases. Excluding the parking orbit (as previously explained) from consideration, it becomes evident that the albedo and Earth IR heat fluxes can be neglected at first glance, due to their insignificance compared to the solar heat flux as also previously stated in Table 25. Consequently, the selection of the hot and cold cases focuses on analyzing the solar heat flux, which is more intense closer to the Sun. Hence, it is straightforward that the hot case corresponds to when the spacecraft is the closest to the Sun, namely in the halo orbit around L_1 , where also all instruments and subsystems are fully operational, while the cold case occurs at the beginning of the transfer when the satellite is farther from the Sun and not performing any scientific observation.

Solar radiations play a crucial role in the present sizing, thus, it is reasonable not to rely on medium approximation blindly. It can be noticed that the launch is foreseen during a minimum of solar cycle¹¹. The identified cold case is approximately near the launch, so the minimum value for the solar constant $q_{0,min} = 1321.6 \text{ W/m}^2$ at 1 AU can be taken into account. Furthermore, the extension of the mission for an additional 6 years was already foreseen during the design phase to exploit the chance to cover the entirety of the solar cycle. Therefore, the most sizing condition for the hot case is certainly in correspondence with maximum solar activity, modelled with a solar constant of $q_{0,max} = 1412.9 \text{ W/m}^2$ at 1 AU.

5.3.2 Heat Fluxes and Powers

To proceed with the analysis, both external and internal heat fluxes (and associated powers) must be determined. Even though in both hot and cold cases IR and albedo fluxes are negligible, they are still modelled to prove it. The heat flux coming from the Sun is modelled as follows:

$$q_{Sun-SC} = q_0 \left(\frac{R_{Earth}}{R_{SC}} \right)^2 \quad (10)$$

Where q_0 is the solar flux at 1 AU, which has already been fixed to $q_{0,max}$ for the hot case and $q_{0,min}$ for the cold case. R_{SC} is the distance of the spacecraft from the Sun, which is properly normalized by R_{Earth} , the distance of the Earth with respect to the Sun. The albedo heat flux is retrieved as:

¹¹This has already been treated in Section 1.9

$$q_{\text{albedo},E} = q_{\text{Sun-SC}} \cdot a \cdot \cos(\theta) \left(\frac{R_{PL}}{R_{\text{orbit}}} \right)^2 \quad (11)$$

Where R_{orbit} is the spacecraft orbital radius, expressed with respect to the centre of the planet around which the S/C is orbiting, R_{PL} is the radius of the planet considered which, in SOHO case, is the Earth and $R_{PL} = 6371 \text{ km}$. The irradiance angle between the spacecraft and the planet is θ and in the preliminary sizing adopted it is considered null, while a is the albedo factor. Considering the Earth planet, the tabulated albedo factor is within the interval [0.31, 0.39] [48], and the value of $a = 0.35$ was chosen to obtain average results. The IR flux coming from the planet Earth is computed as:

$$q_{IR,PL} = \sigma \varepsilon_{PL} T_{PL}^4 \left(\frac{R_{PL}}{R_{\text{orbit}}} \right)^2 \quad (12)$$

Where $\sigma = 5.67 \cdot 10^{-8} \frac{\text{W}}{\text{m}^2 \text{K}^4}$ is the Boltzmann constant and T_{PL} is the surface temperature of the planet, assumed equal to 250 K. The ε_{PL} is the infrared emissivity of the planet considered. For the Earth, ε_{PL} can range between 0.6 and 1 [89]; the value of 1 is chosen following the conservative sizing philosophy. To determine the coldest point along the transfer, a linear variation for R_{SC} (distance from the Sun) and R_{orbit} (distance from the Earth) is assumed. Starting from Earth's radius (1 AU), R_{SC} decreases to 0.990 AU at the L_1 point, while R_{orbit} increases from the parking orbit radius (180 km above Earth) to the L_1 point (0.01 AU). This leads to identifying a point at 0.999 AU from the Sun, assumed to be after Centaur detachment, confirming the hypothesis from Subsection 5.3.1. Instead, the analysis of the halo orbit is performed by considering the S/C in the L_1 point. In Table 26 the results are reported.

Phase	Case	Distance from Sun	$q_{\text{Sun-SC}}$ [W/m ²]	$q_{\text{albedo,E}}$ [W/m ²]	q_{IR} [W/m ²]	q_{tot} [W/m ²]
TTP	Cold	0.999 AU	1323.97	1.05	0.50	1325.52
HOP	Hot	0.990 AU	1441.71	0.01	3.98×10^{-3}	1441.72

Table 26: Heat Fluxes in hot and cold cases

Having determined the external heat fluxes, the **external heat powers** are retrieved as:

$$Q_{\text{Sun-SC}} = A_{cross} \alpha q_{\text{Sun-SC}} \quad Q_{\text{albedo,E}} = A_{cross} \alpha q_{\text{albedo,E}} \quad Q_{IR} = A_{cross} q_{IR,PL} \varepsilon \quad (13)$$

Where A_{cross} is the cross-sectional area previously computed from the equivalent sphere, $\alpha = 0.0064$ and $\varepsilon = 0.0018$ are the absorptivity in the visible and emissivity in the infrared coefficients of the spacecraft. These values are assumed equal to the ones of the Type A of MLI, already described in Subsection 5.1.2, which covers the majority of the S/C surfaces. In order to model its optical properties, a series of radiative resistances is considered using the following formula [84]:

$$\varepsilon = \left(\frac{1}{\varepsilon_{int}} + \frac{1}{\varepsilon_{ext}} - 1 + \left(\frac{2}{\varepsilon_{lay}} - 1 \right) N \right)^{-1} \quad (14)$$

Where $N = 14$ is the number of the internal layers having $\varepsilon_{lay} = 0.05$, $\varepsilon_{int} = 0.4$ is the emissivity of the innermost layer, $\varepsilon_{ext} = 0.72$ the emissivity of the outermost layer [85] [94]. Regarding α , this is retrieved by knowing the typical ratio α/ε , for the aluminized Kapton MLI of 3.5 [87]. These low values highlight the insulation capabilities of the MLI with respect to the external environment. Furthermore, it can be assumed that all the power produced at some point becomes thermal energy. Therefore, in the initial modelling stage, the entirety of the produced power should be considered as the **internal heat power**. From literature [75], it is deduced that the total power required by the spacecraft instruments is 479 W and from the SVM subsystems is 424 W. Due to the fact that SOHO activates its instruments only after reaching the halo orbit, the power allocated to the instruments can be disregarded until it reaches the L_1 point.

In Table 27, the main results regarding the heat powers for the cold and hot cases of the mission are summarized.

Phase	Case	Distance from Sun	$Q_{\text{Sun-SC}}$ [W]	$Q_{\text{albedo,E}}$ [W]	Q_{IR} [W]	Q_{internal} [W]	Q_{tot} [W]
TTP	Cold	0.999 AU	158.34	0.12	0.02	424	581.48
HOP	Hot	0.990 AU	172.42	1.09×10^{-3}	1.36×10^{-4}	903	1074.40

Table 27: Heat Powers in hot and cold cases

The numerical analysis clearly indicates that the fluxes related to Earth albedo and IR Earth emission, along with their respective powers, are negligible as expected. This reaffirms the hypotheses previously established during the selection of hot and cold cases. Moreover, the analysis confirms the thermal stability of the environment: as a matter of fact the discrepancy between the hot and cold cases is dictated primarily by the internal generated power rather than the external one, also due to the fact that there are no eclipses. These, in fact, would have a large impact on the incoming heat flux discrepancy.

5.3.3 Passive Control

The following step of the analysis is the sizing of the passive thermal control starting from the hot case condition. Therefore, it is necessary to identify the A_{rad} required to guarantee the S/C to stay within the limit set by the T_{max} . By imposing the steady state equilibrium for the hot case, the following relation is obtained:

$$Q_{tot,HOT} - Q_{emitted,HOT} = 0 \Rightarrow T_{SC_{hot}} = \sqrt[4]{\frac{Q_{tot_{hot}}}{\sigma \varepsilon A} + T_{DS}^4} \quad (15)$$

Where A is the total surface area of the S/C (mono-node) and $T_{DS} = 3 K$. The only unknown is the maximum temperature reached by the S/C, which can be computed as reported in the second equation. This is found to be $T_{SC_{hot}} = 610.2 K$, which is higher than the allowed value T_{max} . The minimum area of the radiators needed to guarantee to stay within the maximum allowed temperature $T_{SC_{hot}} = T_{max}$ is the only unknown in the following equation:

$$Q_{tot_{hot}} = \sigma \varepsilon A_e (T_{max}^4 - T_{DS}^4) + \sigma \varepsilon_{rad} A_{rad} (T_{max}^4 - T_{DS}^4) \quad (16)$$

Where $A_e = A - A_{rad}$ is the area of the S/C not covered by the radiators. Additionally, according to the reference [80], the radiators are coated with PSG 120 FD white paint, which has an emissivity of $\varepsilon_{rad} = 0.88$ [93]. The area found is $A_{rad} = 2.57 m^2$ and corresponds to the 3.43% of the total area A of the S/C, therefore it is an acceptable value. The heat power emitted by the radiators is computed as $Q_{rad} = \sigma \varepsilon_{rad} A_{rad} (T_{max}^4 - T_{DS}^4)$ and is found to be $Q_{rad} = 1015.27 W$. It can be observed that typically most spacecraft radiators reject $100 - 350 W/m^2$, while in this case the amount is slightly higher, corresponding to $394.28 W/m^2$. This discrepancy may arise from the simplification inherent to the mono-node analysis discussed earlier, which overlooks the heterogeneous materials and temperatures in the actual spacecraft configuration.

5.3.4 Active Control

After the computation of the minimum required area of the radiators found relative to the hot case, it is necessary to evaluate the need to introduce heaters dictated by the study of the cold case, considering the coupled problem where both heaters and radiators would be present. In the first step, as already done for the hot case, the minimum temperature reached by the S/C can be retrieved from the cold case equilibrium at steady state condition:

$$T_{SC_{cold}} = \sqrt[4]{\frac{Q_{tot_{cold}}}{\sigma(\varepsilon A_e + \varepsilon_{rad} A_{rad})}} + T_{DS}^4 \quad (17)$$

Since $T_{SC_{cold}} = 255.73 K$ is lower than T_{min} , then the presence of heaters is required to ensure the proper working condition for the SOHO components also in the cold case. The minimum power furnished by the heaters to maintain SOHO within the acceptable temperature range, by imposing $T_{SC_{cold}} = T_{min}$, is computed as:

$$Q_{heaters} = \sigma (\varepsilon A_e + \varepsilon_{rad} A_{rad}) (T_{min}^4 - T_{DS}^4) - Q_{tot_{cold}} \quad (18)$$

The resulting power $Q_{heaters} = 355.87 W$ appears reasonable compared to the actual power demand of the TCS subsystem, which is $303 W$ [75], considering it is solely allocated to heaters, the only active component. As a concluding note, in the typical TCS sizing process, the active strategy is often the final consideration due to its reliance on onboard power. In fact, a more refined multi-node analysis can be run on critical nodes, which means S/C components whose acceptable range is not respected by the spacecraft temperature $T_{SC_{cold}}$ calculated. This may result in finding a passive strategy to maintain the S/C within the prescribed range, thus, reducing the amount of power needed by the TCS.

5.3.5 Mass, Power and Data Budget

After having determined the area of the radiators and the power required by the heaters it is possible to make an estimation of the mass. Firstly the MLI mass can be determined from the knowledge of the areal density of each layer [85], as follows:

$$M_{MLI} = (\sigma_{ext} + \sigma_{lay} \cdot N + \sigma_{int}) \cdot (A - A_{rad}) \quad (19)$$

Where the considered surface area is the one only covered by the MLI, thus excluding the radiator surface, and $N = 14$ is the number of the internal layers. Considering the areal density of a general radiator panel, $\sigma_{rad} = 3.3 kg/m^2$ [48], the radiator mass can be retrieved as:

$$M_{rad} = \sigma_{rad} A_{rad} \quad (20)$$

Finally, the mass of the heaters can be estimated starting from the knowledge of the required power, considering the following equation:

$$M_{heaters} = \frac{Q_{heaters}}{\Pi_{heaters}} \sigma_{heaters} \quad (21)$$

Where $\sigma_{heaters} = 2 kg/m^2$ is the areal density [86] and $\Pi_{heater} = 1 \cdot 10^4 W/m^2$ is the heater power density. This value is taken within the range in literature [101] for a selected Kapton technology, a classical choice for heaters. No information could be retrieved on the data budget regarding the sized elements, therefore the data assumed for the thermal control subsystem are taken from literature [48] and are based on 1750A-class Instruction Set Architecture. This is reasonable since the 1750A is a general-purpose processor and it is the one used in SOHO mission [76], thus, the numbers reported represent a good first estimate. The results of the analysis are reported in Tables 35 and 29:

Size [Kwords]		Typical Throughput [KIPS]	Typical Execution Frequency [Hz]
code	data		
0.8	1.5	3	0.1

Table 28: Data Budget of TCS

	MLI	Radiators	Heaters	Total
Mass [Kg]	14.78	8.50	0.07	23.35
Power [W]	0	0	355.87	355.87

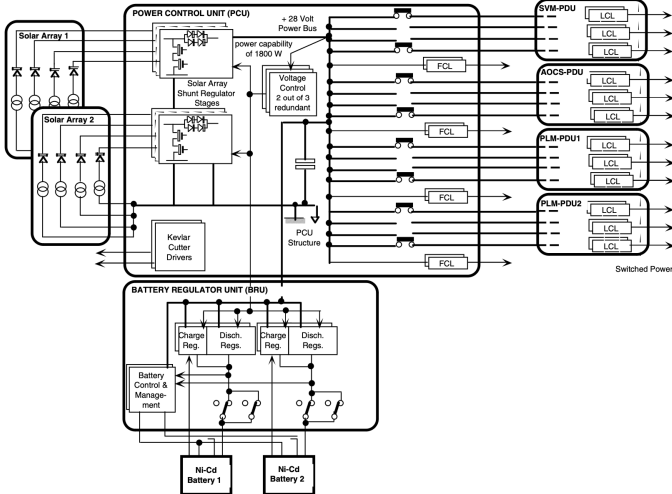
Table 29: Mass and Power Budget of TCS

The mass budget corresponds to the 1.45% of the dry mass, which is less than the typical values in the range 2 – 10% [48], probably due to the assumptions made to perform the mono-nodal analysis.

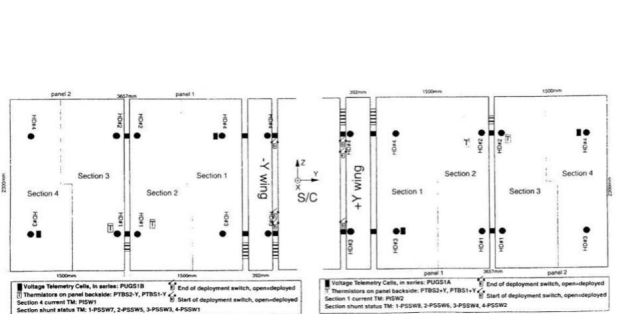
6 EP Subsystem

6.1 EPS Architecture

The SOHO electrical power system has to regulate, distribute and control power from its solar array panels and two Ni-Cd batteries [103]. In the following figures the SOHO EPS general architecture 15a and solar panels layout 15b are shown:



(a) The SOHO Electrical Power System



(b) The SOHO Solar array layout and dimensions

The SOHO power subsystem supplies 28 V regulated power to the spacecraft from a four-panel solar array with silicon cells (initially 1500 W) and two batteries with 20 Ah each and of 32 cells. A Battery Regulator Unit (BRU) manages battery charge and discharge. The Power Control Unit (PCU) handles central power regulation, while 112 Latching Current Limiters (LCLs), located in four Power Distribution Units (PDUs), manage power distribution [102]. Subsequent sections provide detailed explanations of these components.

6.1.1 Power Sources Architecture

In the list below the main sources of power of SOHO are presented in detail:

- **Solar Array (SA):** the solar array is the **primary power source** of SOHO and it has two deployable wings along $\pm Y_b$, each with two $1.5 \text{ m} \times 2.3 \text{ m}$ rigid panels and one yoke panel as shown in Figure 15b. The silicon solar cell network has two independent electrical sections per panel, totaling eight for overall the array. Each section has four double strings: three with two cells in parallel and 77 in series, and one with two cells in parallel and 78 in series. Each double string includes two blocking diodes, and shunt diodes are placed in parallel for blocks of 12 or 13 double parallel cells. The array is a $2 \Omega \text{cm}$ BSR silicon cell ($3.78 \text{ cm} \times 6.38 \text{ cm}$) with an attendant $100 \mu\text{m}$ CMX cover glass¹² and $20 \mu\text{m}$ thick silver interconnections with stress relief loops. Each section provides a minimum of 6.3 A to the 28 V power bus at end-of-life [113].
- **Ni-Cd Batteries:** the two batteries represent the **secondary power source** of SOHO and each of them consists of 32 series-connected, 20 Ah nickel-cadmium cells. Placed in the Service Module (SVM), these higher-mass rechargeable batteries are chosen to fulfill peak power demands throughout the mission and to provide limited energy in case of significant spacecraft Sun de-pointing [103].

6.1.2 Power Regulation and Control

The power regulation of the S/C and the power control are guaranteed by the following units [103]:

- **Power Control Unit (PCU):** the main DC power bus of SOHO is regulated to $28 \text{ V} \pm 1\%$ by PCU, functioning as an integrated shunt, charger and discharger for direct energy transfer. Regulation employs a 'majority voted', three-domain analog control loop. As bus demand rises, dormant SA sections are progressively activated, and battery discharge regulators supply power when necessary. The SA shunt employs the Sequential Switching Shunt Regulator (S3R) concept, with eight serial redundant dump switches per electrical section. When operating, the shunt regulator selects the required number of SA sections to meet the spacecraft load and battery charging requirements. The imprecise selection often results in either an excess or deficiency of current to the main bus, causing continuous modulation of one of the eight dump switch pairs. The SOHO PCU also manages main bus load switching and power distribution, including redundant Foldback Current Limiters (FCLs) for the spacecraft's command receivers/decoders and attitude control failure detection electronics. Additionally, conventional power relays activate the power bus for the four downstream PDUs.

¹²CMX cover glasses are thin, transparent and brittle materials cerium doped that protect the solar cells from the harmful UV, proton, and electron radiations present in space condition [104]

- **Battery Regulator Unit (BRU)**: it is a separate equipment consisting of six multi-cavity power hybrids, which are four battery discharge regulators and two battery charge regulators, along with discrete electronics for each spacecraft battery. During normal operations, when battery voltages exceed power bus voltages, each battery discharge regulator includes an input current limiter and a PWM 'buck' regulator with its own current control loop. Furthermore, protection circuitry automatically deactivates any faulty battery discharger module with full angle output drive. The two battery charge regulators feature a 'buck' switching circuit for controlled charge current, followed by a push-pull inverter and rectification stage. The 'buck' stage of the charge regulator automatically limits input and output current to safeguard the main power bus from failures in the push-pull or DC output stage. Additionally, for protection purposes, circuitry switches the BCR on/off in case of overcurrent detection. This is achieved by detecting a current exceeding 5.6 *amps* in the return line of the stage inverter. Lastly, the BRU houses battery management electronics, including programmable, temperature-compensated end-of-charge (EOC) level, battery overtemperature, and over/undervoltage detectors.

6.1.3 Power distribution

The four PDUs, two in the SVM and two in the Payload Module (PLM)¹³, use electronic Latching Current Limiters (LCLs) for output power switching. Each unit receives four independent power feeds from the PCU: two lines with 12 redundant LCLs for electronic load/experiment switching, and two lines with 16 redundant LCLs for spacecraft heater loads [103]. The electrical subsystem of SOHO revolves around two main buses: the On Board Data Handling (OBDH) data link and the dedicated 28 V regulated power line. Interfaces between these buses and subsystems/experiments use standard units: Remote Terminal Units (RTUs) for data links and Power Distribution Units (PDUs) for power buses [2]. In particular, one PDU is dedicated to the OBDH, one to the Attitude and Orbit Control Subsystem (AOCS), and two to the PLM, achieving a modular design for each spacecraft major component. In addition, all unit communications use isolated links (relays or opto-couplers), or differential lines using a Standard Balanced Digital Link (SBDL).

6.1.3.1 SVM-PLM modularity

To ensure a modular approach for the PLM and SVM, dedicated service electronics units (2 PDUs and 1 RTU) are installed on the PLM. The two PLM PDUs offer 2 x 26 power lines for the experiments' main supply, with one main and one redundant power line for each experiment [82]. Design features, such as the *keep alive line*, ensure continuous low current for maintaining essential equipment functions and prevent lengthy software reloading processes. As for the TCS, the PDUs also power the various heater circuits of the PLM's thermal control. All power lines are divided into 8 buses (4 for each PDU) to provide nominal and redundant configurations for easy reconfiguration in case of anomalies. The RTU provides interface signals for each experiment, including telecommands (on/off, memory load, OBDH block commands) and telemetry. It also handles temperature acquisition for all thermistors used in PLM thermal control. At the PLM integration level, the PDUs and RTU are connected to a SVM simulator, which replicates the SVM's data handling subsystem interfaces (OBDH bus, acquisition and sending of telemetry packets, telecommands, timing functions) and power subsystem interfaces (power supply to PDUs with protections and monitoring).

6.2 EPS Design and Justifications

The EPS design *rationale* revolves around providing continuous electrical power throughout the spacecraft's operational life, considering its 3-axis stabilization, modularity, and available power sources.

Solar panels are strategically positioned in the $\pm Y_b$ direction in order to maximize sunlight exposure, as the spacecraft always faces the Sun along its $+X_b$ direction. This is also the reason why SAs are chosen as **primary energy source**. Opting for solar panels over a RTG is logical due to the spacecraft's consistent Sun-pointing ability and safe distance, ensuring ample solar flux for power generation without risking damage to the solar cells from proximity. Silicon solar panels are chosen for their cost-effectiveness and reliability in space missions, despite requiring larger arrays and additional mass compared to gallium arsenide cells. Additionally, the spacecraft's 3-axis stabilized configuration favours rigid deployable solar arrays because of their higher performance and no area constraints, but they necessitate Sun sensors, deployment and rotational mechanisms [86].

At the time of the design phase, Nickel-based batteries, including Ni-H₂ and Ni-Cd, were commonly used [105]. Ni-H₂ batteries offer higher energy density, longer lifecycle and greater reliability, while Ni-Cd batteries are lighter, cost-effective and have better packing efficiency and lower self-discharge rates. For power demands below 1-2 kW, Ni-Cd batteries are preferred due to their efficiency and cost-effectiveness, while Ni-H₂ batteries are chosen for higher power demands exceeding 2 kW. Consequently, Ni-Cd batteries are selected as the **secondary energy source** for providing power during the initial acquisition phase and for peak power requirements [2]. Batteries are nominally never used during the mission due to the absence of eclipses and the unlikelihood of significant Sun de-pointing, as assumed during the design phase [102]. The choice of rechargeable batteries over primary ones is motivated by the necessity to meet peak power demands and the advantage of retaining limited energy even in the event of significant Sun de-pointing [103].

The EPS component selection emphasizes **standardization** and **high modularity** for efficient power distribution, as already pointed out in Subsection 6.1.3.1. This philosophy is dictated by the need of facilitating early interfaces validation

¹³The difference between the Payload Module and the Service Module has already been treated in Section 4.1

and making them independent of the integration level. In the PLM, complex experiment interfaces require parallel development and testing with the SVM, highlighting the autonomy and decoupling between modules. Dedicated electronic units in the PLM facilitate this strategy and reduce interface debugging at integration levels [82]. A combination of nominal and redundant power buses within each PDU maintains consistent dissipation, preserving thermo-elastic stability of the PLM during bus reconfiguration.

Concerning **bus configuration**, three main typologies are available: unregulated, sunlight regulated and fully regulated. As spacecraft power requirements increase, the fully regulated solution, although more complex, is preferred for its flexibility. In the case of SOHO, that has a power demand below 2000 W but still significant, the power distribution relies on a standard regulated 28 V bus [48]. This choice is also dictated by the need for standardization in the power distribution unit, a philosophy that guided the design of the EPS, as already pointed out. Regarding **power control techniques**, two primary power control techniques are considered: Direct Energy Transfer (DET) and Power Peak Tracker (PPT). DET, chosen for SOHO, is favored for its lightweight design and efficiency, suitable for high-power requirements and extended missions exceeding 5 years. However, DET can face lock-up issues due to its fixed operating point regulated by a shunt regulator. DET transmits power directly from solar panels to loads, prioritizing simplicity and efficiency while avoiding complexities and potential failure modes associated with a PPT integrated into the main power bus [86].

6.2.1 Operational Profiles and Power Budget

To size the EPS system, a power budget breakdown of the SOHO mission has been conducted for each subsystem in each phase and each mode, considering the operational profiles in Table 30 whose reasoning behind is described in the following lines.

Subsystem	LEOP					TTP					HOP				
	ISA	Corrective manoeuvre	ESR	CRP	RMW	NM	ESR	CRP	RMW	NM	ESR	CRP	RMW	NM	ESR
AOCS	gyros	SASs, gyros	FPSS, Star Tracker, gyros	SASs,gyros	FPSS,gyros,RWs	FPSS, Star Tracker,gyros,RWs(desat)	FPSS, Star Tracker,RWs	SASs,gyros	FPSS,gyros,RWs	FPSS, Star Tracker,gyros,RWs(desat)	FPSS, Star Tracker,RWs	SVM,PLM	SVM,PLM	SVM,PLM	SVM
TCS	SVM	SVM,PLM	SVM,PLM	SVM,PLM	SVM,PLM	SVM,PLM	SVM,PLM	SVM,PLM	SVM,PLM	SVM,PLM	SVM,PLM	SVM,PLM	SVM,PLM	SVM,PLM	SVM
TMTI	X	X	✓	✓	✓	✓	✓	✓	✓	✓	✓	✓	✓	✓	✓
OBDH	✓	✓	✓	✓	✓	✓	✓	✓	✓	✓	✓	✓	✓	✓	✓
Propulsive	X	8thrusters (A-branch)	8thrusters (A-branch)	4thrusters (B-branch)	X	8thrusters (A-branch)	X	4thrusters (B-branch)	X	8thrusters (A-branch)	X	8thrusters (A-branch)	X	8thrusters (A-branch)	X
EPS	✓	✓	✓	✓	✓	✓	✓	✓	✓	✓	✓	✓	✓	✓	✓
PAYOUTLOAD	X	X	X	X	X	X	X	X	X	X	X	X	X	X	✓
Energy source	Batteries	Batteries	Solar Panels	Solar Panels	Solar panels	Solar Panels	Solar Panels	Solar Panels	Solar Panels	Solar Panels	Solar Panels	Solar Panels	Solar Panels	Solar Panels	Solar Panels

Table 30: Operational Profiles

During **LEOP**, after lift-off, the spacecraft is powered by the batteries which activate only the OBDH, the gyroscopes (IRU) and the SVM thermal control. Concerning the **TTP**, the first mode temporally encountered is the ISA: after the separation from the Centaur, the AOCS cancels the angular rates imparted by the separation and coarsely aligns the spacecraft towards the Sun using hydrazine thrusters and Sun-acquisition sensors. Until the deployment of the SA, occurring just after ISA, communication is not available. In all the subsequent modes and phases, it is considered to be always active, since it is of vital importance. After full solar-panel deployment has been achieved, the AOCS performs the transition to the NM where fine Sun pointing and roll-angle control are performed using a fine-pointing Sun sensor, a star tracker and three reaction wheels [9]. During the TTP also corrective manoeuvres should be taken into account. The attitude sensors are considered to be the same as in the NM, since impulses are planned to have always the Sun in the FOV of the FPSS but, being a ΔV manoeuvre, the S/C is controlled by the thrusters [42], whose presence is always associated to the one of the gyroscopes [114]. Concerning the payload, this is considered to be officially activated only after the insertion in the **HOP**, due to the fact that commissioning ends two months after the insertion. Therefore, the NM in the HOP is nominally equal to the one described in the TTP with the difference that the payload is active. During the TTP, RMW is primarily concerned with the desaturation of the RWs, while during the HOP it involves both Station Keeping (SK) manoeuvres and RW desaturation, which are planned to occur simultaneously. During this mode the payload is switched off because, according to literature [37], the manoeuvres are planned to be as infrequent as possible to avoid interruption to scientific observation. The AOCS set up, in this case, is the typical one associated to ΔV manoeuvres, as already described for corrective ones, with the difference that the RWs are considered powered since their speed is monitored to predict their future secular variation and next dumping needed [34]. Furthermore, the ESR mode is the final "safety net" for SOHO, where attitude is controlled by SAS-1, thrusters and gyroscopes to maintain a coarse alignment with the Sun. In this mode, only vital subsystems are active (e.g. thermal control, communication, etc) to guarantee that the spacecraft is not harmed or lost. Finally, the CRP mode is the first step "up" from ESR, where the reaction wheels are used for attitude control (i.e. no thruster firings) and FPSS and gyroscopes are used as attitude sensors [63].

Given the lack of specific data regarding the number of thrusters utilized in each mode, it is assumed that there are always eight operational thrusters when the spacecraft is 3-axis stabilized. The exception is the ESR mode, where attitude control is more relaxed and only four thrusters are utilized [41]. Concerning the OBDH, this is considered to be always operational as well as the EPS and TCS, being of primary importance for the survival of the S/C, and they are assumed to have constant power consumption as a first approximation. The latter has the peculiarity that the PLM TCS is switched on only when instruments are not operational, to guarantee a stable thermal environment and avoid causing damage to the payload [75]. Regarding the **power sources**, batteries are basically used only during the LEOP and ISA phases, where solar panels are not deployed yet. After solar array deployment, batteries are nominally never used but they can supply additional power during power peak or a little amount of energy in case of a significant Sun de-pointing, although such event was stated to be non-credible during the design phase [103]. Hence, even during the ESR mode, the solar arrays serve as the primary power source for SOHO. This is because, even in this mode, the spacecraft maintains its alignment with the

Sun to facilitate power generation, although with reduced accuracy. The results of this reasoning are reported in Table 31:

Power Budget Breakdown		LEOP		TTP					HOP				Reference
Subsystem	Total [W]	ISA	CM ¹⁴	ESR	CRP	RMW	NM	ESR	CRP	RMW	NM		
AOCS	140,5	43	43	53,5	43	130,5	140,5	97,5	43	130,5	140,5	97,5	
Star Tracker	10	0	0	10	0	0	10	10	0	0	10	10	[48]
FPSS	0,5	0	0	0,5	0	0,5	0,5	0,5	0	0,5	0,5	0,5	[48]
RWS	87	0	0	0	0	87	87	87	0	87	87	87	[71]
IRU	43	43	43	43	43	43	0	43	43	43	0	0	[73]
SASS	0	0	0	0	0	0	0	0	0	0	0	0	[69]
TCS	303	133	303	303	303	303	303	303	303	303	303	133	
SVM TCS	133	133	133	133	133	133	133	133	133	133	133	133	[75]
PLM TCS	170	0	170	170	170	170	170	170	170	170	170	0	[75]
EPS	90,9	90,9	90,9	90,9	90,9	90,9	90,9	90,9	90,9	90,9	90,9	90,9	
PDUs	50	50	50	50	50	50	50	50	50	50	50	50	[102]
BRU	22	22	22	22	22	22	22	22	22	22	22	22	[102]
FCLs	14,1	14,1	14,1	14,1	14,1	14,1	14,1	14,1	14,1	14,1	14,1	14,1	[103]
PCU	4,8	4,8	4,8	4,8	4,8	4,8	4,8	4,8	4,8	4,8	4,8	4,8	[103]
Propulsive	68	0	68	68	34	0	68	0	34	0	68	0	
Thruster	8,5	0	8,5	8,5	8,5	0	8,5	0	8,5	0	8,5	0	[39]
TMTC	109,5	0	0	109,5	109,5	109,5	109,5	109,5	109,5	109,5	109,5	109,5	
S-Band receiver	17,5	0	0	17,5	17,5	17,5	17,5	17,5	17,5	17,5	17,5	17,5	[48]
S-Band transmitter	40	0	0	40	40	40	40	40	40	40	40	40	[48]
HPA (SSPA)	52	0	0	52	52	52	52	52	52	52	52	52	Section 3
Payload	479	0	0	0	0	0	0	0	0	0	0	479	[75]
OBDH	20,00	20,00	20,00	20,00	20,00	20,00	20,00	20,00	20,00	20,00	20,00	20,00	
Processor	20,00	20,00	20,00	20,00	20,00	20,00	20,00	20,00	20,00	20,00	20,00	20,00	[48]
Total	1210,90	286,90	524,90	644,90	600,40	653,90	731,90	620,90	600,40	653,90	731,90	929,90	
Margin (20%)	242,18	57,38	104,98	128,98	120,08	130,78	146,38	124,18	120,08	130,78	146,38	185,98	
Total with margins	1453,08	344,28	629,88	773,88	720,48	784,68	878,28	745,08	720,48	784,68	878,28	1115,88	

Table 31: Power Budget for phase/mode

A 20% margin has been taken into account for minor components not found in literature and for battery recharging, whose power consumption cannot yet be considered before the effective sizing. Notice that the second column represents a scenario where all subsystems are operating at their maximum power. However, this situation should not be factored into the reverse sizing, as it never occurs during the mission's lifetime. Be aware that if there is a considerable deviation from the Sun due to a malfunction, a revised power budget must be prepared because this would represent an unexpected situation not anticipated in the initial design [102]. Under these circumstances, power consumption should be minimized to ensure survival using the restricted power available from the batteries until the spacecraft can be directed back towards the Sun.

6.3 EPS Reverse Sizing

6.3.1 Solar Arrays

As already discussed in Section 6.2, the SAs are the more suitable primary source for the SOHO mission. The starting point of the preliminary EPS sizing is Table 31, resuming the power budget considering the operational profiles designed for the mission. From the cited table, the maximum power mode is the NM during HOP, where SOHO performs its scientific observations. This is taken as a sizing condition with $P_{max} = 1115.88 \text{ W}$. The other parameters (with their relative references) used in the analysis are listed in the following table:

Parameter	Symbol	Value	Reference
Sun irradiance	I_0	1395.27 W/m^2	Equation below
Nominal lifetime	$T_{lifetime}$	2.5 years	[102]
Degradation per year	d_{py}	0.04	[81] ¹⁵
Sun incidence angle	θ	20°	[103]
Inherent degradation	I_d	0.7	[48]
BOL efficiency of single SA cell	ε_{BOL}	11.2%	[113]
Operating voltage of the system	V_{sys}	28 V	[102]
Operating voltage of a single cell of SA	$V_{cell,SA}$	0.404 V	[113]
Area of single cell	A_{cell}	$2.41 \times 10^{-3} \text{ m}^2$	[113]
Efficiency factor in daylight	X_d	0.85	[48]

Table 32: Parameters chosen for SA sizing

The I_0 value is retrieved from the following formula of solar flux $I_0 = q_0 \cdot (R_{Earth}/R_{SC})^2$, where the solar flux $q_0 = 1367.5 \text{ W/m}^2$ is the solar flux at 1 AU, R_{Earth} is the distance of Earth with respect to Sun, whose mean value is 1 AU, and R_{SC} is the S/C distance from Sun. In this preliminary sizing, the spacecraft is assumed to be exactly in L_1 point, so R_{SC} is set to be 0.99 AU. The chosen lifetime for the SOHO satellite is 2.5 years, accounting for 2 years of nominal mission and half a year for the transfer. The latter is included since the transfer leg is also powered by the main power source at some point. The value of $\theta = 20^\circ$ is selected to maximise the associated cosine losses, accounting for eventual non-nominal conditions. This choice is coherent with the conservative philosophy followed for the solar panel sizing. The inherent degradation value I_d , collectively including design and assembly, temperature of array and shadowing of cells sources of degradations, is set to 0.7, which is a reasonable mean value between the proper range [0.49, 0.88] [48]. Moreover, as reported in Subsection 6.2, the chosen power control technique is DET, whose associated value of efficiency factor in daylight is $X_d = 0.85$. The correspondent eclipse value $X_e = 0.65$ can be safely neglected, since no total eclipse is foreseen, also in case of safe mode. For this reason, the time in eclipse can be set to $T_e = 0 \text{ s}$, and the total power required to the solar arrays to satisfy the S/C power demand can be computed as follows:

¹⁴Correction Manoeuvres

¹⁵The value is referred to the requirements for the SOHO sizing

$$P_{SA} = \frac{P_d}{X_d} = 1312.80 \text{ W} \quad (22)$$

The power (per unit area) at the beginning of life produced by the SA is computed as $P_{BOL} = I_0 \varepsilon_{BOL} I_d \cos\theta$. Notice that P_{BOL} must account for cell efficiency ε_{BOL} , inherent degradation I_d due to the explained causes and the not always perfect alignment of the SA normal direction with the Sun rays direction, which is the definition of θ parameter. Taking the parameters from Table 32, the power per unit area initially generated is $P_{BOL} = 102.79 \text{ W/m}^2$. To have a comparison, the corresponding power, obtained by multiplying P_{BOL} by the real area of the solar panel, is 1418.53 W . This is similar to the value of initial power of 1500 W found in literature [102]. SA degrades for many reasons, such as corrosion, thermal cycling and radiation, that are the most relevant for this type of mission. Yearly, all those causes are summed up in the d_{py} . The associated degradation factor along the whole mission, whose (nominal) duration is $T_{lifetim}$, can be determined as $L_d = (1 - d_{py})^{T_{lifetim}} = 0.903$. From this value, the end-of-life power produced by the SA and the total required area of solar panels can be computed as:

$$P_{EOL} = P_{BOL} L_d = 92.82 \text{ W/m}^2 \quad A_{SA} = \frac{P_{SA}}{P_{EOL}} = 14.14 \text{ m}^2 \quad (23)$$

The actual area of the SOHO solar panels is 13.80 m^2 [113], indicating that the two values are quite similar. This suggests that the inherent degradation of the chosen panel is close to the design conditions considered, and, in fact, slightly conservative.

In addition to the silicon cells and CMX cover glass discussed previously, several other components are essential for the SOHO solar array. Adhesive substrates are necessary for thermal stress damping and structural integrity, bonding the cover glass to the solar cells and the solar cells to the Kapton foil, which acts as a reflector and insulator. Two carbon fibre substrates provide structural rigidity and thermal management, while an aluminium honeycomb between the carbon fibre layers adds structural stability. Note that the interconnectors are not included, as their exact number and configuration cannot be determined at this stage of sizing. The complete list of substrates for the SA is provided in the following table:

Substrate material	Number of substrate	Density		Thickness [m]
		Value [kg/m ³]	Reference	
Silicon cells	1	$\rho_{Si} = 2330$	[107]	$t_{Si} = 210 \times 10^{-6}$
CMX cover glass	1	$\rho_{CMX} = 2600$	[108]	$t_{CMX} = 100 \times 10^{-6}$
Aluminium honeycomb	1	$\rho_{AH} = 68.88$	[109]	$t_{AH} = 4 \times 10^{-2}$
DC 93-500 adhesive ¹⁶	2	$\rho_A = 1030$	[110]	$t_A = 100 \times 10^{-6}$
Kapton foil	1	$\rho_K = 1420$	[111]	$t_K = 100 \times 10^{-6}$
Carbon fiber	2	$\rho_{CF} = 1780$	[112]	$t_{CF} = 60 \times 10^{-6}$

Table 33: Resuming table of substrates characteristics

The first two thickness values are taken from the literature (Subsection 6.1.1); the others, which could not be retrieved for the SOHO mission, are chosen between the proper ranges following the conservative philosophy of the design. Hypothesising that all the substrates are characterized by the same area of the SA found from Equation 23, the total mass of the solar arrays m_{SA} can be evaluated as follows:

$$m_{SA} = A_{SA} (\rho_{Si} t_{Si} + \rho_{CMX} t_{CMX} + \rho_{AH} t_{AH} + \rho_A t_A + \rho_K t_K + \rho_{CF} t_{CF}) = 54.60 \text{ kg} \quad (24)$$

From the surface area of a single cell A_{cell} , the evaluated A_{SA} , the voltage for the system V_{sys} and the one related to the single cell V_{cell} , it is possible to determine the number of cells needed to cover the entire surface, the part of them which must be put in series and, consequently, the actual number of cells needed to provide the voltage and guarantee the desired power:

$$N = ceil \left(\frac{A_{SA}}{A_{cell}} \right) = 5865 \quad N_{series} = ceil \left(\frac{V_{sys}}{V_{cell}} \right) = 70 \quad N_{real} = ceil \left(\frac{N}{N_{series}} \right) N_{series} = 5880 \quad (25)$$

For what concerns the number of cells, it can be noted that both the quantity of cells per string and their total number are close to the real values, respectively, 77/78 and 5740 [113]. The actual voltage is $V_{real} = N_{series} V_{cell}$, which is equal to 28.28 V. The real surface area can be computed as $A_{SA,real} = N_{real} A_{cell}$, which results in 14.18 m^2 , obviously still different from the real value, as already pointed out multiple times. Using the same hypotheses and the same Equation 24, the real mass of the solar array can be retrieved, and it is equal to 54.74 kg.

6.3.2 Secondary Batteries

As previously seen in Section 6.2, for the SOHO design two Ni-Cd batteries are selected, $N_{Bat} = 2$, and their data, picked from the documentation [48] [106], are shown in the table below:

E_m [Wh/kg]	E_v [Wh/dm ³]	DoD [-]	η [-]	$V_{cell,Bat}$ [V]	μ [-]
30	90	0.9	0.9	1.35	0.8

Table 34: Parameters chosen for Battery sizing

Where E_m is the specific energy, E_v is the energy density, DoD is the Depth of Discharge, $V_{cell,Bat}$ is the single cell voltage, η is the line efficiency and μ is the package efficiency. Considering that these batteries are designed to be used in exceptional

¹⁶This adhesive was chosen since from literature [92] it provides low outgassing and have great gluing capabilities.

cases, it follows that they have a low number of cycles and therefore a very high DoD can be considered, as found in literature [48] [9].

The sizing is based on the batteries' nominal design condition, which involves providing power during LEOP and ISA until SA deployment, as shown in Table 30. This choice is supported by the assertion that significant Sun de-pointing was stated to be "non-credible", meaning the batteries were nominally unused during the mission [102]. The correctness of the selection of this sizing condition is further highlighted by the fact that the possibility of using primary batteries, intended solely to supply power during the mission's initial stages, instead of secondary ones, was taken into account during the design phase [103]. The two considered phases with their required electrical powers and durations are the LEOP, with $P_{LEOP} = 344.28 \text{ W}$ for $T_{LEOP} = 2.417 \text{ h}$, and the ISA with $P_{ISA} = 629.88 \text{ W}$ for $T_{ISA} = 0.217 \text{ h}$ [7]. Therefore, the capacity, mass and volume of one battery can initially be roughly estimated as in the formulas:

$$C = \frac{T_{LEOP} P_{LEOP} + T_{ISA} P_{ISA}}{\text{DoD } N_{Bat} \eta} = 597.83 \text{ Wh} \quad m_{1Bat} = \frac{C}{E_m} = 19.93 \text{ kg} \quad v_{1Bat} = \frac{C}{E_v} = 6.64 \text{ dm}^3 \quad (26)$$

Considering a nominal bus voltage $V_{sys} = 28 \text{ V}$, as seen in Subsection 6.1.2, dividing it by $V_{cellBat}$ and applying the ceiling function, it is obtained that $N_{series} = 21$ cells in series are required with a real battery voltage of $V_{Bat} = 28.35 \text{ V}$. Then, the capacity of a single string of cells can be computed from the knowledge of the single cell capacity ($C_{cell} = 20 \text{ Ah}$ [103]), and from that value the number of strings in parallel $N_{parallel}$ and the real battery system capacity C_{Bat} is obtained:

$$C_{string} = \mu C_{cell} V_{Bat} = 453.60 \text{ Wh} \quad N_{parallel} = \text{ceil} \left(\frac{C}{C_{string}} \right) = 2 \quad C_{Bat} = N_{parallel} C_{string} = 907.20 \text{ Wh} \quad (27)$$

Notice that the result obtained for $N_{parallel}$ is consistent with the value N_{Bat} . To retrieve the overall weight and size of the battery pack, the values of specific energy and energy density are used as follows:

$$m_{Bat} = \frac{C_{Bat}}{E_m} = 30.24 \text{ kg} \quad v_{Bat} = \frac{C_{Bat}}{E_v} = 10.08 \text{ dm}^3 \quad (28)$$

The number of cells on a string obtained differs from the real number, that is 32 (as seen in Section 6.1.1), due to the battery sizing model, which uses the voltage of the entire system V_{sys} and not the operating value of the battery of 42 V, but it is nevertheless consistent with the values found in the literature [48]. Then, also battery system capacity obtained C_{Bat} slightly differs from the real value adopted in the mission of 900 Wh, and the reasons may be linked to the computation of the power budget, the expected time duration of use and the computed number of cells in series [9].

After the sizing of the batteries based on the nominal condition has been carried out, an off-nominal design condition is considered in order to evaluate the possibility of surviving during a strong Sun de-pointing condition, not foreseen in the original design, where the batteries would result in being the only source of power. In order to do that, the available power for the maximum period between two subsequent communications with the ground is calculated by considering a period of $T_{FC} = 3.73$ hours between two following communications and assuming a constant power demand. The batteries (sized as described) can supply a power of $P_{FC} = C_{Bat} \text{DoD} \eta / T_{FC} = 197.01 \text{ W}$. This is insufficient to meet the power requirements in ESR mode, necessitating the implementation of an additional mode to address this potential situation. This is what has been done during the 1998 anomaly [103], already discussed in Section 6.2.1.

6.3.3 Mass, Power, Data and Volume Budget

The total mass of the EPS can be computed as the sum of the SAs and the batteries masses, to which a 25% margin is added in order to consider the harness and cabling that interconnects the S/C subsystems:

$$m_{EPS} = 1.25 (m_{Bat} + m_{SA}) = 106.23 \text{ kg} \quad (29)$$

It is worth noting that this subsystem amounts to the 6.59% of the overall dry mass of the satellite. The volume budget can be retrieved considering both the volumes of battery and solar arrays. The former has already been computed in Subsection 6.3.2 and corresponds to the 0.0235% of the overall S/C volume. The latter can be easily determined as follows $v_{SA} = A_{SA,real} \cdot t_{TOT} = 0.58 \text{ m}^3$, where t_{TOT} is the sum of all the substrates thickness. The power budget for the EPS has already been deepened in Subsection 6.2.1 relying on information found in literature [103]. No data was available for the sized elements' data budget. Therefore, the EPS data is sourced from literature [48] and based on the 1750A-class Instruction Set Architecture, a general-purpose processor used in the SOHO mission [76]. This makes the estimates reliable. The analysis results are summarized in the following table:

Size [Kwords]		Typical Throughput [KIPS]	Typical Execution Frequency [Hz]
code	data		
1.2	0.5	5.0	1.0

Table 35: Data Budget of EPS

7 Configuration & OBDH Subsystem

7.1 Space segment configuration and justification

The SOHO space segment design is based on a modular concept and includes two main elements: the **Service Module** (SVM) and the **Payload Module** (PLM) [2].

The PLM contains all the scientific instruments and provides a stable optical bench. It houses the attitude sensors used for spacecraft pointing reference (as will be deepened in Subsection 7.1.5).

The optical bench features 2.6-meter-high faces split into large flat panels for heavy sensors and smaller lower panels for the electronics associated with the instruments. This arrangement ensures satisfactory thermo-elastic decoupling, preventing sensor pointing disturbances caused by power dissipation variations from the electronics. Meanwhile, it meets all functional requirements of the instruments, particularly regarding viewing direction, field of view clearance, straylight prevention, and pointing stability [82].

The SVM consists of two sub-modules: one carrying the service equipments and the other the propulsion unit, which includes the spacecraft's propulsion elements. The appendages, deployable solar wings and antennas, are attached to the SVM. It is a relatively flat rectangular box with slightly cut corners for late-stage inspection access. Most service electronic units are mounted on the four main dismountable hinged side walls, each corresponding to a specific electrical subsystem and its interface electronics. The modularity of this approach down to the subsystem level makes the pre-integration possible already at the subsystem responsible premises, therefore minimising the schedule risks. The modules are linked together by bolting them at the level of their central tube, ensuring the stiffness required for each one [82].

The following paragraphs will deepen the different subsystems configurations, positioning with respect to the modular concept of SOHO, and the relative *rationale*.

7.1.1 Launcher adapter and appendages

SOHO is mounted on the Atlas IIAS/Centaur launcher through an adapter that connects the spacecraft to the second stage. The mass of the adapter can be estimated using statistical data from previous missions, exploiting Table 6, and it amounts to 190.9 kg, supporting an overall mass of 1863.7 kg. The spacecraft must fit within the dimensions available in the fairing of the launcher. According to literature [2], SOHO dimensions are $4.3 \times 2.7 \times 3.7 \text{ m}^3$, fitting into the large configuration of the fairing [46], which has a maximum diameter of 4.2 m and a height of 12.2 m. The Atlas launcher also offers a stretched large configuration with an increased diameter of 1 m, providing a greater volume, but this configuration is generally avoided due to its negative impact on booster performance [48].

In Figure 16, it is possible to see the SOHO spacecraft inside the fairing of the launcher. In the folded launch configuration, the spacecraft is almost cylindrically symmetric, with the axis of symmetry parallel to the thrust axis. The solar arrays are folded during launch and secured with hold-down points mounted on the lower and upper floors of the SVM. All service dissipative equipment is mounted on the lateral walls, providing important mounting surfaces and radiative areas. The high-gain antenna is integrated into the spacecraft central tube, while the two low-gain antennas, mounted on fixed booms at the bottom section of the service module, protrude from the main body to provide full geometrical coverage. A central tube transfers loads to the SVM central tube via the propulsion support ring.

7.1.2 Payloads

Installing 12 different scientific experiments presents significant challenges due to numerous and sometimes conflicting constraints which can be categorized into several areas.

Mechanical constraints involve the physical parameters of the experiments, such as their dimensions, mass properties, interface loads on the supporting structure, and the size and orientation of their fields of view.

Thermal constraints ensure that each experiment maintains its required thermal environment. This includes providing unobstructed fields of view for radiators and controlling temperatures within dedicated enclosures for electronics.

Pointing constraints require precise alignment of the scientific instruments on the ground and stringent stability of their pointing directions during flight. Additionally, **electrical constraints** affect the layout by determining the cable lengths between the units of each experiment and the routing of these cables to avoid electromagnetic compatibility issues between noisy and sensitive lines. **Cleanliness constraints** necessitate locating the most sensitive instrument parts away from potential sources of contamination. Finally, **integration constraints** ensure good access to each experiment unit for all test activities on the PLM, including mechanical, electrical, and alignment tests, regardless of the presence of other previously installed experiments [82].

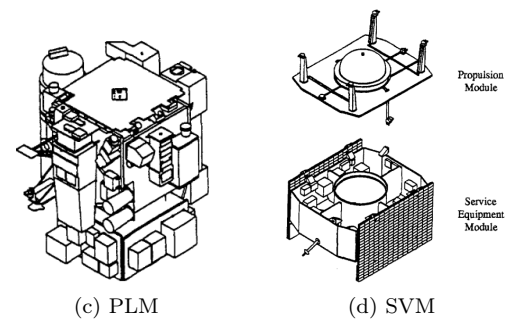


Figure 15: S/C modular design



Figure 16: SOHO prepared for encapsulation in the fairing

To meet all the above constraints, a square-shaped PLM with externally mounted units was designed, offering ample mounting surfaces and easy integration access.

This design layout can accommodate both side-mounted and top-mounted instruments, providing an optimal size and orientation towards the Sun for the instruments FOV, fulfilling scientific objectives. The design features an even distribution of large and heavy instruments for balance, with detector radiators giving unobstructed views to deep space to maintain cold temperatures. The PLM is divided into an upper part, which serves as a stable optical bench for the instruments, and a lower part which houses most of the experiment electronics. To avoid contamination, all instruments except for SWAN sensors, which have specific FOV requirements and dedicated shields, are placed at the top of the PLM, away from potential pollution sources like thruster plume impingement. Unit locations were optimized to group all units of the same experiment on the same or adjacent panels, with electronics units under spacecraft thermal control placed inside thermal enclosures covered by Multi-Layer Insulation (MLI) [82] [6].

7.1.3 TMTC subsystem

The positioning of the TMTC components is based on the need to guarantee continuous communication and pointing towards the Earth. The **HGA**, essential for high-rate scientific data transmission, is integrated into the spacecraft central tube and is aligned with the $-X_b$ direction in the body frame to facilitate direct communication with Earth [9].

This positioning serves dual purposes: firstly, it fulfills the Earth-pointing requirement, and secondly, it places the antenna in a shaded area, minimizing potential interference. Additionally, the HGA is gimbaled to allow a maximum deviation of 32° from the anti-Sun direction. This adjustment is crucial to avoiding S-band radio interference from the Sun during downlink transmissions. Moreover, the presence of a rotating mechanism grants the HGA two degrees of freedom, facilitating precise pointing towards both the Earth and the DSN, regardless of the highly elliptical orbit traced by the spacecraft around the L_1 point [51].

The two **LGAs**, situated on fixed booms at the bottom section of the SVM, extend along the $\pm Z_b$ sides of the spacecraft, ensuring complete geometrical coverage. The antenna pattern exhibits quasi-rotational symmetry and quasi-isotropy within the elevation range of 0° – 108.5° (LGA reference axis) [2].

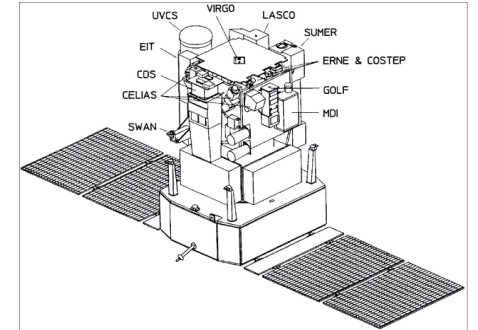


Figure 17: SOHO spacecraft instruments view

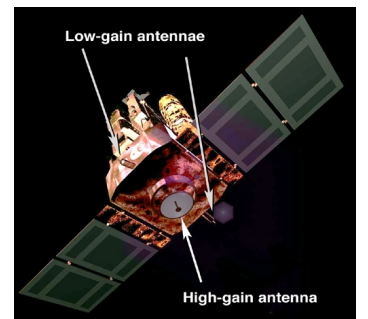


Figure 18: SOHO antennas highlighted

7.1.4 Propulsion Subsystem

The propulsion subsystem of SOHO S/C is equipped with two fully redundant branches of 8 4.4 N MRE-1.0 monopropellant hydrazine [39] **thrusters** each. The dual-branch configuration ensures redundancy and reliability in propulsion (and control) systems. Figure 19 illustrates the adopted thrusters layout, detailing their arrangement and orientation, while the configuration adopted is described in Table 36, in which the roles of each thruster pair regarding ΔV and attitude control are also highlighted:

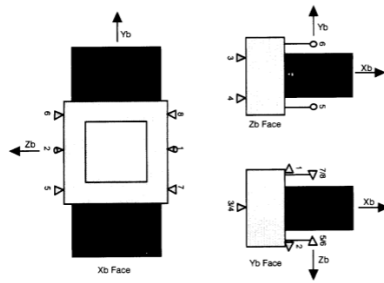


Figure 19: SOHO thruster configuration

Thruster Pair	Thruster Locations	ΔV Direction (body frame)	Primary Attitude Control
1 and 2 (1 is canted 30° down and 2 is 30° up)	Fore (Sunward $+X_b$)	$-X_b$	Pitch
3 and 4	Aft (Earthward $-X_b$)	$+X_b$	Yaw
5 and 6	Top ($+Z_b$)	$-Z_b$	Roll
7 and 8	Bottom ($-Z_b$)	$+Z_b$	Roll

Table 36: SOHO thrusters (applies to both A and B branches)

As can be seen, thrusters are only positioned in $\pm X_b$ and $\pm Z_b$ directions. In fact, based on mission needs, the manoeuvres are designed to consist of two main segments: those along the Earth-Sun line (x-axis) and those perpendicular to it (z-axis) [34], which are completely fulfilled by the chosen thruster architecture. Furthermore, this configuration ensures, as shown in Table 36, three-axis attitude control, allowing SOHO to maintain its desired orientation in space, enabling scientific observations, fulfilling mission requirements, and ensuring reaction wheels off-loading. Cleanliness, which is a driver for the SOHO mission, significantly influences the positioning of thrusters to minimize the impact of their plumes on sensitive equipment. Specifically, thrusters 1 and 2 are canted 30° out to minimize plume impingement on the payload module, as the $+X_b$ direction aligns with the instrument bore-sights aimed at the Sun [34]. This arrangement is essential for preserving the integrity of scientific observations and data collection onboard [2].

A specific interface cylinder supports the propulsion **storage tank** and related **propulsion tubing** and is connected on one side to the PLM internal cylinder and on the other to the SVM thrust tube [82]. The tank has a prolate spheroidal shape [44] and is housed in the upper panel of the SVM, aligned with the principal axis of the spacecraft and with the centre of mass of it. This positioning minimizes changes in the principal inertia matrix during fuel consumption and helps control the generation of strong disturbance torques caused by propellant sloshing. Additionally, the tank position shields the electronics from radiation and helps to keep the hydrazine warm. Finally, the propulsion equipment is mounted on the upper platform of the SVM, except for two thruster blocks positioned on the lower floor [2].

7.1.5 AOCS

The **sensors** of SOHO AOCS are: two Fine Pointing Sun Sensors (FPSS), two star trackers also referred to as SSU, three gyroscopes, which composes the Inertial Reference Unit (IRU), and three Solar Acquisition Sensors (SAS). FPSSs, SSU and SASs are located in the PLM, to benefit from its accurate pointing stability [2]. FPSSs point toward $+X_b$ direction directly facing the Sun [2], which is necessary due to their narrow FOV around $\pm 4.5^\circ$ [72]. Star trackers' FOV is narrow $3^\circ \times 4^\circ$ [67] and they must be precisely oriented. They face the deep space in a direction perpendicular to the Sun-Earth line so that they are shielded from the radiations and disturbances coming from the Earth and the Sun. Moreover, they are placed along the Y_b directions not to be impinged by thrusters plumes [63]. The SAS units are characterized by almost hemispherical FOV [69], allowing them to be strategically placed along the spacecraft to ensure omnidirectional coverage and partial overlapping. This configuration is particularly useful for regaining proper orientation when the spacecraft experiences significant deviations from its intended alignment with the Sun. As a final remark, the AOCS sensors are mounted close to the instruments and the electronics used for power, to minimize cabling and harness size and mass [82]. The **actuators** of the AOCS SOHO mission are sixteen thrusters and four RWs. The thrusters' positioning and related *rationale* are already treated in Subsection 7.1.4, while pyramidal configured RWs [34] are placed in SVM [2].

7.1.6 TCS

The TCS consists of several components: the Sunshield, heaters, radiators, MLI blankets and coatings. The placement of each component is influenced by crucial mission requirements, such as the pointing stability for the payload compartment and the autonomy requirement [77]. The **Sunshield**, located on the $+X_b$ side, faces the Sun and acts as a radiator for the instruments and electronics mounted on that panel. The **heaters** are divided into three types: Substitution, Sunshield and Structure heaters. The Sunshield heaters are positioned on the same panel as the Sunshield, while the Structure and Substitution ones are placed on the upper lateral panels $\pm Z_b$ and $\pm Y_b$ where instrument sensors are mounted. This arrangement helps smooth thermal gradients from a structural perspective and maintains components at the correct operating temperature [75]. **Radiators** are oriented perpendicular to the solar radiation direction, with only the solar reflection from the solar arrays reaching the $\pm Y_b$ panels. They are located on the lateral walls, the corner panel $+Y_b / -Z_b$ and on the lower platform [80]. This placement allows them to face deep space directly without any obstructions, thereby facilitating efficient heat emission. The S/S units housed in the SVM are thermally controlled by wrapping their structures with **MLI blanket** as also the panels on which the instrument sensors are mounted [75]. Concerning **coatings**, they are applied to various parts of the spacecraft according to the specific requirements of each surface. Each subsystem having a particular thermal requirement is equipped with its own thermal components to ensure that the correct operating temperature is maintained throughout the mission, as already explained in Section 5.

7.1.7 EPS

The EPS configuration is primarily driven by the need of a symmetrical design, a balanced mass distribution and limited cabling. Consequently, the **Solar Array** (SA) configuration features two deployable wings positioned along the $\pm Y_b$ axis, ensuring symmetry. This configuration is also driven by the fact that the S/C always faces the Sun along its $+X_b$ direction, therefore, the sunlight exposure of SAs is maximized owing to this positioning. Due to the SA external surface area of $13.80\ m^2$ [113], a folded configuration is necessary to save space in the launcher, and it necessitates unfolding and rotating mechanisms. Typically being bulky and massive, the **batteries** are important components of the configuration. In particular, they are positioned symmetrically and aligned with the principal axis of the S/C, in order to minimize changes in the inertia matrix and disturbance torques. A risk of the batteries is that containing liquid electrolysis they may vent gasses in space. Therefore, they are placed far from the active thrusters since they may become a small disturbance. **Power regulation, control, and distribution units** are strategically placed close to their respective subsystems to minimize cabling. Also, the routing of these cables is critically designed with the purpose of avoiding EMC problems between noisy and sensitive lines. Moreover, the **experiment electronics** are grouped in the opposite side of the PLM with respect to the payload, such that the thermo-elastic distortions induced by the electronics power dissipation are minimized and do not affect the instruments pointing [82].

7.1.8 OBDH Subsystem

The OBDH components are strategically positioned within the spacecraft to optimize functionality and operational efficiency, typically near the center of mass to ensure balance and stability. This placement serves multiple purposes: it minimizes signal attenuation and processing delays by situating components close to scientific instruments, enabling rapid data acquisition and processing, while also facilitating efficient communication with other subsystems from a centralized location, promoting coordinated spacecraft operations. Thermal stability is carefully considered in component placement

to maintain optimal operating temperatures, and shielded locations are chosen to mitigate electromagnetic interference, preserving signal integrity and system reliability.

7.2 OBDH Subsystem

The OBDH subsystem generally receives, validates, decodes, and distributes commands to other spacecraft S/S and gathers, processes, and formats spacecraft housekeeping and mission data for downlink or use by an onboard computer. On the SOHO spacecraft the main functions of this subsystem are [2]:

- data acquisition and formatting from experiments and SVM;
- data storage during periods of no ground data collection;
- acquisition, decoding, validation and distribution of commands from ground to experiments and SVM;
- thermal control of SVM and PLM;
- maintenance and distribution of time base references for synchronization and time tag purposes;
- inter-instrument data exchange;
- on board surveillance and monitoring to ensure the safety of the spacecraft.

For the accomplishment of these functions some specific components of the OBDH subsystem are required, and they will be deepened in the following paragraphs together with their operating method. The general data flow architecture of the SOHO S/C has a centralized structure with respect to the subsystems, as clearly visible in Figure 20:

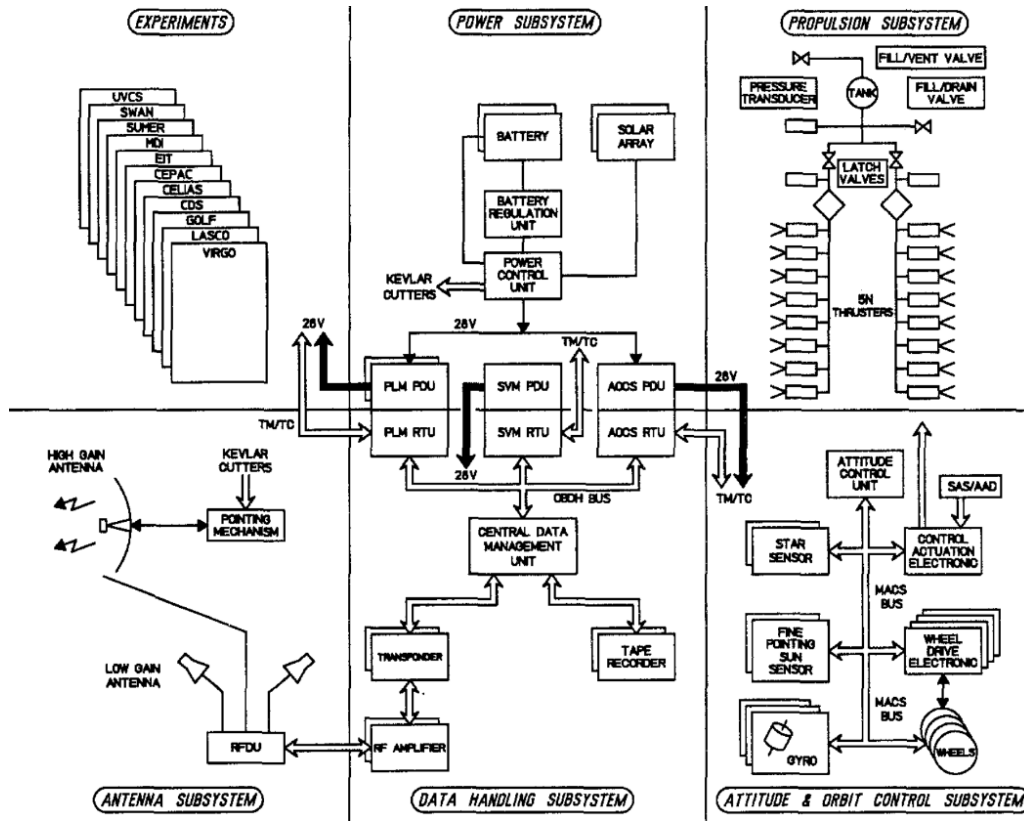


Figure 20: OBDH Architecture [2]

The centralization of the architecture is a feature that contributes to increasing the reliability of the OBDH subsystem and supports isolated failure management. However, it results in extensive wiring, which adds mass to the S/C and necessitates specific interfaces, leading to increased testing and integration complexity.

7.2.1 Components and Adopted Buses

The core of the subsystem is the **Central Data Management Unit** (CDMU), which consists of a redundant intelligent processing unit with a 16-bit MAS281 microprocessor. The latter is a high-performance implementation of the MIL-STD-1750A instruction set architecture and it consists of three CMOS/SOS large-scale integration (LSI) chips [116]. For the software implementation, it has been used the ADA language, while the TLD cross compiler provides valid code for the MIL-1750A standard instruction set and it has the possibility of acting as the interface with the assembly language [115]. The microprocessor is in charge of managing and distributing the onboard time, performing the thermal monitoring and thermal control of the satellite, managing the antenna pointing and handling the inter-instrument data exchange.

The exchanges between on board computers and users are realized by the **digital OBDH bus** which is controlled by the central processor and uses separate lines for interrogation (computer commands or requests) and response (data or acknowledge to computer). It has a federated data flow architecture and it is a Litton coded bus, whose bit rate is 524 kHz [2].

7.2.2 Interfaces

For the on-board data management, proven interfaces have been selected through the use of an ESA OBDH bus for the data handling, and an ESA MACS bus for the AOCS. These two subsystems make use of an identical processor type [82]. In addition, all communications between units are done through isolated links (relays or opto-couplers), or differential lines using a standard balanced digital link (SBDL), which means that two circuits are used for each signal, where a positive differential voltage represents logic "0" and a negative represents logic "1" for the signal [118].

In order to simplify the data interfaces as much as possible, the telemetry and command functions (monitoring, actuating, switching) are combined into three **Remote Terminal Units** (RTUs), that work as an interface between the central OBDH system and the remote devices or equipment distributed throughout the satellite, receiving commands from the former and transmitting them to the corresponding subsystems. These RTUs operate under the control of the main computer via the OBDH bus and they provide all interface signals needed by each experiment in terms of both telecommands (on/off, memory load, and OBDH block commands) and telemetry (serial acquisition, bilevel digital, relay status, thermistors interface, analogue signals, timing and clock signals), thus allowing the complete operation and monitoring of the experiments. The RTUs also perform the temperature acquisition for all thermistors used as part of the PLM thermal control. The RTUs are respectively dedicated to the PLM, to the SVM equipment (data handling/telecommunications and power subsystems), and to the **Attitude Control Unit** (ACU). The ACU is based on the same microprocessor used in the CDMU of the data handling subsystem (MAS281), making the system fully redundant.

7.2.3 Data

During the nominal operational phase, when the ground link is not active, data are recorded through one **magnetic tape recorder** of 1 Gigabit capacity and one fully self-redundant **solid-state recorder** with 2 Gigabits capacity. Subsequently, data are transferred to and from the data recorder via a dedicated link connected to the transfer frame generator [2]. Furthermore, there are specific services offered to the experiments in order to allow a better scientific return. One of these is an inter-instrument flag system, implemented in the OBDH system, called **Inter Instrument Data Exchange** (IIDE), which allows the participating instruments to communicate between them. A master instrument is selected by a command sent by the ground station, and the other instruments, then acting as receivers can obtain from the master and through the S/C on-board software data related to a solar event [82]. In order to limit the complexity and potential clashes, at any one time only one pre-defined instrument may flag one pre-defined event in response to a specified observation, defined through planning at the Experimenter's Operations Facility (EOF), and this will only have one potential reaction by the receiving instruments [2]. So, specific spacecraft data handling modes can be enabled in order to establish specific functions. Moreover, the MDI high data rate transmission allows to transfer directly from the MDI instrument a telemetry flow to the spacecraft CDMU at a rate of 160 *k*bps [82].

7.2.4 Autonomy

Although the maximum non visibility time between the S/C and the ground segment is twenty minutes, a 48-hours autonomy is provided by the spacecraft to allow an easy restart of the observations in case of any problem. Moreover, an independent (hardwired) mode provides a safe mode in case of failures. Related to instruments safety, it is worth mentioning [82]:

- the Emergency Sun Re-acquisition flag (ESR), which is a specific message (block command) sent by the on-board software to the experiments if an attitude anomaly is detected allowing the instruments to adopt safe configuration;
- the actions undertaken by the S/C to ensure a minimal monitoring of the experiments: a variety of reconfiguration actions can be initiated by the on-board software depending on the anomaly detected, which consist of switching off one or all experiments, reconfiguring the PLM thermal control and the non-operational heaters.

7.2.5 On Board Time (OBT)

The time tags for the spacecraft and instrument housekeeping packets are generated by the OBDH system, and then the time tags for the instrument science data packets are inserted by the instruments generating the science data. A redundant, oven-controlled, Ultra Stable Oscillator (USO), with a stability better than $3.6 \cdot 10^{-8}$ per day, drives the spacecraft On Board Time (OBT) clock, maintaining within $\pm 20\text{ ms}$ with respect to International Atomic Time (TAI reference, 1958 January 1 epoch) ground reference time during the whole mission. Ground adjustments of the OBT are anticipated every 2.5 days to maintain the above accuracy. This process ensures precise time-tagging of onboard events and telemetry data. The time tags are provided in 6 bytes; the first 4 bytes are TAI seconds (2^0 to 2^{31} seconds) and the last 2 bytes are fractions of a second with the resolution of the On Board Time Pulse (2^{-11} seconds). The Coordinated Universal Time (UTC) is used as the operational time reference in the EOF. Therefore, the "SOHO operations day" is defined to begin at 00:00 UTC and the computer systems in the SOHO Mission Operations Control Center (SMOCC) and EOF are synchronized to run on UTC [2] [65].

7.2.6 OBDH Reverse Sizing

The method used to obtain all the subsystem data is known as *estimation by similarity*.

Firstly, the functions managed by the OBDH within each subsystem are identified and broken down into basic elements.

For each element in all subsystems, average values of memory data and lines of code, along with typical throughput (TP) and execution frequency, are extracted from reference tables [48]. Then, a desired execution (or acquisition) frequency is determined for each element. In most cases, the actual acquisition frequency was not available, so it was chosen critically. For instance, functions that require fast processing are assigned a high frequency. Conversely, for functions where the computer does not have stringent speed requirements and exact frequency values are unavailable, a typical execution frequency is used. Using this estimation by similarity approach, the actual throughput (measured in *KIPS*) required by each function is calculated based on the desired acquisition frequency f , employing the following equation:

$$KIPS = \frac{KIPS_{typ}f}{f_{typ}} \quad (30)$$

Then, the total throughput, data and code needed by each subsystem can be determined simply through a summation of the various functions requests:

$$KIPS_{tot} = \sum_{i=1}^{n_{fun}} k_{fun} KIPS_{fun} \quad CODE_{tot} = \sum_{i=1}^{n_{fun}} k_{fun} CODE_{fun} \quad DATA_{tot} = \sum_{i=1}^{n_{fun}} k_{fun} DATA_{fun} \quad (31)$$

Where k_{fun} is the number of elements of each function and $KIPS_{fun}$, $CODE_{fun}$ and $DATA_{fun}$ are the real throughput, code and data of each function. Tables 37 enumerate the requests for each subsystem. The final row displays the outcomes of Equation 31, considering all elements of the S/S active, and the final column shows the results of Equation 30.

It is important to note that green cells denote actual frequencies cited in literature, whereas yellow cells indicate frequencies assumed based on critical analysis. These assumptions are based on the knowledge of SOHO mission objectives and environment. The reduced frequency for thruster control with respect to the typical one is justified by SOHO stable and controllable configuration, as it operates in an environment with minimal external disturbances. Additionally, the higher frequency for the star tracker accommodates the mission's stringent pointing requirements for scientific observations. Lastly, given SOHO placement in a stable thermal environment during its nominal scientific phase, the lower frequency for thermal control is considered to be appropriate.

AOCS							
Components	Number	Code [Words]	Data [Words]	Typical KIPS	Typical Freq [Hz]	Acquisition Freq [Hz]	KIPS
RWs control	4	1000	300	5	2	10 (in [71])	100
Thruster Control	16	600	400	1,2	2	1	9,6
IRU	1	800	500	9	10	10	9
Star Tracker	2	2000	15000	2	0,01	1	400
FPSS	2	500	100	1	1	1	2
SAS	3	500	100	1	1	1	3
Kinematic Integration	1	2000	200	15	10	10	15
Error Determination	1	1000	100	12	10	10	12
Attitude Determination	1	15000	3500	150	10	10	150
Attitude Control	1	24000	4200	60	10	10	60
Ephemeris Propagation	1	2000	300	2	1	1	2
Complex Ephemeris	1	3500	2500	4	0,5	0,5	4
Orbit Propagation	1	13000	4000	20	1	1	20
Total		81400	53400				1638,6

PS							
Components	Number	Code [Words]	Data [Words]	Typical KIPS	Typical Freq [Hz]	Acquisition Freq [Hz]	KIPS
Tank	1	-	-	-	-	-	-
Tank Control Valve	2	800	1500	3	0,1	0,1	6
Latch Valves	2	800	1500	3	0,1	0,1	6
Tank Pressure Sensor	2	800	1500	3	0,1	0,1	6
Total		4800	9000				36

EPS							
Components	Number	Code [Words]	Data [Words]	Typical KIPS	Typical Freq [Hz]	Acquisition Freq [Hz]	KIPS
Solar Panels	2	-	-	-	-	-	-
Batteries	2	-	-	-	-	-	-
Cables & Harness	1	-	-	-	-	-	-
Power Voltage Control	1	1200	500	5	1	1	5
Power Current Control	1	1200	500	5	1	1	5
Total		2400	1000				10

TCS							
Components	Number	Code [Words]	Data [Words]	Typical KIPS	Typical Freq [Hz]	Acquisition Freq [Hz]	KIPS
Thermal Control	1	800	1500	3	0,1	0,01	0,3
Total		800	1500				0,3

TMTC							
Components	Number	Code [Words]	Data [Words]	Typical KIPS	Typical Freq [Hz]	Acquisition Freq [Hz]	KIPS
HGA	1	-	-	-	-	-	-
LGA	2	-	-	-	-	-	-
Uplink Card	2	1000	4000	7	10	10	14
Downlink Card	2	1000	2500	3	10	10	6
Total		4000	13000				40

System								
Components	Number	Code [Words]	Data [Words]	Typical KIPS	Typical Freq [Hz]	Acquisition Freq [Hz]	KIPS	
I/O Device Handlers	1	2000	700	50	5	5	50	
Test and Diagnostic	1	700	400	0,5	0,1	0,1	0,5	
Math Utilities	1	1200	200	0,5	0,1	0,1	0,5	
Executive	1	3500	2000	60	10	10	60	
Run Time Kernel	1	8000	4000	60	10	10	60	
Complex Autonomy	1	15000	10000	20	10	10	20	
Fault Detection (Monitors)	1	4000	1000	15	5	5	15	
Fault Correction	1	2000	10000	5	5	5	5	
Total		36400	28300				211	

Table 37: Data of all subsystem components
(green=real value; yellow=assumed value; white=typical value)

Note that the payloads are not taken into account in this preliminary analysis. This exclusion stems from the fact that during scientific activities, telemetry related to experiment housekeeping is solely stored, compressed by dedicated DCU [119] and subsequently transmitted by the spacecraft without undergoing analysis [82].

To aid in the analysis of the final results, from Tables 37, the percentages on code, data and KIPS per subsystem with respect to the total are retrieved and reported in Table 38:

	% on Code	% on Data	% on Instructions
AOCS	62,71%	50,28%	84,64%
PS	3,70%	8,47%	1,86%
EPS	1,85%	0,94%	0,52%
TCS	0,62%	1,41%	0,02%
TMTC	3,08%	12,24%	2,07%
System (OS)	28,04%	26,65%	10,90%

Table 38: Percentage on code, data and KIPS per S/S

It can be observed that, as expected, the highest values are related to the AOCS and OS. Notably, due to the high demands of the AOCS, it seems reasonable to adopt a second microprocessor dedicated to this subsystem (ACU), as discussed in Subsection 7.2.2. Consequently, the analysis of memory usage per mode considers two scenarios: one where overall data management is handled by a single processor and another where data are split between two microprocessors, one dedicated to the AOCS and the other to the remaining subsystems. Given that the system is 16-bit word-based, as already mentioned in Subsection 7.2.1, the required memory can be computed using the following formulas:

$$ROM[kb] = \frac{Code[words]16[\frac{bit}{word}]}{8[\frac{bit}{byte}]1000[\frac{byte}{kbyte}]} \quad RAM[kb] = \frac{(Code[words] + Data[words])16[\frac{bit}{word}]}{8[\frac{bit}{byte}]1000[\frac{byte}{kbyte}]} \quad (32)$$

The results regarding each mode are shown in Table 39, where TP stands for throughput and is measured in MIPS, Code/Data are measured in words, and ROM/RAM in kb:

Mode	Overall					ACU					CDMU				
	Code	Data	ROM	RAM	TP	Code	Data	ROM	RAM	TP	Code	Data	ROM	RAM	TP
NM	552000	375500	1104	1855	6.1315	334000	156500	668	981	4.825	218000	219000	436	874	1.3065
ESR	568000	350000	1136	1836	3.0835	326000	86000	652	824	1.597	242000	264000	484	1012	1.4865
CRP	542000	300500	1084	1685	4.1765	324000	81500	648	811	2.87	218000	219000	436	874	1.3065
RWM	600000	436500	1200	2073	6.7405	358000	172500	716	1061	5.254	242000	264000	484	1012	1.4865
All active	649000	531000	1298	2360	9.6795	407000	267000	814	1348	8.193	242000	264000	484	1012	1.4865

Table 39: Final results and systems data usage per each S/S in each mode

Notice that the reported data already consider a **400% margin** on the computed values. This significant margin is included because the analysis is in its early stages and relies on statistical data, making it necessary to enhance its robustness.

The precise computation leading to the final values, along with the applied margin, is based on Equations 31 and 32 and detailed in Tables 42 to 49 in the Appendix. In particular, the value of the number of elements of each function k_{fun} , is based on the number of active components of each subsystem per mode retrieved from the literature and described in previous sections. This is summarized in Table 41 (in Appendix), which presents a comprehensive list of active elements within each subsystem across all modes considered for the SOHO mission.

It is evident from the analysis that the most demanding mode is the RWM mode. Therefore, it is chosen as the sizing condition for further considerations. Finally, a comparison between the most demanding computed values and real values, retrieved from literature, is reported in Table 40:

Results	Computed			Real		
	Total	ACU	Data Handling	ACU	Data Handling	References
ROM [Mb]	1,2	0,716	0,484	0,064	0,08	[9]
RAM [Mb]	2,073	1,061	1,012	0,128	0,128	[9]
TP [MIPS]	6,7405	5,254	1,4865	0,5	0,5	[117]

Table 40: Comparison between computed and real data

Based on the observation of the OBDH budgets, it is evident that the Data Handling requirements align with the performance characteristics of a typical 1750A 16-bit architecture [48] [117], while the high throughput of the ACU exceeds the capability of such architecture, meaning that some kind of overestimation has occurred. The observed significant deviation between real and computed values could arise from various factors. Firstly, not all OS and AOCS processing functions are active simultaneously in every mode. Secondly, the margin applied to the computed values of 400% may be too high contributing to the observed deviation.

Appendix

Subsystem	Modes							
	ESR		CRP		RMW		NM	
AOCS	SASs (3), IRU	FPSS(1), IRU, RWs(3)	FPSS(1), Star Tracker(1), IRU, RWs(desat)			FPSS(1), Star Tracker(1), RWs(3)		
TCS	SVM, PLM	SVM, PLM	SVM, PLM			SVM		
TMTC	✓	✓	✓			✓	✓	
OBDH	✓	✓	✓			✓	✓	
Propulsive	4 thrusters	X	8 thrusters			X		
EPS	✓	✓	✓			✓	✓	
PAYLOAD	X	X	X			X	✓	

Table 41: Resuming table of subsystems elements active for each mode

Data	AOCS	EPS	PS	TCS	TMTC	Payload	OS	TOT
RMW	1	1	1	1	1	0	1	
$T_p [KIPS]$	1050,8	10	36	0,3	40	0	211	1348,1
Margined	5254	50	180	1,5	200	0	1055	6740,5
Code	71600	2400	4800	800	4000	0	36400	120000
Margined	358000	12000	24000	4000	20000	0	182000	600000
Data	34500	1000	9000	1500	13000	0	28300	87300
Margined	172500	5000	45000	7500	65000	0	141500	436500

Table 42: Systems data usage per each S/S in RMW mode

Data	AOCS	EPS	PS	TCS	TMTC	Payload	OS	TOT
ESR	1	1	1	1	1	0	1	
$T_p [KIPS]$	319,4	10	36	0,3	40	0	211	616,7
Margined	1597	50	180	1,5	200	0	1055	3083,5
Code	65200	2400	4800	800	4000	0	36400	113600
Margined	326000	12000	24000	4000	20000	0	182000	568000
Data	17200	1000	9000	1500	13000	0	28300	70000
Margined	86000	5000	45000	7500	65000	0	141500	350000

Table 44: Systems data usage per each S/S in ESR mode

RMW					
TOT CODE [kb]	TOT Data [kb]	TOT T_p [KIPS]	ROM [kb]	RAM [kb]	T_p [MIPS]
		1348,1			
		6740,5			
240			240	414,6	1.3481
1200			1200	2073	6.7405
174,6					
873					

Table 46: Total results for RMW mode

ESR					
TOT CODE [kb]	TOT Data [kb]	TOT T_p [KIPS]	ROM [kb]	RAM [kb]	T_p [MIPS]
		616,7			
		3083,5			
227,2			227,2	367,2	0,6167
1136			1136	1836	3.0835
140					
700					

Table 48: Total results for ESR mode

Data	AOCS	EPS	PS	TCS	TMTC	Payload	OS	TOT
NM	1	1	0	1	1	0	1	
$T_p [KIPS]$	965	10	0	0,3	40	0	211	1226,3
Margined	4825	50	0	1,5	200	0	1055	6131,5
Code	66800	2400	0	800	4000	0	36400	110400
Margined	334000	12000	0	4000	20000	0	182000	552000
Data	31300	1000	0	1500	13000	0	28300	75100
Margined	156500	5000	0	7500	65000	0	141500	375500

Table 43: Systems data usage per each S/S in NM mode

Data	AOCS	EPS	PS	TCS	TMTC	Payload	OS	TOT
CRP	1	1	0	1	1	0	1	
$T_p [KIPS]$	574	10	0	0,3	40	0	211	835,3
Margined	2870	50	0	1,5	200	0	1055	4176,5
Code	64800	2400	0	800	4000	0	36400	108400
Margined	324000	12000	0	4000	20000	0	182000	542000
Data	16300	1000	0	1500	13000	0	28300	60100
Margined	81500	5000	0	7500	65000	0	141500	300500

Table 45: Systems data usage per each S/S in CRP mode

NM					
TOT CODE [kb]	TOT Data [kb]	TOT T_p [KIPS]	ROM [kb]	RAM [kb]	T_p [MIPS]
		1226,3			
		6131,5			
220,8					
1104					
150,2					
751					

Table 47: Total results for NM mode

CRP					
TOT CODE [kb]	TOT Data [kb]	TOT T_p [KIPS]	ROM [kb]	RAM [kb]	T_p [MIPS]
		835,3			
		4176,5			
216,8					
1084					
120,2					
601					

Table 49: Total results for CRP mode

Bibliography

- [1] *Overview of the SOHO mission*
Authors: R. M. Bonnet, & F. Felici
Date: 1997
Journal: *Advances in Space Research*, 20(12), 2207–2218.
DOI: [https://doi.org/10.1016/s0273-1177\(97\)00894-6](https://doi.org/10.1016/s0273-1177(97)00894-6)
- [2] *The SOHO mission: An overview*
Authors: V. Domingo, B. Fleck, & A. I. Poland
Date: 1995
Journal: *Solar Physics*, 162(1–2), 1–37.
DOI: <https://doi.org/10.1007/bf00733425>
- [3] *SOHO factsheet*
Authors: ESA
Date: 30 June 2003
Available at: https://www.nasa.gov/wp-content/uploads/2015/04/156578main_soho_fact_sheet.pdf
- [4] *SOHO Commissioning phase*
Authors: ESA
Date: December 11, 1997
Available at: <https://soho.nascom.nasa.gov/operations/commissioning/>
- [5] *Official SOHO webpage*
Authors: ESA
Available at: <https://www.cosmos.esa.int/web/soho>
- [6] *SOHO (Solar and Heliospheric Observatory) - EOPortal*
Date: July 27, 2022
Available at: <https://www.eoportal.org/satellite-missions/soho#SOHO.html.4>
- [7] *ESA Bulletin Nr. 84: "The SOHO Ground Segment and Operations"*
Authors: W. Worrall, D. Muñoz, R. Menrad & C. Berner
Date: November 1995
Available at:
[https://www.esa.int/esapub/bulletin/bullet84/worral84.htm#:~:text=The%20operational%20mission%20is%20divided,Halo%20orbit%20Phase%20\(HOP\).](https://www.esa.int/esapub/bulletin/bullet84/worral84.htm#:~:text=The%20operational%20mission%20is%20divided,Halo%20orbit%20Phase%20(HOP).)
- [8] *ESA Bulletin Nr. 84: "The SOHO Payload and Its Testing"*
Author: C. Berner & V. Domingo
Date: November 1995
Available at: <https://www.esa.int/esapub/bulletin/bullet84/domi84.htm>
- [9] *ESA Bulletin Nr. 84: "The SOHO Spacecraft"*
Authors: J. Candé, G. Coupé, P. Rumler, P. Strada and F. Teston.
Date: November 1995
Available at: <https://www.esa.int/esapub/bulletin/bullet84/vdbus84.htm>
- [10] *ESA Bulletin Nr. 86: "SOHO - The Trip to the L1 Halo Orbit"*
Authors: F. C. Vandenbussche & P. Temporelli
Date: November 1996
Available at: <https://www.esa.int/esapub/bulletin/bullet86/huber86.htm>
- [11] *ESA Bulletin Nr. 88: "The History of the SOHO Mission"*
Authors: M.C.E. Huber , R.M. Bonnet , D.C. Dale , Monique Arduini , C. Fröhlich , V. Domingo & G. Whitcomb
Date: May 1996
Available at: <https://www.esa.int/esapub/bulletin/bullet88/vande88.htm>
- [12] *Operations*

Authors: NASA Date: 1995
Available at: <https://soho.nascom.nasa.gov/publications/soho-documents/sop/node11.html>

[13] *L1, the first Lagrangian Point*

Authors: ESA
Available at:
https://www.esa.int/Science_Exploration/Space_Science/L1_the_first_Lagrangian_Point

[14] *Global Oscillations at Low Frequencies - Instrument*

Authors: Patrick Boumier (Institut d'Astrophysique Spatiale, France)
Available at: <https://www.ias.u-psud.fr/golf/templates/instrument.html>

[15] *NASA Technical Reports Server (NTRS) 19980201678: AAS/GSFC 13th International Symposium on Space Flight Dynamics. Volume 2: NASA Technical Reports Server (NTRS).*

Date: 1998, May 1
Available at: https://archive.org/details/NASA_NTRS_Archive_19980201678/page/587/mode/1up?q=SOHO&view=theater

[16] *Variability of solar IRradiance and Gravity Oscillations*

Authors: Institut d'Astrophysique Spatiale, France
Available at: <https://www.ias.u-psud.fr/virgo/virgomain.html>

[17] *The Michelson Doppler Imager*

Authors: Stanford-Lockheed Institute for Space Research, USA
Available at: <http://soi.stanford.edu/>

[18] *Stationkeeping techniques for Libration-Point satellites. The Journal of the Astronautical Sciences, 49(1), 127–144.*

Authors: Dunham, D., and Roberts
Date: 2001
Available at: <https://doi.org/10.1007/bf03546340>

[19] *Solar Ultraviolet Measurements of Emitted Radiation*

Authors: Max Planck Institute for Solar System Research (MPS), Germany
Available at: <https://www2.mps.mpg.de/projects/soho/sumer/>

[20] *Coronal Diagnostic Spectrometer on SOHO*

Authors: CDS Operations Management Team in the Space Science and Technology Department at CCLRC Rutherford Appleton Laboratory
Available at: <https://solar.bnsc.rl.ac.uk/>

[21] *The SOHO Extreme ultraviolet Imaging Telescope*

Authors: The EIT Consortium (NASA/Goddard Space Flight Center, USA)
Available at: https://umbra.nascom.nasa.gov/eit/EIT.html#WHAT_EIT

[22] *The Ultraviolet Coronagraph Spectrometer for the SOHO*

Authors: Raid Suleiman, Harvard-Smithsonian Center for Astrophysics, USA
Available at: <https://lweb.cfa.harvard.edu/uvcs/>

[23] *LASCO, Large Angle ans Spectrometric Coronagraph*

Authors: U.S. Naval Research Laboratory
Available at: https://lasco-www.nrl.navy.mil/index.php?p=content/about_lasco

[24] *SWAN Far Side Imaging*

Authors:
Available at: <https://soho.nascom.nasa.gov/data/summary/swan/>

[25] *The CELIAS Experiment*

Authors: Verena Heidrich-Meisner, Lars Berger (University of Kiel, Germany)
Available at: <http://www2.physik.uni-kiel.de/SOHO-CELIAS/instrument.html#Introduction>

- [26] *What is COSTEP?*
Authors: Ole Staack (University of Kiel, Germany)
Available at: <http://www2.physik.uni-kiel.de/et/ag-heber/costep/index.php>
- [27] *ERNE project*
Authors: Space Research Laboratory, Department of Physics and Astronomy, FI-20500 University of Turku, FINLAND
Available at: <https://srl.utu.fi/projects/erne/>
- [28] *The "IADC Space Debris Mitigation Guidelines" and supporting documents*
Authors: M. Yakovlev
Date: 2005
Available at:
<https://conference.sdo.esoc.esa.int/proceedings/sdc4/paper/35/SDC4-paper35.pdf>
- [29] *The Solar and Heliospheric Observatory(SOHO) Mission: An Overview of Flight Dynamics Support of the Early Mission Phase*
Authors: R. Short,J Behuncik
Available at: <https://ntrs.nasa.gov/citations/19960035770>
- [30] *Design and analysis of quasi-halo orbits and optimal transfers from the Earth under different Sun-Earth frameworks using differential evolution. Journal of Astrophysics and Astronomy, 44(2).*
Authors: Neelakantan and Ramanan.
Date: 2023
Available at: <https://doi.org/10.1007/s12036-023-09969-1>
- [31] *SOHO mission update*
Author:Bernhard Fleck
Date:2018
Available at: https://soho2018.sciencesconf.org/data/pages/SOHO_29_SOHO_Status_2018_Fleck.pdf
- [32] *On the reentry design for the SOHO mission*
Authohors: E. M. Alessi, G. Tommei, I. Holbrough, and J. Beck
Date: 2020
Available at: <https://conference.sdo.esoc.esa.int/proceedings/sdc7/paper/478/SDC7-paper478.pdf>
- [33] SOHO: Frequently Asked Questions (FAQ)
Available at: <https://soho.nascom.nasa.gov/explore/faq.html>
- [34] *The Solar and Heliospheric Observatory(SOHO) Mission: An Overview of Flight Dynamics Support of the Early Mission Phase*
Authors: R. Short,J Behuncik
Available at: <https://ntrs.nasa.gov/citations/19960035770>
- [35] *Mission design for a halo orbiter of the Earth. Astrodynamics Conference*
Authors: Farquhar, R. W., Muononen, D. P., & Richardson, D. L.
Date: 1976
DOI: <https://doi.org/10.2514/6.1976-810>
- [36] How is SOHO Orbit Location (The L1 point) Calculated?
Available at: <https://solar-center.stanford.edu/FAQ/QL1.html>
- [37] *Stationkeeping techniques for Libration-Point satellites. The Journal of the Astronautical Sciences, 49(1), 127–144.*
Authors: Dunham, D., and Roberts
Date: 2001
Available at: <https://doi.org/10.1007/bf03546340>
- [38] *NASA Technical Reports Server (NTRS) 19980201678: AAS/GSFC 13th International Symposium on Space Flight Dynamics. Volume 2: NASA Technical Reports Server (NTRS).*
Date: 1998, May 1

Available at: https://archive.org/details/NASA_NTRS_Archive_19980201678/page/587/mode/1up?q=SOHO&view=theater

[39] *MRE-1.0 Monopropellant Thruster Datasheet.*

Available at: https://wpcontent.ot5o9s93syrb.net/wp-content/uploads/MRE-10_MonoProp_Thruster.pdf

[40] *ISEE-3 / ICE (International Cometary Explorer) mission*

Author: European Space Agency

DOI: <https://www.eoportal.org/satellite-missions/isee-3#launch>

[41] *The Soho Mission L1 Halo orbit recovery from the Attitude Control Anomalies of 1998*

Author: ROBERTS, C.E

Date: 2002

DOI: https://doi.org/10.1142/9789812704849_0009

[42] *Long term missions at the Sun-Earth Libration point L1: ACE, SOHO, and WIND*

Author: Craig E. Roberts

Date: 2002

Available at: <https://core.ac.uk/download/pdf/158348809.pdf>

[43] *Pressure fed rockets*

Author: Derek Honkawa. M.S. Aerospace Engineering, California State University

Date: 2016

Available at: <https://www.honkawarocketry.com/propulsion-systems>

[44] *Diaphragm Tanks Data Sheets*

Author: Northrop Grumman

Available at: <https://www.northropgrumman.com/space/diaphragm-tanks-data-sheets-sorted-by-volume>

[45] *Resurrected DSCOVR Propulsion System – Challenges and Lessons Learned*

Author: Apurva P. Varia and Ashley R. Scroggins

Available at: <https://ntrs.nasa.gov/api/citations/20150022915/downloads/20150022915.pdf>

[46] *Atlas Mission Planner's Guide*

Author: General Dynamics Commercial Launch Services, INC

Available at: <https://apps.dtic.mil/sti/tr/pdf/ADA258845.pdf>

[47] *NASA Horizon web software*

Available at: <https://ssd.jpl.nasa.gov/horizons/app.html#/>

[48] *Space Mission Analysis and Design*

Author: Wiley J.Larson and James R. Wertz

Date: 2005

[49] *Margin philosophy for science assessment studies*

Author: European Space Agency

Date: 2012

Available at: https://sci.esa.int/documents/34375/36249/1567260131067-Margin_philosophy_for_science_assessment_studies_1.3.pdf

[50] *What is the Deep Space Network?*

Author: NASA Jet Propulsion Laboratory

Available at: <https://www.nasa.gov/directorates/somd/space-communications-navigation-program/what-is-the-deep-space-network/>

[51] *Keyhole Periods: Problem Definition and Solving Model.*

Author: Policella, Nicola & Oliveira, Henrique & Siili, Tero.

Year: 2009

Available at: <https://www.nasa.gov/directorates/somd/space-communications-navigation-program/what-is-the-deep-space-network/>

- [52] *Injection contingency recovery strategies for halo orbit transfer trajectory-AIAA/AAS Astrodynamics Conference, San Diego, CA, July 29-31, 1996, Collection of technical papers (A96-34712 09-12), Reston, VA, American Institute of Aeronautics and Astronautics, 1996, p. 241-256*
 Author: C.E.Roberts, R. Short
 Date: 1996
- [53] *Efficient Modulation Methods Study at NASA/JPL PHASE 3: END-TO-END System Performance*
 Author: Warren L. Martin Tsun-Yee Yan Loc V. Lam
 Year: September 1997
 Available at: <https://deepspace.jpl.nasa.gov/files/phase3.pdf>
- [54] *Building a Quadrifilar Helix Antenna for Undergraduate Researchers*
 Available at: https://www.theremino.com/files/Building_QFH_Antenna_ENG.pdf
- [55] *26-m Antenna Subnet Telecommunications Interfaces*
 Year: November 30, 2000
 Available at: <https://deepspace.jpl.nasa.gov/dsndocs/810-005/102/102.pdf>
- [56] *Extremely low-profile helix radiating a circularly polarized wave*
 Author: H. Nakano; H. Takeda; T. Honma; H. Mimaki; J. Yamauchi
 Year: June 1991
 Available at: <https://ieeexplore.ieee.org/document/86872>
- [57] *SOHO, an international success*
 Author: F.Felici; European Space Agency; ESTEC
 Year: October 1996
- [58] *Deep Space Network Services Catalog*
 Author: Jeff Berner; DSN Project Chief Engineer
 Year: February 24, 2015
 Available at: <https://deepspace.jpl.nasa.gov/files/820-100-F1.pdf>
- [59] *Soho Recovery*
 Authors: Olive, J.
 Date: 1999
 Journal: NASA Conference Publication (pp. 449-462)
- [60] *"Solar and Heliospheric Observatory (SOHO) Flight Dynamics Simulations Using MATLAB."*
 Authors: Headrick, R., and J. Rowe
 Date: 1996
 Journal: NASA CONFERENCE PUBLICATION
 Available at: <https://ntrs.nasa.gov/api/citations/19960035757/downloads/19960035757.pdf>
- [61] *SOHO Mission Interruption Preliminary Status and Background Report*
 Date: July 15, 1998
 Available at: https://umbra.nascom.nasa.gov/soho/prelim_and_background_rept.html
- [62] *SOHO, What Happened After 1999?*
 Authors: van Overbeek, T.
 Date: May, 2006
 Available at: <https://articles.adsabs.harvard.edu/full/2006ESASP.617E..30V/0000030.001.html>
- [63] *SOHO Spacecraft Emergencies and Modes*
 Available at: <https://soho.nascom.nasa.gov/soc/esr/>
- [64] *AOCS technology (attitude and orbit control subsystem)*
 Author: W.J. Alldridge
 Date: 1990
 Available at: <https://ieeexplore.ieee.org/document/190835/authors#authors>

- [65] *SOHO Ancillary Data*
Available at: <https://soho.nascom.nasa.gov/data/ancillary/>
- [66] *SOHO Spacecraft rolls*
Available at: <https://soho.nascom.nasa.gov/operations/commissioning/SC-rolls.html>
- [67] *The Officine Galileo Autonomous Star Tracker*
Authors: Franco Boldrini, Andrea Landi
Available at: <https://www.cosmos.esa.int/documents/12133/1028864/THE+OFFICINE+GALILEO+AUTONOMOUS+STAR+TRACKER>
- [68] *Leonardo Star Trackers - Flight Experiences and Introduction of SPACESTAR Product on GEO Platforms*
Date: October 18, 2017
Available at: https://indico.esa.int/event/182/contributions/1506/attachments/1456/1682/1710_-_Boldrini.pdf
- [69] *TNO Coarse Sun Sensor using European cells - ESA CSC*
Date: 19 April, 2024
Available at: <https://connectivity.esa.int/projects/tno-coarse-sun-sensor-using-european-cells>
- [70] *The Million-Mile Rescue*
Date: April 2021
Available at: <https://appel.nasa.gov/2012/04/25/the-million-mile-rescue/>
- [71] *Reaction Wheel Unit W45E*
Available at: <https://satsearch.co/products/bradford-reaction-wheel-unit-w45e>
- [72] *REDWIRE FINE POINTING SUN SENSOR*
Date: May 2021
Available at: <https://redwirespace.com/wp-content/uploads/2023/06/redwire-fine-pointing-sun-sensor-flysheet.pdf>
- [73] *Scalable SIRU™ Family - Datasheet.*
Authors: Northrop Grumman.
Available at: <https://www.satcatalog.com/component/scalable-siru-1/>
- [74] *Reaction Wheel Unit W45*
Available at: <https://satsearch.co/products/bradford-reaction-wheel-unit-w45>
- [75] *SOHO spacecraft thermal control aspects*
Authors: Poinas Philippe & Cande Jacques
Date: July 31, 1997
Available at: https://www.researchgate.net/publication/234368253_SOHO_spacecraft_thermal_control_aspects
- [76] *ESA Bulletin Nr. 84: "The SOHO Spacecraft"*
Author: F.C. Vandenbussche, J. Candé, G. Coupé, P. Rumler, P. Strada & F. Teston
Date: November 1995
Available at: <https://www.esa.int/esapub/bulletin/bullet84/vdbus84.htm>
- [77] *The SOHO thruster temperature control*
Authors: Fabrizio Felici
Date: May, 1997
Available at: <https://adsabs.harvard.edu/full/1997ESASP.400..133L>
- [78] *High precision device for the LASCO instrument on SOHO*
Authors: F. Burger, J. Eder
Available at: <https://adsabs.harvard.edu/full/1995ESASP.374....9B>
- [79] *The Thermal Control of the Coronal Diagnostic Spectrometer*
Authors: Simon Peskett

Date: July 12-15,1993
Available at: <https://www.sae.org/publications/technical-papers/content/932080/>

[80] *SOHO SVM Thermal Control*

Authors: Jose L. Garcia
Date: August 21, 2018
DOI: <https://doi.org/10.4271/941427>

[81] *Space Weather Effects on SOHO and its leading role in the Early-Warning system for space weather*

Authors: P. Brekke, B. Fleck, S.V. Haugan, RSSD, European Space Agency T. van Overbeek, H. Schweitzer, SCI-P, European Space Agency M. Chaloupy, Astrium, GSFC
Available at: <https://ams.confex.com/ams/pdffiles/74187.pdf>

[82] *SOHO: a modular spacecraft concept to allow flexible payload integration and efficient development*

Authors: M Bouffard, J.P Gardelle, M Le Moine, P Temporelli
Date: October, 1995
Available at: <https://www.sciencedirect.com/science/article/pii/009457659500070G>

[83] *Results from proton damage tests on the Michelson Doppler Imager CCD for SOHO*

Authors: Igor Zayer, Ira Chapman, Dexter W. Duncan, G. A. Kelly, Keith E. Mitchell
Date: 12 July 1993
Available at: <https://www.spiedigitallibrary.org/conference-proceedings-of-spie/1900/0000/Results-from-proton-damage-tests-on-the-Michelson-Doppler-Imager/10.1117/12.148604.short>

[84] *Effective Emittance MLI*

Available at: https://www.thermalengineer.com/library/effective_emittance.htm

[85] *Multilayer Insulation Material Guidelines*

Authors: Finckenor, M. M., & Dooling, D.
Date: 1999
Available at: <https://ntrs.nasa.gov/api/citations/19990047691/downloads/19990047691.pdf>

[86] *Elements of spacecraft design*

Authors: Brown, C. D.
Date: 2002
DOI: <https://doi.org/10.2514/4.861796>

[87] *Aluminized Kapton® Fabric Laminate*

Available at: <https://dunmore.com/products/aluminized-polyimide-fabric-laminate.html>

[88] *Information for the Safe Handling of Ni-Cd Batteries*

Available at: https://www.enersys.com/493bb4/globalassets/documents/product-documentation/_enersys/emea/instructions-for-safe-handling/nicd/enersys-information-for-safe-handling-of-nicd-batteries-january-2018.pdf

[89] *NASA Spacecraft Maps Earth's Global Emissivity*

Available at: <https://www.jpl.nasa.gov/images/pia18833-nasa-spacecraft-maps-earths-global-emissivity>

[90] *NASA Reference Publication 1121, Solar Absorptance and Thermal Emittance of Some Common Spacecraft Thermal Control Coatings*

Available at: <https://ntrs.nasa.gov/api/citations/19840015630/downloads/19840015630.pdf>

[91] *Spacecraft Thermal Control Handbook*

Author: David G. Gilmore
Date: 2002

[92] *Transformational Solar Array Final Report*

Authors: Gaddy, Edward and Ballarotto, Mihaela and Drabenstadt, Christian and Nichols, John and Douglas, Mark and Spence, Brian and Stall, Richard A. and Sulyma, Chris and Sharps, Paul
Available at: <https://ntrs.nasa.gov/api/citations/20170010684/downloads/20170010684.pdf>

- [93] *PSG120FD paint datasheet*
Available at: <https://www.spacematdb.com/spacemat/datasearch.php?name=PSG%20120%20FD>
- [94] *MLI Polyimide Kapton datasheet*
Available at: <https://www.spacematdb.com/spacemat/m-datasearch.php?name=Sheldahl%20146633>
- [95] *Electrodag 501 paint datasheet*
Available at: <https://www.spacematdb.com/spacemat/m-datasearch.php?name=Electrodag%20501>
- [96] *Optical Solar Reflector datasheet*
Available at: <https://www.excelitas.com/product/optical-solar-reflectors#documentation>
- [97] *Chemglaze Z306 datasheet*
Available at: <https://www.spacematdb.com/spacemat/m-datasearch.php?name=Chemglaze%20Z306>
- [98] *SOHO power system performance during 6 years in orbit*
Authors: Rumler, Peter and Schweitzer, H.
Journal: European space power conference 141-146
Date: May 2002
Available at: <https://ui.adsabs.harvard.edu/abs/2002ESASP.502..141R/abstract>
- [99] *Lessons learned from the thermal design of an instrument (EIT, the Extreme-UV Imaging Telescope) on board SOHO*
Authors: J.M. Defise, P. Rochus
Date: July, 1997
Available at: <https://www.sae.org/publications/technical-papers/content/972528/>
- [100] *Software Implementation of Systems Engineering in Space Applications*
Authors: Yilmaz, Özgün
Date: 2011
Available at: <https://www.diva-portal.org/smash/record.jsf?pid=diva2%3A1018270&dswid=8749>
- [101] *7.0 Thermal Control - NASA*
Available at: <https://www.nasa.gov/smallsat-institute/sst-soa/thermal-control/#7.3.1>
- [102] *Soho Power System Performance during 6 years in orbit*
Authors: Peter Rumler, Helmut Schweitzer
Date: 2002
Available at: <https://ui.adsabs.harvard.edu/abs/2002ESASP.502..141R/abstract>
- [103] *Power System Performance of the SOHO Spacecraft During the 1998 Attitude Recovery*
Authors: H. Fiebrich, J. E. Haines, P. Perol, P. Rumler
Date: 1999
Available at: <https://www.sae.org/publications/technical-papers/content/1999-01-2484/>
- [104] *Spectroscopic Behavior of Composite, Black Thermal Paint, Solar Cell, and Multilayered Insulation Materials in a GEO Simulated Environment*
Authors: Jacqueline A. Reyes, Ryan C. Hoffmann, Daniel P. Engelhart, Heather M. Cowardin, Darren Cone
Date: 2002
Available at: <https://ntrs.nasa.gov/api/citations/20190033943/downloads/20190033943.pdf>
- [105] *Batteries and fuel cells in space*
Authors: Halpert, G., Frank, H., & Surampudi, S.
Date: 1999
Available at: <https://doi.org/10.1149/2.f06993if>
- [106] *Saft spacecraft batteries*
Author: Saft ©
Available at: <https://www.saft.com/market-sectors/aerospace-defense/space>

- [107] *Silicon density*
Available at: <https://www.periodic-table.org/Silicon-density/>
- [108] *CMX cover glass datasheet*
Available at: https://www.excelitas.com/file-download/download/public/58456?filename=Qioptiq_Space-Qualified_Cover_Glass_Datasheet.pdf
- [109] *Honeycomb datasheet*
Available at: https://www.hexcel.com/user_area/content_media/raw/CR_PAA_us.pdf
- [110] *DC 93-500 adhesive datasheet*
Available at: <https://www.dow.com/documents/en-us/productdatasheet/11/11-39/11-3982-01-dowsil-space-grade-silicone-sealants.pdf?iframe=true>
- [111] *Kapton datasheet*
Available at: https://www.dupont.com/content/dam/dupont/amer/us/en/ei-transformation/public/documents/en/EI-10142_Kapton-Summary-of-Properties.pdf
- [112] *Carbon fiber datasheet*
Available at: https://www.hexcel.com/user_area/content_media/raw/IM2C_HexTow_DataSheet.pdf
- [113] *SOHO Solar Array: a performance evaluation of 2,5 years in orbit and capabilities for a mission extension of 5 years*
Authors: P.Rumler, H. Schwetzer, H. Evans
Date: 1998
Available at: <https://ui.adsabs.harvard.edu/abs/1998ESASP..416..621R/abstract>
- [114] *ESA Bulletin Nr. 97:"SOHO's Recovery – An Unprecedented Success Story"*
Author: F.C. Vandenbussche
Date: November 1995
Available at: <https://www.esa.int/esapub/bulletin/bullet97/vandenbu.pdf>
- [115] *CDPU for SOHO-CEPAC collaboration*
Authors: D. Meziat, J. Sequeiros, J. Medina, S.Sanchez
Date: January, 1993
Available at: <https://www.sciencedirect.com/science/article/pii/016560749390012A>
- [116] *MIL-STD-1750A Microprocessor Datasheet*
Available at: <https://pdf.datasheetcatalog.com/datasheet/dynex/MAS281.pdf>
- [117] *Space System Engineering and Operations-On board Data Handling*
Author: M. Lavagna
Date: 2023/2024
- [118] *A Configurable Interface Unit for Telemetry Monitoring in Satellites*
Authors: Fredrik Hagglärt, Fredrik Johansson, Chalmers University of Technology, University of Gothenburg, Sweden
Date: 2018
Available at: <https://odr.chalmers.se/server/api/core/bitstreams/45dab46c-dfca-4227-bdfc-022c84d21557/content>
- [119] *Adaptive on-board data compression for spacecraft*
Authors: Ward, A. K. ; Nicholls, J. P. ; Chaturvedi, D. C.

Date: Oct. 7-13, 1989

Available at: <https://ui.adsabs.harvard.edu/abs/1989mala.iafcQ....W/abstract>